X72-10667

~~CONFIDENTIAL~~

NASA TECHNICAL MEMORANDUM

NASA TM X-2622

NATIONAL AERONAUTICS AND SPACE ADMINISTRATION U.S.A.

NASA TM X-2622

WIND-TUNNEL INVESTIGATION AT MACH NUMBERS FROM 0.25 TO 1.01 OF A TRANSPORT CONFIGURATION DESIGNED TO CRUISE AT NEAR-SONIC SPEEDS

by Richard A. Langhans and Stuart G. Flechner

Langley Research Center
Hampton, Va. 23365

NATIONAL AERONAUTICS AND SPACE ADMINISTRATION • WASHINGTON, D. C. • AUGUST 1972

~~CONFIDENTIAL~~

[redacted]

[redacted]

1. Report No.	2. Government Accession No.	3. Recipient's Catalog No.
NASA TM X-2622		

4. Title and Subtitle
WIND-TUNNEL INVESTIGATION AT MACH NUMBERS FROM 0.25 TO 1.01 OF A TRANSPORT CONFIGURATION DESIGNED TO CRUISE AT NEAR-SONIC SPEEDS (U)

5. Report Date
August 1972

6. Performing Organization Code

7. Author(s)
Richard A. Langhans and Stuart G. Flechner

8. Performing Organization Report No.
L-8226

10. Work Unit No.
501-15-01-01

9. Performing Organization Name and Address
NASA Langley Research Center
Hampton, Va. 23365

11. Contract or Grant No.

13. Type of Report and Period Covered
Technical Memorandum

12. Sponsoring Agency Name and Address
National Aeronautics and Space Administration
Washington, D.C. 20546

14. Sponsoring Agency Code

15. Supplementary Notes

16. Abstract

A wind-tunnel investigation was conducted in the Langley 8-foot transonic pressur tunnel at Mach numbers from 0.25 to 1.01 and angles of attack from about 0° to 30° on a transport configuration designed to cruise at near-sonic speeds. Included are results showing the static longitudinal and lateral-directional aerodynamic characteristics for sideslip angles.

17. Key Words (Suggested by Author(s))
Transonic aerodynamics
Supercritical-wing transport aircraft
Advanced technology transport configuration
Supercritical airfoil application

19. Security Classif. (of this report)	20. Security Classif. (of this page)	21. No. of Pages	22. Price
[redacted]	Unclassified	108	

[redacted]

[redacted]

[redacted]

WIND-TUNNEL INVESTIGATION AT MACH NUMBERS FROM 0.25 TO 1.01 OF A TRANSPORT CONFIGURATION DESIGNED TO CRUISE AT NEAR-SONIC SPEEDS*

By Richard A. Langhans and Stuart G. Flechner
Langley Research Center

SUMMARY

A wind-tunnel investigation was conducted at Mach numbers from 0.25 to 1.01 to determine the static aerodynamic characteristics of a transport configuration designed to cruise at near-sonic speeds.

The results of the investigation show that the configuration exhibits a sufficiently high drag-divergence Mach number to cruise at near-sonic speeds. The configuration is longitudinally stable through the cruise Mach number and lift-coefficient range, but at higher lift coefficients displays pitchup and becomes unstable. A rapid degradation in stability occurs with decreasing Mach number for Mach numbers below 0.95. Trim drag penalties, associated with increases in the static margin with Mach number, are reduced by the positive trend of the zero-lift pitching moment.

The configuration was directionally stable at all test conditions and laterally stable in the angle-of-attack range required for cruise.

INTRODUCTION

The NASA supercritical airfoil, which has been under development for a number of years (refs. 1 to 4), is designed to delay shock-induced boundary-layer separation to Mach numbers and lift coefficients notably higher than those of conventional sections. Configurations employing this new concept have demonstrated the potential for obtaining significant increases in drag-divergence Mach number.

Wind-tunnel investigations of a configuration with a sweptback supercritical wing designed for possible application to a transport aircraft (refs. 5 and 6) showed that the configuration had a drag-divergence Mach number of about 0.97; yet the flow over the wing was still satisfactory with only a small degree of trailing-edge separation to a Mach number of approximately 1.00. It was conjectured that the drag divergence was primarily

*Title, Unclassified.

associated with the nonoptimum cross-sectional area development of the configuration. Recent experimental results (ref. 7) indicate that this drag divergence could be substantially reduced by improving the longitudinal development of the normal cross-sectional area. This improvement was based on a refined area-rule concept at a Mach number of 1.00 which considers second-order effects.

These results suggest the possibility of developing a transport configuration having a drag-divergence Mach number which would allow economically competitive cruise at near-sonic speeds. The purpose of this paper is to present the results from a wind-tunnel investigation at Mach numbers from 0.25 to 1.01 and angles of attack from about 0° to 30° on a transport configuration designed to cruise at near-sonic speeds. Included are results showing the static longitudinal and lateral-directional aerodynamic characteristics for sideslip angles of 0°, 2.0°, 2.5°, and 5.0°.

SYMBOLS

The results presented herein are referred to the stability axis system for the longitudinal characteristics and the body axis system for the lateral and directional characteristics. (See fig. 1(a).) All coefficients are based on the geometry of the basic trapezoidal wing panel, which does not include the leading-edge glove or the trailing-edge extension but includes the fuselage intercept. (See fig. 1(b).) The moment reference center is located longitudinally at 37.86 percent of the mean geometric chord of the basic trapezoidal wing, 80.47 cm (31.68 in.) aft of the fuselage nose, and vertically at 0.686 cm (0.270 in.) above the fuselage reference line. (See fig. 1(b).)

Values are given in both SI and U.S. Customary Units. The measurements and calculations were made in U.S. Customary Units.

Coefficients and symbols used herein are defined as follows:

A cross-sectional area

A_{max} maximum cross-sectional area

A_R area removed for stream-tube expansion at any x

$A_{R,max}$ maximum area removed for stream-tube expansion, 24.4 cm^2 (3.79 in^2)

$$\left(\frac{A}{A_{max}}\right)'' = \frac{d^2\left(A/A_{max}\right)}{d(x/l)^2}$$

b wing span, 109.22 cm (43.0 in.)

c — streamwise chord of total wing planform, which includes leading-edge glove and trailing-edge extension

$\bar{c}$ — mean geometric chord of basic wing panel

C_D — drag coefficient, $\frac{\text{Drag}}{qS}$, where drag is total measured drag minus base drag and internal drag of flow-through nacelles

$(C_{D,o})_{eff}$ — effective zero-lift drag, computed from $(C_{D,o})_{eff} = (C_D)_{C_L=0.4} - \frac{\Delta C_D}{\Delta C_L{}^2}(0.16)$

$\frac{\Delta C_D}{\Delta C_L{}^2}$ — drag-due-to-lift parameter, slope of C_D against $C_L{}^2$ at $C_L = 0.40$

C_L — lift coefficient, $\frac{\text{Lift}}{qS}$

C_{L_α} — lift-curve slope, $\partial C_L/\partial\alpha$, per degree

C_l — rolling-moment coefficient, $\frac{\text{Rolling moment}}{qSb}$

C_{l_β} — rate of change of rolling-moment coefficient with sideslip (effective-dihedral parameter), $\Delta C_l/\Delta\beta$, per degree

C_m — pitching-moment coefficient, $\frac{\text{Pitching moment}}{qS\bar{c}}$

$C_{m_{C_L}}$ — longitudinal stability derivative, $\partial C_m/\partial C_L$

$C_{m,o}$ — pitching-moment coefficient at zero lift

C_n — yawing-moment coefficient, $\frac{\text{Yawing moment}}{qSb}$

C_{n_β} — rate of change of yawing-moment coefficient with sideslip (directional stability parameter), $\Delta C_n/\Delta\beta$, per degree

C_Y — side-force coefficient, $\frac{\text{Side force}}{qS}$

C_{Y_β} — rate of change of side-force coefficient with sideslip, $\Delta C_Y/\Delta\beta$, per degree

K	constant used to define zero-lift area distribution
l	total length of zero-lift body
M	Mach number of undisturbed stream
q	dynamic pressure of undisturbed stream
R	Reynolds number based on mean geometric chord
S	wing area (trapezoidal wing) including fuselage intercept
x	longitudinal distance from model nose
x_{max}	distance from model nose to maximum cross-sectional area of zero-lift shape
x_o	distance from model nose to origin of region of stream-tube expansion compensation
$x_{R,max}$	distance from model nose to point of maximum stream-tube expansion compensation
x_T	distance from model nose to end of region of stream-tube expansion compensation
Δx	longitudinal distance from leading edge to point of interest
y	distance measured spanwise from plane of symmetry, zero at fuselage reference line
z	distance measured along a line parallel to plane of symmetry and perpendicular to x and y, zero at fuselage reference line
α	angle of attack, referenced to fuselage reference line
β	angle of sideslip, referenced to fuselage reference line (positive when nose is left)
δ_h	horizontal-tail deflection, referenced to fuselage reference line (positive when trailing edge is down)

APPARATUS AND PROCEDURES

Tunnel Description

The investigation was conducted in the Langley 8-foot transonic pressure tunnel, a continuous, single-return tunnel with a slotted, rectangular test section. This facility has the capability for independent variation of Mach number, density, temperature, and humidity. A more complete description of this facility is contained in reference 8.

For earlier investigations on models with a similar wing and of approximately the same size (refs. 5 and 6), tunnel slots with an open ratio of about 22 percent (designed on the basis of ref. 9 to give theoretically zero three-dimensional blockage) were used instead of the normal slots with an open ratio of 6 percent to alleviate tunnel wall blockage. However, there is some question as to the accuracy of this theory at Mach numbers approaching 1.00.

Tunnel operating difficulties associated with the wider slots necessitated a return to the normal slots with 6-percent open ratio, which appeared likely to produce significant blockage effects at the higher subsonic Mach numbers for a model of this size. However, since generally good correlation has been shown between unpublished drag-divergence data obtained with the slots with 22-percent open ratio and results obtained with the slots with 6-percent open ratio when wooden test-section wall inserts were used (fig. 1(c)), these wall inserts were included for the present investigation.

Because of the nature of the flow field surrounding a lifting configuration, 60 percent of the streamline displacement was assumed to occur in the vertical direction. The wall inserts were therefore indented to account for 40 percent of the longitudinal development of the model cross-sectional area, effectively a bulging of the walls away from the model to reduce streamline distortion. (See ref. 10.) Fore and aft of the model, these inserts reduced tunnel test-section cross-sectional area by approximately 0.24 percent.

Model Description

Drawings of the wind-tunnel model and sting support are presented in figures 1(b) and 1(d), and several photographs are shown in figure 2. This configuration incorporated an NASA supercritical wing with lower surface leading-edge vortex generators, an extensively-area-ruled fuselage, three aft-mounted nacelles (two side-mounted flow-through nacelles and one simulated S-duct nacelle), and a T-tail.

The configuration incorporated a low wing with a root incidence of approximately 2° and with approximately 6° of twist (washout) between the root and tip chords. On the basis of the deflection characteristics presented in reference 5, aeroelastic effects at a Mach number of 0.99 and a dynamic pressure of 35 910 N/m^2 (750 psf) can be expected to increase the twist at the tip approximately 2.6°. The wing airfoil coordinates are presented in table I. The data presented in this report were based on preliminary measurements of the wing, and the final measurements varied from those originally used as shown in the table below. These final values were computed by use of the coordinates in table I at $\frac{y}{b/2} = 0.4651$ and $\frac{y}{b/2} = 0.9302$.

	Original values	Final values
Root chord	24.727 cm (9.735 in.)	24.620 cm (9.693 in.)
Tip chord	9.703 cm (3.820 in.)	9.538 cm (3.755 in.)
S	0.1880 m^2 (2.024 ft^2)	0.1865 m^2 (2.008 ft^2)
b	109.22 cm (43.0 in.)	109.22 cm (43.0 in.)
$\bar{c}$	18.308 cm (7.208 in.)	18.189 cm (7.161 in.)
Aspect ratio	6.3	6.4
Taper ratio	0.392	0.387

The lower surface leading-edge vortex generators (ref. 7), which were 10-percent Clark-Y airfoils with the flat lower surface facing inboard, were located at $\frac{y}{b/2} = 0.6163$.

The fuselage was shaped by use of an area rule refined to account for second-order effects. The forebody is described in table II, and the rest is defined by the normal cross sections presented in figure 3. The longitudinal development of the cross-sectional area for the fuselage and the other model components is presented in figure 4(a).

The flow-through nacelles, used to simulate the side-mounted engines (fig. 1(b)) are described by the coordinates presented in table III. The nacelles were mounted on pylons with the leading edge located 104.14 cm (41.0 in.) aft of the fuselage nose.

Because of the particular sting arrangement utilized for this investigation, it was not possible to provide for flow through the vertical-tail-mounted S-duct nacelle. An alternate method was selected which would approximate the flow-field disturbances produced by a flow-through nacelle. This consisted of a swept wedge having a cross-sectional area equal to the nacelle area minus the stream-tube area. (See figs. 2 and 3.) It should be noted that this is an approximate method of simulating the external inlet flow-field disturbance only. Other tests would be necessary for determining the nacelle flow effects on the model afterbody. The vertical tail had 50° of leading-edge sweep and incorporated a symmetrical supercritical airfoil section. Coordinates for the middle engine and vertical tail are presented in table IV.

The horizontal tail had 45° of leading-edge sweep and was mounted at the top of the vertical tail. (See fig. 1(b).) The hinge line of the horizontal tail was located 21.84 cm (8.6 in.) above the fuselage reference line and at 33.8 percent of the mean geometric chord of the horizontal tail. Coordinates for the horizontal tail, measured at a deflection of 5°, are presented in table V.

Cross-Sectional Area Development

The first objective in the cross-sectional area development was to define the design envelope. (See fig. 4(b).) A zero-lift area distribution was derived from tests of a zero-lift body of revolution and theory. The body of revolution had the characteristics of the NASA supercritical airfoil: a high subsonic drag-divergence Mach number, a blunt nose, and low curvature in the midregion. The zero-lift area distribution is defined by the following equations:

Forward of the maximum area,

$$\left(\frac{A}{A_{max}}\right)'' = \frac{K}{A/A_{max}}$$

and rearward of the maximum area,

$$\left(\frac{A}{A_{max}}\right)'' = K\left(\frac{A}{A_{max}}\right)$$

where

$$\left(\frac{A}{A_{max}}\right)'' = \frac{d^2(A/A_{max})}{d(x/l)^2} \qquad \left(\left(\frac{A}{A_{max}}\right)'' \text{ constrained to be continuous at } A = A_{max}\right)$$

A — cross-sectional area at any x

A_{max} — maximum cross-sectional area, 203.9 cm^2 (31.6 in^2)

K — constant dependent upon body parameters A_{max}, l, and x_{max}

l — total length of zero-lift body, 152.4 cm (60.0 in.)

x — distance from body nose

x_{max} — distance from body nose at which $A = A_{max}$, 67.1 cm (26.4 in.)

The particular zero-lift area distribution obtained from the equation and parameters above is shown as (A) in figure 4(b) and presented in nondimensional form in table VI.

The zero-lift area distribution was reduced as shown in figure 4(b) to account for second-order effects which allow for expansion of the supersonic stream tubes about the upper surface of a lifting wing. The amount and extent of the area compensation was determined experimentally, and for the configuration discussed herein, the empirically derived equations for this second-order area consideration are

Forward of the maximum area decrease,

$$A_R = \frac{A_{R,max}}{2}\left[1 - \cos\left(\pi \frac{x - x_o}{x_{R,max} - x_o}\right)\right]$$

and rearward of the maximum area decrease,

$$A_R = A_{R,max}\left[\cos\left(\frac{\pi}{2}\frac{x - x_{R,max}}{x_T - x_{R,max}}\right)\right]$$

where the cosine is of an angle in radians and

A_R area that must be removed from zero-lift distribution at any x

$A_{R,max}$ maximum area to be removed from the zero-lift distribution 24.4 cm^2 (3.79 in^2), constrained to be 1.3 percent of original wing area S

x_o location for origin of area reduction; intersection of basic wing-panel leading edge and model center line

$x_{R,max}$ distance from nose at which $A_R = A_{R,max}$, constrained to be the most forward point of actual wing trailing edge, 86.9 cm (34.2 in.)

x_T distance from model nose at which area reduction is terminated, constrained to be 2/3 wing tip chord, 110.2 cm (43.4 in.)

The area compensation for stream-tube expansion is shown as (B) in figure 4(b). The design envelope is now defined as the difference between these two area distributions, shown as (A) – (B) in figure 4(b).

This design envelope was used to match the model components together for the configuration under investigation. The longitudinal development of the cross-sectional area for the complete configuration and the model components is presented in figure 4(a). The total area distribution almost identically matches the design envelope area distribution.

Boundary-Layer Transition

For Mach numbers from 0.95 to 1.00, the boundary-layer trips were sized and located on the wing upper and lower surfaces by use of the techniques discussed in references 11 to 13 to simulate boundary-layer and shock-induced separation characteristics at full-scale Reynolds numbers. The trips were applied to the wing lower surface at 45 percent of the local streamwise chord and to the outboard region of the upper surface at 45 percent of the local streamwise chord. On the basis of observations of the boundary-layer flow during earlier tests with the fluorescent-oil film method described in reference 14, the trips on the wing upper surface were modified over the inboard region (moved slightly forward) to prevent the occurrence of laminar separation ahead of the trip. This laminar separation would not be expected at full-scale conditions since turbulent boundary-layer flow is usually established near the leading edge. This trip arrangement is designated as type I and is shown in figures 5(a) and 5(b).

For Mach numbers of 0.90 and below, the boundary-layer trip on the wing upper surface was moved nearer the leading edge to prevent laminar separation from occurring ahead of the trip at high angles of attack. This trip is designated as type II and is shown in figure 5(c).

For all Mach numbers, the fuselage boundary-layer trip was applied 3.81 cm (1.50 in.) aft of the fuselage nose. The trips on the vertical tail were located at 45 percent of the local streamwise chord, beginning below the horizontal tail and ending 6.60 cm (2.6 in.) above the fuselage. The trips on the horizontal tail were located at 45 percent of the streamwise chord on the upper surface, and from 22.5 percent of the local streamwise chord 1.27 cm (0.5 in.) inboard from the tip to 45 percent of the local streamwise chord of the root. These trips consisted of No. 100 carborundum grains and were 0.127 cm (0.05 in.) wide.

The trips on the flow-through nacelles were located 0.51 cm (0.20 in.) behind the aftmost point of the inlet, inside and outside, and were perpendicular to the center line of the nacelle. The trip on the wedge, which simulated the third engine, was located 1.27 cm (0.50 in.) aft of, and parallel to, the wedge leading edge. These trips consisted of No. 180 carborundum grains. All trips were 0.127 cm (0.05 in.) wide.

The forward boundary-layer trips were located and sized by the procedures described in reference 13. The rearward boundary-layer trips were also sized by the procedures discussed in reference 13 although located according to reference 12.

When employing the technique described in reference 12 to simulate boundary-layer and shock-induced separation characteristics at full-scale Reynolds numbers, transition must occur only at the prescribed trip locations. As a result, it is important to maintain the model region ahead of the boundary-layer trips in an extremely smooth condition to prevent premature transition to turbulent flow. However, for the present investigation, natural transition to turbulent flow occurred on several model regions despite the smooth condition of the model. These regions were the glove, inboard of the 20.32-cm (8-in.) semispan station, and most of the vertical tail.

To aid in the analysis of the data obtained with the rearward boundary-layer trips, the skin-friction drag coefficient was computed for the wing by use of two-dimensional boundary-layer theory and the experimental pressure distributions presented in reference 6 for lift coefficients near 0.40. For the laminar portions of the boundary layer, an approximate procedure from reference 15 was used, and for the turbulent portions, references 16 and 17 were used. For the horizontal and vertical tails, average dynamic pressures based on available experiments and estimates were used. On the basis of these computations, the following corrections should be applied to the wind-tunnel data to adjust to a condition for which transition occurs at the 5-percent chord on the wing and tail surfaces. For the wing at Mach numbers of 0.80 to 0.90, ΔC_D of 0.0007 should be added, and at Mach numbers of 0.95 to 1.00, ΔC_D of 0.0015 should be added. For the horizontal and vertical tails, $\Delta C_D = 0.0006$ should be added at all Mach numbers from 0.80 to 1.00.

Test Conditions

Tests were conducted at Mach numbers from 0.25 to 1.01. The stagnation temperature of the tunnel air was automatically maintained at a value of approximately 322 K (120° F), and the air was dried until the dewpoint temperature in the test section was reduced sufficiently to avoid condensation effects. Test conditions are summarized in table VII.

Measurements

Aerodynamic forces and moments on the model were measured by means of a six-component electrical strain-gage balance housed within the fuselage cavity. Differential pressure transducers referenced to free-stream static pressure were used to measure the sting-cavity and model-base pressures. Measurements were taken over a Mach number range from 0.25 to 1.01 for angles of attack that generally varied from 0° to 16°. Several additional runs were made at Mach numbers of 0.25 and 0.50 to obtain data at angles of attack to 32. These data were obtained by use of an offset coupling, which is shown in figure 1(d). Force and moment data were also obtained through the lower angle-of-attack range for sideslip angles of 2.0°, 2.5°, and 5.0°.

To aid in the analysis of the boundary-layer flow patterns, photographs were taken at selected test conditions of the wing upper and lower surfaces by employing the fluorescent-oil film technique described in reference 14. Schlieren photographs were also taken at selected test conditions.

Corrections

The drag results presented herein have been adjusted to correspond to free-stream static pressure acting over the cross-sectional area of the sting at the model base and for the internal drag of the flow-through nacelles.

The model support sting (with the exception of the offset coupling) was designed on the basis of the results in reference 18 to minimize sting interference at near-sonic Mach numbers.

Corrections have been made to the measured angles of attack for model support sting and balance deflections as a result of aerodynamic loads on the model. Further corrections have been made to the measured angle of attack for tunnel flow angularity and for first-order boundary-induced lift-interference effects. This boundary-induced lift-interference correction, based on the theory of reference 19, amounted to reductions in the measured angles of attack of 0.09 times the normal force coefficient.

The large size of the present model relative to the tunnel size (ratio of model cross-sectional area to tunnel area is 0.005) raises a question of the absolute accuracy of the results at test Mach numbers approaching 1.00. Unpublished drag-divergence data obtained for the model of reference 5 by use of the same wind-tunnel test-section geometric configuration as for the present investigation have been compared with flight test results. This comparison indicates that the wind-tunnel drag characteristics at Mach numbers greater than 0.99 are questionable. Therefore, no drag data above this Mach number are included herein.

PRESENTATION OF RESULTS

The results of this investigation are presented in the following figures:

	Figure
Longitudinal aerodynamic characteristics:	
Longitudinal aerodynamic characteristics with type I transition; $\beta = 0^{\circ}$	6
Longitudinal aerodynamic characteristics with types I and II transition; $\beta = 0^{\circ}$	7
Effect of horizontal-tail deflections on longitudinal aerodynamic characteristics at high angles of attack; transition type II, $\beta = 0^{\circ}$	8
Variation of longitudinal aerodynamic characteristics with Mach number; $\beta = 0^{\circ}$, $\delta_h = -1.0^{\circ}$	9
Effect of sideslip on longitudinal aerodynamic characteristics; transition type II, $\delta_h = -1.0^{\circ}$	10

RESULTS AND DISCUSSION

Longitudinal Aerodynamic Characteristics

Lift characteristics.- As shown by the data presented in figures 6 and 7, the lift curves are nearly linear to a lift coefficient of approximately 0.40, at which point the lift-curve slopes decrease probably because of progressive wing tip and trailing-edge separation. The variation of lift-curve slope with Mach number is presented in figure 9(d) for a horizontal-tail deflection of -1.0°. These slopes, measured at the design cruise lift coefficient of 0.40, increase with Mach number to a maximum value at $M = 1.00$. The rearward transition location (type I), which was used to obtain the performance data at Mach numbers of 0.95 and above, increased the lift-curve slopes at Mach numbers above 0.95.

The data for the high angle-of-attack range, obtained with the offset sting arrangement shown in figure 1(d), are presented in figure 8. These data show a significant loss of lift at angles of attack between 18° and 20°. It is conjectured that the outboard region of the wing has stalled at these angles of attack and that the inboard region of the wing and the glove continue to produce lift at the higher angles of attack.

Pitching-moment characteristics.- The pitching-moment characteristics presented in figures 6 and 7 show the model to be longitudinally stable through the cruise lift coefficient and Mach number range. Pitchup and static longitudinal instability are noted at the higher lift coefficients for all horizontal-tail deflection angles for which data were obtained. A rapid degradation in static longitudinal stability with decreasing Mach numbers occurs for Mach numbers below 0.95.

The data for the high angle-of-attack range (fig. 8) show that the horizontal tail remained effective in providing pitch increments over the angle-of-attack range investigated for horizontal-tail deflections up to $+5^{\circ}$. The higher tail deflections indicate reduced control effectiveness probably caused by flow separation on the horizontal tail. As was previously discussed, the break in the pitching-moment curves is mainly associated with stalling of the outboard region of the wing, as indicated by the tail-off data.

The summary of the longitudinal stability characteristics, measured at the design cruise lift coefficient of 0.40, is presented in figure 9(c) for a horizontal-tail deflection of -1.0°. Although the static margin increases with Mach number $\left(\text{more negative } C_{m_{C_L}}\right)$, the associated trim drag penalties are reduced by the increasing values of $C_{m,o}$. With the rearward transition (type I), there is a large increase in static margin and less positive $C_{m,o}$, as would be expected with the shock in a more rearward location.

Drag characteristics.- The variation of the drag coefficient with Mach number, measured at the design cruise lift coefficient of 0.40 is presented in figure 9(b) for a horizontal-tail deflection of -1.0°. A drag-divergence Mach number above 0.99 is indicated by the data $\left(\text{drag-divergence Mach number being defined as the Mach number at which } \frac{\partial C_D}{\partial M} = 0.1\right)$. The data presented in figure 9(a) support this view, as there is little change in the drag-due-to-lift parameter and no rapid increase in the effective zero-lift drag. However, because the drag data at the higher Mach numbers (above 0.99) were considered to be questionable, the exact drag-divergence Mach number could not be determined.

Lateral-Directional Aerodynamic Characteristics

Figure 10 presents the effects of sideslip angle on the longitudinal aerodynamic characteristics, referenced to the stability axis system (fig. 1(a)). Little effect is noted for a sideslip angle of 2.5°. However, a sideslip angle of 5.0° results in the pitching moments becoming more negative with little change in the curve shape. Sideslip had little effect on the lift characteristics.

The lateral-directional aerodynamic characteristics are presented in figures 11 and 12 and are summarized in figure 13. These data show that the complete model was directionally stable at all Mach numbers and angles of attack at which data were obtained. Removing the horizontal tail decreased the directional stability, and the configuration with the vertical tail removed was directionally unstable.

The data of figure 13 show that the model was laterally stable over the angle-of-attack range investigated at the lower Mach numbers. (See figs. 13(a) and 13(b).) However, as the Mach number increased, the lateral stability became nonlinear with angle of attack and the model became unstable at small positive angles and between approximately 4° to 6° angle of attack (figs. 13(d) and 13(e)), but remained stable at the angle of attack required for cruise. Removal of the horizontal and vertical tails decreased the lateral stability at all test conditions.

CONCLUSIONS

Wind-tunnel tests to determine the static aerodynamic characteristics of a transport configuration designed to cruise at near-sonic speeds have indicated the following conclusions:

1. The configuration exhibits a sufficiently high drag-divergence Mach number to cruise at Mach numbers approaching 1.00.

2. The configuration is longitudinally stable in the cruise lift-coefficient and Mach number range, but at higher lift coefficients pitches up and becomes unstable. A rapid degradation in stability occurs with decreasing Mach number for Mach numbers below 0.95.

3. Although the static margin increases significantly with Mach number, excessive trim drag penalties are reduced by an associated increase in the zero-lift pitching moment.

4. The complete configuration was directionally stable at all test conditions and was laterally stable in the angle-of-attack range for cruise.

Langley Research Center,
National Aeronautics and Space Administration,
Hampton, Va., July 5, 1972.

REFERENCES

1. Whitcomb, Richard T.; and Clark, Larry R.: An Airfoil Shape for Efficient Flight at Supercritical Mach Numbers. NASA TM X-1109, 1965.

2. Whitcomb, Richard T.; and Blackwell, James A., Jr.: Status of Research on a Supercritical Wing. Conference on Aircraft Aerodynamics, NASA SP-124, 1966, pp. 367-381.

3. Harris, Charles D.: Wind-Tunnel Investigation of Effects of Trailing-Edge Geometry on a NASA Supercritical Airfoil Section. NASA TM X-2336, 1971.

4. Harris, Charles D.; and Blackwell, James A., Jr.: Wind-Tunnel Investigation of Effects of Rear Upper Surface Modification on an NASA Supercritical Airfoil. NASA TM X-2454, 1972.

5. Bartlett, Dennis W.; and Re, Richard J.: Wind-Tunnel Investigation of Basic Aerodynamic Characteristics of a Supercritical-Wing Research Airplane Configuration. NASA TM X-2470, 1972.

6. Harris, Charles D.: Wind-Tunnel Measurements of Aerodynamic Load Distribution of an NASA Supercritical-Wing Research Airplane Configuration. NASA TM X-2469, 1972.

7. Harris, Charles D.; and Bartlett, Dennis W.: Wind-Tunnel Investigation of Effects of Underwing Leading-Edge Vortex Generators on a Supercritical-Wing Research Airplane Configuration. NASA TM X-2471, 1972.

8. Schaefer, William T., Jr.: Characteristics of Major Active Wind Tunnels of the Langley Research Center. NASA TM X-1130, 1965.

9. Davis, Don D., Jr.; and Moore, Dewey: Analytical Study of Blockage- and Lift-Interference Corrections for Slotted Tunnels Obtained by the Substitution of an Equivalent Homogeneous Boundary for the Discrete Slots. NACA RM L53E07b, 1953.

10. Goethert, Bernhard H.: Transonic Wind Tunnel Testing. AGARDograph No. 49, Pergamon Press, 1961.

11. Loving, Donald L.: Wind-Tunnel—Flight Correlation of Shock-Induced Separated Flow. NASA TN D-3580, 1966.

12. Blackwell, James A., Jr.: Preliminary Study of Effects of Reynolds Number and Boundary-Layer Transition on Location of Shock-Induced Separation. NASA TN D-5003, 1969.

13. Braslow, Albert L.; and Knox, Eugene C.: Simplified Method for Determination of Critical Height of Distributed Roughness Particles for Boundary-Layer Transition at Mach Numbers From 0 to 5.0. NACA TN 4363, 1958.

14. Loving, Donald L.; and Katzoff, S.: The Fluorescent-Oil Film Method and Other Techniques for Boundary-Layer Flow Visualization. NASA MEMO 3-17-59L, 1959.

15. Schlichting, Hermann (J. Kestin, transl.): Boundary-Layer Theory. Sixth ed., McGraw-Hill Book Co., 1968.

16. Nash, J. F.; and Macdonald, A. G. J.: The Calculation of Momentum Thickness in a Turbulent Boundary Layer at Mach Numbers up to Unity. C.P. No. 963, Brit. A.R.C., 1967.

17. Nash, J. F.; and Macdonald, A. G. J.: A Turbulent Skin-Friction Law for Use at Subsonic and Transonic Speeds. C.P. No. 948, Brit. A.R.C., 1967.

18. Lee, George; and Summers, James L.: Effects of Sting-Support Interference on the Drag of an Ogive-Cylinder Body With and Without a Boattail at 0.6 to 1.4 Mach Number. NACA RM A57I09, 1957.

19. Wright, Ray H.; and Barger, Raymond L.: Wind-Tunnel Lift Interference on Sweptback Wings in Rectangular Test Sections With Slotted Top and Bottom Walls. NASA TR R-241, 1966.

TABLE I.- WING AIRFOIL COORDINATES

Δx/c	$\frac{y}{b/2} = 0.1395$ c = 46.068 cm (18.137 in.) x = 41.252 cm (16.241 in.)		$\frac{y}{b/2} = 0.1860$ c = 35.639 cm (14.031 in.) x = 51.173 cm (20.147 in.)		$\frac{y}{b/2} = 0.2791$ c = 23.604 cm (9.293 in.) x = 63.701 cm (25.079 in.)		$\frac{y}{b/2} = 0.3721$ c = 19.126 cm (7.530 in.) x = 70.495 cm (27.754 in.)		$\frac{y}{b/2} = 0.4651$ c = 17.605 cm (6.931 in.) x = 75.565 cm (29.750 in.)	
	z/c		z/c		z/c		z/c		z/c	
	Upper surface	Lower surface	Upper surface	Lower surface	Upper surface	Lower surface	Upper surface	Lower surface	Upper surface	Lower surface
0										
.0025	-0.0725	-0.0869	-0.1109	-0.1255	-0.1995	-0.2159	-0.2688	-0.2827	-0.3044	-0.3204
.0050	-.0721	-.0894	-.1084	-.1279	-.1962	-.2193	-.2659	-.2857	-.3014	-.3233
.0100	-.0673	-.0925	-.1048	-.1315	-.1919	-.2233	-.2614	-.2896	-.2976	-.3274
.0200	-.0638	-.0967	-.1003	-.1365	-.1862	-.2289	-.2560	-.2948	-.2925	-.3320
.0300	-.0612	-.1002	-.0971	-.1403	-.1824	-.2328	-.2525	-.2984	-.2891	-.3352
.0400	-.0590	-.1030	-.0945	-.1435	-.1794	-.2360	-.2497	-.3011	-.2867	-.3375
.0500	-.0573	-.1056	-.0924	-.1460	-.1771	-.2386	-.2474	-.3032	-.2844	-.3393
.1000	-.0511	-.1148	-.0862	-.1557	-.1706	-.2474	-.2406	-.3101	-.2774	-.3454
.1500	-.0474	-.1214	-.0830	-.1630	-.1671	-.2528	-.2361	-.3139	-.2731	-.3486
.2000	-.0455	-.1271	-.0810	-.1686	-.1646	-.2568	-.2327	-.3163	-.2699	-.3502
.2500	-.0449	-.1319	-.0798	-.1733	-.1635	-.2590	-.2304	-.3177	-.2678	-.3507
.3000	-.0454	-.1358	-.0797	-.1768	-.1629	-.2602	-.2290	-.3181	-.2661	-.3507
.3500	-.0465	-.1391	-.0806	-.1792	-.1633	-.2603	-.2284	-.3178	-.2648	-.3500
.4000	-.0482	-.1415	-.0823	-.1803	-.1642	-.2594	-.2286	-.3167	-.2639	-.3486
.4500	-.0508	-.1429	-.0847	-.1802	-.1657	-.2576	-.2290	-.3149	-.2635	-.3466
.5000	-.0539	-.1431	-.0875	-.1790	-.1677	-.2549	-.2296	-.3122	-.2633	-.3434
.5500	-.0575	-.1420	-.0912	-.1770	-.1701	-.2512	-.2305	-.3085	-.2633	-.3395
.6000	-.0617	-.1400	-.0954	-.1737	-.1730	-.2462	-.2317	-.3032	-.2639	-.3343
.6500	-.0667	-.1370	-.0999	-.1693	-.1760	-.2405	-.2333	-.2964	-.2649	-.3275
.7000	-.0724	-.1329	-.1049	-.1638	-.1796	-.2345	-.2353	-.2884	-.2662	-.3187
.7500	-.0784	-.1275	-.1103	-.1579	-.1835	-.2278	-.2380	-.2798	-.2681	-.3092
.8000	-.0845	-.1218	-.1158	-.1519	-.1878	-.2210	-.2410	-.2717	-.2707	-.3004
.8500	-.0910	-.1166	-.1216	-.1467	-.1923	-.2152	-.2450	-.2657	-.2744	-.2942
.9000	-.0978	-.1134	-.1276	-.1433	-.1974	-.2118	-.2497	-.2631	-.2793	-.2916
.9500	-.1049	-.1131	-.1341	-.1433	-.2027	-.2120	-.2551	-.2644	-.2861	-.2955
.9700	-.1079	-.1142	-.1368	-.1443	-.2052	-.2128	-.2578	-.2667	-.2896	-.2984
.9800	-.1093	-.1148	-.1382	-.1448	-.2064	-.2134	-.2592	-.2681	-.2916	-.3008
.9900	-.1110	-.1153	-.1397	-.1457	-.2079	-.2141	-.2610	-.2693	-.2939	-.3030
.9950	-.1113	-.1152	-.1406	-.1460	-.2087	-.2147	-.2618	-.2701	-.2952	-.3036
.9975	-.1114	-.1149	-.1410	-.1462	-.2090	-.2146	-.2624	-.2701	-.2961	-.3040
1.0000										

TABLE I.- WING AIRFOIL COORDINATES – Concluded

$\Delta x/c$	$\frac{y}{b/2} = 0.5581$ c = 16.248 cm (6.397 in.) x = 80.513 cm (31.698 in.)		$\frac{y}{b/2} = 0.6512$ c = 14.836 cm (5.841 in.) x = 85.474 cm (33.651 in.)		$\frac{y}{b/2} = 0.7442$ c = 13.419 cm (5.283 in.) x = 90.442 cm (35.607 in.)		$\frac{y}{b/2} = 0.8372$ c = 12.014 cm (4.730 in.) x = 95.410 cm (37.563 in.)		$\frac{y}{b/2} = 0.9302$ c = 10.589 cm (4.169 in.) x = 100.396 cm (39.526 in.)	
	z/c		z/c		z/c		z/c		z/c	
	Upper surface	Lower surface	Upper surface	Lower surface	Upper surface	Lower surface	Upper surface	Lower surface	Upper surface	Lower surface
0										
.0025	-0.3439	-0.3595	-0.3917	-0.4054	-0.4488	-0.4613	-0.5182	-0.5313	-0.6097	-0.6213
.0050	-.3408	-.3622	-.3883	-.4081	-.4454	-.4643	-.5150	-.5334	-.6076	-.6234
.0100	-.3367	-.3658	-.3840	-.4121	-.4414	-.4681	-.5112	-.5370	-.6037	-.6272
.0200	-.3317	-.3705	-.3792	-.4165	-.4365	-.4725	-.5061	-.5412	-.5980	-.6311
.0300	-.3283	-.3733	-.3760	-.4194	-.4331	-.4751	-.5027	-.5440	-.5939	-.6332
.0400	-.3258	-.3755	-.3734	-.4215	-.4306	-.4770	-.5000	-.5457	-.5905	-.6349
.0500	-.3237	-.3772	-.3715	-.4230	-.4285	-.4787	-.4979	-.5469	-.5882	-.6359
.1000	-.3166	-.3827	-.3643	-.4280	-.4212	-.4825	-.4905	-.5503	-.5788	-.6378
.1500	-.3119	-.3855	-.3594	-.4301	-.4162	-.4840	-.4850	-.5513	-.5718	-.6371
.2000	-.3084	-.3866	-.3554	-.4307	-.4121	-.4842	-.4803	-.5510	-.5661	-.6354
.2500	-.3056	-.3869	-.3523	-.4304	-.4083	-.4836	-.4763	-.5495	-.5608	-.6328
.3000	-.3034	-.3864	-.3496	-.4295	-.4051	-.4823	-.4723	-.5476	-.5562	-.6294
.3500	-.3019	-.3852	-.3474	-.4278	-.4022	-.4802	-.4689	-.5446	-.5517	-.6256
.4000	-.3006	-.3833	-.3455	-.4258	-.3996	-.4778	-.4655	-.5412	-.5476	-.6213
.4500	-.2997	-.3810	-.3439	-.4230	-.3973	-.4745	-.4624	-.5372	-.5438	-.6162
.5000	-.2990	-.3777	-.3427	-.4194	-.3956	-.4708	-.4594	-.5323	-.5402	-.6105
.5500	-.2987	-.3735	-.3417	-.4150	-.3941	-.4658	-.4569	-.5264	-.5368	-.6037
.6000	-.2987	-.3681	-.3414	-.4092	-.3926	-.4596	-.4543	-.5192	-.5339	-.5961
.6500	-.2992	-.3610	-.3412	-.4018	-.3918	-.4518	-.4522	-.5104	-.5315	-.5870
.7000	-.3000	-.3520	-.3414	-.3926	-.3914	-.4422	-.4505	-.4998	-.5291	-.5764
.7500	-.3014	-.3422	-.3422	-.3826	-.3916	-.4321	-.4495	-.4886	-.5275	-.5651
.8000	-.3036	-.3334	-.3439	-.3737	-.3922	-.4229	-.4493	-.4784	-.5267	-.5546
.8500	-.3070	-.3269	-.3469	-.3671	-.3945	-.4159	-.4499	-.4702	-.5272	-.5469
.9000	-.3119	-.3239	-.3515	-.3643	-.3979	-.4126	-.4524	-.4662	-.5296	-.5440
.9500	-.3191	-.3272	-.3582	-.3676	-.4037	-.4153	-.4575	-.4683	-.5344	-.5467
.9700	-.3227	-.3311	-.3618	-.3710	-.4075	-.4179	-.4609	-.4710	-.5375	-.5493
.9800	-.3247	-.3331	-.3638	-.3732	-.4096	-.4200	-.4630	-.4725	-.5397	-.5505
.9900	-.3272	-.3356	-.3664	-.3751	-.4119	-.4219	-.4653	-.4744	-.5426	-.5519
.9950	-.3284	-.3372	-.3679	-.3763	-.4134	-.4227	-.4670	-.4755	-.5440	-.5524
.9975	-.3297	-.3375	-.3688	-.3766	-.4143	-.4229	-.4683	-.4757	-.5452	-.5524
1.0000										

TABLE II.- FUSELAGE FOREBODY RADII

[Center of radii, 0.457 cm (0.180 in.) below reference center line]

Upper and lower			
Longitudinal station		Radius	
cm	in.	cm	in.
0	0	0	0
2.54	1.00	2.769	1.090
5.08	2.00	3.658	1.440
7.62	3.00	4.293	1.690
10.16	4.00	4.801	1.890
12.70	5.00	5.232	2.060
15.24	6.00	5.588	2.200
17.78	7.00	5.893	2.320
20.32	8.00	6.172	2.430
22.86	9.00	6.426	2.530
25.40	10.00	6.655	2.620
27.94	11.00	6.858	2.700
30.48	12.00	7.036	2.770
33.02	13.00	7.188	2.830
35.56	14.00	7.315	2.880
38.10	15.00	7.417	2.920
40.64	16.00	7.468	2.940
43.18	17.00	7.468	2.940
45.72	18.00	7.442	2.930
48.26	19.00	7.391	2.910
50.80	20.00	7.315	2.880
53.34	21.00	7.188	2.830
55.88	22.00	7.036	2.770
58.42	23.00	6.833	2.690
60.96	24.00	6.579	2.590

Upper only			
Longitudinal station		Radius	
cm	in.	cm	in.
63.50	25.00	6.274	2.470
66.04	26.00	5.994	2.360
68.58	27.00	5.766	2.270
71.12	28.00	5.563	2.190
73.66	29.00	5.436	2.140
76.20	30.00	5.385	2.120
78.74	31.00	5.410	2.130
81.28	32.00	5.486	2.160
83.82	33.00	5.613	2.210
86.36	34.00	5.791	2.280
88.90	35.00	5.969	2.350
91.44	36.00	6.147	2.420
93.98	37.00	6.325	2.490
96.52	38.00	6.502	2.560
99.06	39.00	6.579	2.590

TABLE III.- COORDINATES OF FLOW-THROUGH NACELLES

[Inside diameter, 4.928 cm (1.940 in.); x = 98.933 cm (38.950 in.)]

Δx, cm (in.)	Radius, cm (in.)		
	Top	Side	Bottom
0 (0)	2.489 (0.980)		
.254 (.100)	2.540 (1.000)		
.635 (.250)	2.616 (1.030)	2.489 (0.980)	
1.270 (.500)	2.692 (1.060)	2.667 (1.050)	
1.397 (.550)	2.718 (1.070)	2.692 (1.060)	2.489 (0.980)
2.540 (1.000)	2.870 (1.130)	2.845 (1.120)	2.819 (1.110)
3.810 (1.500)	2.972 (1.170)	2.972 (1.170)	2.972 (1.170)
5.080 (2.000)	3.073 (1.210)	3.073 (1.210)	3.073 (1.210)
6.350 (2.500)	3.175 (1.250)	3.175 (1.250)	3.175 (1.250)
7.620 (3.000)	3.200 (1.260)	3.200 (1.260)	3.200 (1.260)
8.890 (3.500)	3.226 (1.270)	3.226 (1.270)	3.226 (1.270)
10.160 (4.000)	3.200 (1.260)	3.200 (1.260)	3.200 (1.260)
11.430 (4.500)	3.175 (1.250)	3.175 (1.250)	3.175 (1.250)
12.700 (5.000)	3.099 (1.220)	3.099 (1.220)	3.099 (1.220)
13.970 (5.500)	2.997 (1.180)	2.997 (1.180)	2.997 (1.180)
15.240 (6.000)	2.870 (1.130)	2.870 (1.130)	2.870 (1.130)
16.510 (6.500)	2.718 (1.070)	2.718 (1.070)	2.718 (1.070)
17.780 (7.000)	2.591 (1.020)	2.591 (1.020)	2.591 (1.020)
19.050 (7.500)	2.464 (.970)	2.464 (.970)	2.464 (.970)

TABLE IV.- MIDDLE-ENGINE AND VERTICAL-TAIL AIRFOIL COORDINATES

$\Delta x/c$	z = 5.944 cm (2.340 in.) c = 29.347 cm (11.554 in.) x = 105.547 cm (41.554 in.)	z = 7.620 cm (3.000 in.) c = 31.892 cm (12.556 in.) x = 104.148 cm (41.003 in.)	z = 10.160 cm (4.000 in.) c = 33.254 cm (13.092 in.) x = 104.785 cm (41.254 in.)	z = 12.446 cm (4.900 in.) c = 34.643 cm (13.639 in.) x = 105.519 cm (41.543 in.)	z = 12.700 cm (5.000 in.) c = 33.104 cm (13.033 in.) x = 106.832 cm (42.060 in.)
	y/c	y/c	y/c	y/c	y/c
0					
.0025	0.0010	0.0014	0.0022	0.0007	0.0015
.0050	.0011	.0018	.0027	.0011	.0021
.0100	.0016	.0025	.0036	.0018	.0030
.0200	.0019	.0041	.0048	.0030	.0042
.0300	.0022	.0055	.0060	.0040	.0052
.0400	.0025	.0068	.0073	.0050	.0064
.0500	.0029	.0080	.0086	.0061	.0072
.1000	.0090	.0145	.0151	.0110	.0116
.1500	.0172	.0213	.0212	.0154	.0154
.2000	.0271	.0283	.0273	.0197	.0206
.2500	.0377	.0355	.0334	.0240	.0253
.3000	.0481	.0428	.0391	.0283	.0298
.3500	.0561	.0496	.0440	.0323	.0341
.4000	.0606	.0546	.0473	.0357	.0376
.4500	.0629	.0570	.0490	.0385	.0401
.5000	.0630	.0573	.0494	.0401	.0417
.5500	.0616	.0566	.0490	.0409	.0421
.6000	.0603	.0540	.0471	.0404	.0414
.6500	.0546	.0502	.0440	.0386	.0396
.7000	.0499	.0457	.0399	.0361	.0368
.7500	.0447	.0405	.0351	.0327	.0331
.8000	.0383	.0343	.0299	.0282	.0281
.8500	.0306	.0272	.0244	.0224	.0224
.9000	.0223	.0196	.0181	.0162	.0163
.9500	.0134	.0121	.0112	.0098	.0098
.9700	.0101	.0092	.0083	.0072	.0072
.9800	.0085	.0070	.0067	.0056	.0058
.9900	.0067	.0059	.0050	.0040	.0041
.9950	.0055	.0049	.0040	.0032	.0032
.9975	.0048	.0043	.0035	.0027	.0028
1.0000	.0042	.0037	.0030	.0022	.0022

CONFIDENTIAL

TABLE IV.- MIDDLE-ENGINE AND VERTICAL-TAIL AIRFOIL COORDINATES – Concluded

Δx/c	z = 15.240 cm (6.000 in.) c = 22.012 cm (8.666 in.) x = 119.819 cm (47.173 in.)	z = 17.780 cm (7.000 in.) c = 20.345 cm (8.010 in.) x = 123.386 cm (48.577 in.)	z = 20.320 cm (8.000 in.) c = 19.167 cm (7.546 in.) x = 126.426 cm (49.774 in.)	z = 21.209 cm (8.350 in.) c = 18.684 cm (7.356 in.) x = 127.485 cm (50.191 in.)	z = 23.495 cm (9.250 in.) c = 16.523 cm (6.506 in.) x = 130.211 cm (51.264 in.)
	y/c	y/c	y/c	y/c	y/c
0					
.0025	0.0073	0.0080	0.0073	0.0076	0.0091
.0050	.0105	.0123	.0103	.0107	.0126
.0100	.0145	.0155	.0144	.0147	.0178
.0200	.0201	.0210	.0197	.0201	.0248
.0300	.0242	.0247	.0235	.0241	.0301
.0400	.0275	.0276	.0264	.0271	.0347
.0500	.0302	.0300	.0288	.0298	.0387
.1000	.0398	.0382	.0379	.0396	.0497
.1500	.0455	.0436	.0443	.0458	.0533
.2000	.0493	.0473	.0482	.0484	.0550
.2500	.0520	.0499	.0502	.0503	.0547
.3000	.0539	.0513	.0502	.0504	.0533
.3500	.0548	.0517	.0497	.0500	.0513
.4000	.0546	.0509	.0482	.0479	.0490
.4500	.0538	.0489	.0455	.0461	.0469
.5000	.0519	.0469	.0437	.0426	.0438
.5500	.0495	.0439	.0403	.0390	.0401
.6000	.0458	.0404	.0360	.0355	.0372
.6500	.0418	.0363	.0337	.0311	.0335
.7000	.0369	.0321	.0278	.0272	.0293
.7500	.0317	.0276	.0237	.0231	.0252
.8000	.0265	.0230	.0197	.0190	.0208
.8500	.0209	.0180	.0154	.0151	.0161
.9000	.0151	.0131	.0110	.0106	.0114
.9500	.0095	.0079	.0062	.0060	.0068
.9700	.0068	.0054	.0042	.0038	.0048
.9800	.0055	.0044	.0030	.0026	.0034
.9900	.0040	.0030	.0016	.0015	.0020
.9950	.0031	.0021	.0009	.0008	.0012
.9975	.0027	.0017	.0005	.0005	.0009
1.0000	.0022	.0012	.0001	.0003	.0005

TABLE V.- HORIZONTAL-TAIL AIRFOIL COORDINATES

Δx/c	y = 1.080 cm (0.425 in.) c = 16.441 cm (6.473 in.) x = 130.947 cm (51.554 in.)		y = 2.540 cm (1.000 in.) c = 15.598 cm (6.141 in.) x = 132.380 cm (52.118 in.)		y = 5.080 cm (2.000 in.) c = 14.178 cm (5.582 in.) x = 134.917 cm (53.117 in.)		y = 7.620 cm (3.000 in.) c = 12.764 cm (5.025 in.) x = 137.467 cm (54.121 in.)	
	z/c		z/c		z/c		z/c	
	Upper surface	Lower surface	Upper surface	Lower surface	Upper surface	Lower surface	Upper surface	Lower surface
0								
.0025	1.4026	1.3876	1.4696	1.4561	1.5991	1.5885	1.7590	1.7485
.0050	1.4049	1.3845	1.4717	1.4533	1.6010	1.5862	1.7604	1.7467
.0100	1.4078	1.3803	1.4748	1.4493	1.6037	1.5828	1.7626	1.7437
.0200	1.4114	1.3743	1.4778	1.4431	1.6070	1.5772	1.7652	1.7397
.0300	1.4117	1.3694	1.4792	1.4387	1.6086	1.5735	1.7666	1.7365
.0400	1.4122	1.3655	1.4797	1.4345	1.6095	1.5702	1.7676	1.7339
.0500	1.4122	1.3623	1.4799	1.4312	1.6098	1.5670	1.7682	1.7311
.1000	1.4105	1.3488	1.4786	1.4180	1.6093	1.5554	1.7684	1.7214
.1500	1.4078	1.3376	1.4763	1.4082	1.6075	1.5469	1.7666	1.7142
.2000	1.4049	1.3280	1.4735	1.4012	1.6050	1.5405	1.7640	1.7075
.2500	1.4017	1.3215	1.4704	1.3954	1.6019	1.5349	1.7608	1.7027
.3000	1.3983	1.3167	1.4669	1.3902	1.5982	1.5297	1.7572	1.6979
.3500	1.3944	1.3130	1.4631	1.3856	1.5942	1.5262	1.7532	1.6937
.4000	1.3902	1.3097	1.4586	1.3828	1.5896	1.5224	1.7487	1.6896
.4500	1.3853	1.3070	1.4538	1.3802	1.5846	1.5195	1.7441	1.6862
.5000	1.3802	1.3056	1.4488	1.3783	1.5794	1.5172	1.7389	1.6832
.5500	1.3748	1.3047	1.4433	1.3770	1.5740	1.5154	1.7337	1.6806
.6000	1.3691	1.3037	1.4374	1.3763	1.5684	1.5140	1.7284	1.6776
.6500	1.3630	1.3040	1.4312	1.3758	1.5625	1.5125	1.7230	1.6756
.7000	1.3569	1.3045	1.4245	1.3755	1.5564	1.5115	1.7172	1.6732
.7500	1.3504	1.3051	1.4178	1.3755	1.5503	1.5102	1.7108	1.6712
.8000	1.3437	1.3057	1.4112	1.3757	1.5435	1.5091	1.7041	1.6697
.8500	1.3369	1.3065	1.4042	1.3758	1.5364	1.5082	1.6969	1.6685
.9000	1.3300	1.3071	1.3968	1.3760	1.5292	1.5077	1.6898	1.6677
.9500	1.3224	1.3076	1.3885	1.3758	1.5213	1.5073	1.6818	1.6667
.9700	1.3189	1.3077	1.3851	1.3758	1.5181	1.5073	1.6780	1.6665
.9800	1.3167	1.3082	1.3833	1.3760	1.5165	1.5073	1.6760	1.6667
.9900	1.3145	1.3088	1.3812	1.3765	1.5142	1.5075	1.6738	1.6671
.9950	1.3133	1.3091	1.3799	1.3768	1.5125	1.5079	1.6722	1.6673
.9975	1.3084	1.3093	1.3793	1.3770	1.5115	1.5081	1.6712	1.6675
1.0000	1.3119	1.3096	1.3786	1.3773	1.5106	1.5082	1.6702	1.6677

TABLE V.- HORIZONTAL-TAIL AIRFOIL COORDINATES – Concluded

$\Delta x/c$	y = 10.160 cm (4.000 in.) c = 11.346 cm (4.467 in.) x = 139.984 cm (55.112 in.)		y = 12.700 cm (5.000 in.) c = 9.898 cm (3.897 in.) x = 142.517 cm (56.109 in.)		y = 15.240 cm (6.000 in.) c = 8.468 cm (3.334 in.) x = 145.037 cm (57.101 in.)		y = 17.361 cm (6.835 in.) c = 7.244 cm (2.852 in.) x = 147.173 cm (57.942 in.)	
	z/c		z/c		z/c		z/c	
	Upper surface	Lower surface	Upper surface	Lower surface	Upper surface	Lower surface	Upper surface	Lower surface
0								
.0025	1.9590	1.9494	2.2245	2.2132	2.5741	2.5642	2.9842	2.9734
.0050	1.9608	1.9474	2.2258	2.2117	2.5759	2.5618	2.9860	2.9716
.0100	1.9631	1.9447	2.2276	2.2091	2.5783	2.5585	2.9884	2.9695
.0200	1.9653	1.9407	2.2304	2.2050	2.5810	2.5546	2.9909	2.9649
.0300	1.9664	1.9369	2.2320	2.2017	2.5822	2.5513	2.9923	2.9611
.0400	1.9673	1.9337	2.2327	2.1989	2.5831	2.5486	2.9930	2.9583
.0500	1.9680	1.9315	2.2333	2.1963	2.5837	2.5465	2.9940	2.9558
.1000	1.9687	1.9223	2.2338	2.1868	2.5855	2.5369	2.9961	2.9474
.1500	1.9673	1.9156	2.2248	2.1799	2.5846	2.5305	2.9947	2.9400
.2000	1.9649	1.9096	2.2302	2.1737	2.5822	2.5243	2.9954	2.9337
.2500	1.9617	1.9046	2.2271	2.1683	2.5789	2.5189	2.9895	2.9842
.3000	1.9581	1.8993	2.2235	2.1640	2.5753	2.5144	2.9860	2.9236
.3500	1.9546	1.8948	2.2197	2.1599	2.5714	2.5099	2.9814	2.9197
.4000	1.9503	1.8914	2.2156	2.1558	2.5675	2.5063	2.9765	2.9158
.4500	1.9452	1.8878	2.2112	2.1519	2.5627	2.5030	2.9719	2.9120
.5000	1.9405	1.8847	2.2061	2.1491	2.5570	2.4997	2.9674	2.9088
.5500	1.9355	1.8816	2.2012	2.1460	2.5525	2.4964	2.9621	2.9060
.6000	1.9299	1.8787	2.1960	2.1427	2.5474	2.4940	2.9569	2.9036
.6500	1.9243	1.8760	2.1904	2.1404	2.5420	2.4913	2.9520	2.9011
.7000	1.9187	1.8737	2.1848	2.1383	2.5360	2.4892	2.9464	2.8990
.7500	1.9127	1.8719	2.1789	2.1365	2.5303	2.4877	2.9400	2.8973
.8000	1.9062	1.8706	2.1722	2.1350	2.5237	2.4862	2.9341	2.8959
.8500	1.8990	1.8693	2.1655	2.1337	2.5171	2.4850	2.9278	2.8948
.9000	1.8919	1.8681	2.1583	2.1329	2.5102	2.4838	2.9215	2.8940
.9500	1.8838	1.8675	2.1504	2.1324	2.5024	2.4832	2.9130	2.8938
.9700	1.8802	1.8675	2.1468	2.1322	2.4985	2.4838	2.9109	2.8945
.9800	1.8780	1.8677	2.1447	2.1324	2.4964	2.4841	2.9085	2.8952
.9900	1.8751	1.8681	2.1414	2.1327	2.4940	2.4847	2.9043	2.8959
.9950	1.8735	1.8681	2.1396	2.1329	2.4922	2.4847	2.9022	2.8962
.9975	1.8726	1.8684	2.1388	2.1332	2.4910	2.4850	2.9015	2.8962
1.0000	1.8715	1.8684	2.1378	2.1334	2.4901	2.4850	2.9011	2.8966

TABLE VI.- ENVELOPE AREA DEVELOPMENT FOR ZERO LIFT

x/l	A/A_{max}	x/l	A/A_{max}
0	0	0.5307	0.970
.0050	.040	.5562	.950
.0094	.070	.5771	.930
.0193	.130	.6035	.900
.0404	.240	.6190	.880
.0606	.330	.6402	.850
.0807	.410	.6596	.820
.1002	.480	.6832	.780
.1217	.550	.6997	.750
.1385	.600	.7204	.710
.1606	.660	.7400	.670
.1810	.710	.7632	.620
.1989	.750	.7809	.580
.2185	.790	.7980	.540
.2403	.830	.8227	.480
.2587	.860	.8387	.440
.2793	.890	.8581	.390
.3217	.940	.8809	.330
.3440	.960	.9032	.270
.3573	.970	.9215	.220
.3731	.980	.9395	.170
.3938	.990	.9610	.110
.4400	1.000	.9787	.060
.4939	.990	1.0000	0
.5147	.980		

TABLE VII.- SUMMARY OF TEST CONDITIONS

M	q		R
	N/m^2	lb/ft^2	
0.25	4 309	90	0.91×10^6
.50	14 987	313	1.69
.80	35 910	750	2.73
.90	35 910	750	2.52
.95	35 910	750	2.44
.98	35 910	750	2.40
.99	35 910	750	2.38
.995	35 910	750	2.37
1.00	35 910	750	2.37
1.01	35 910	750	2.35

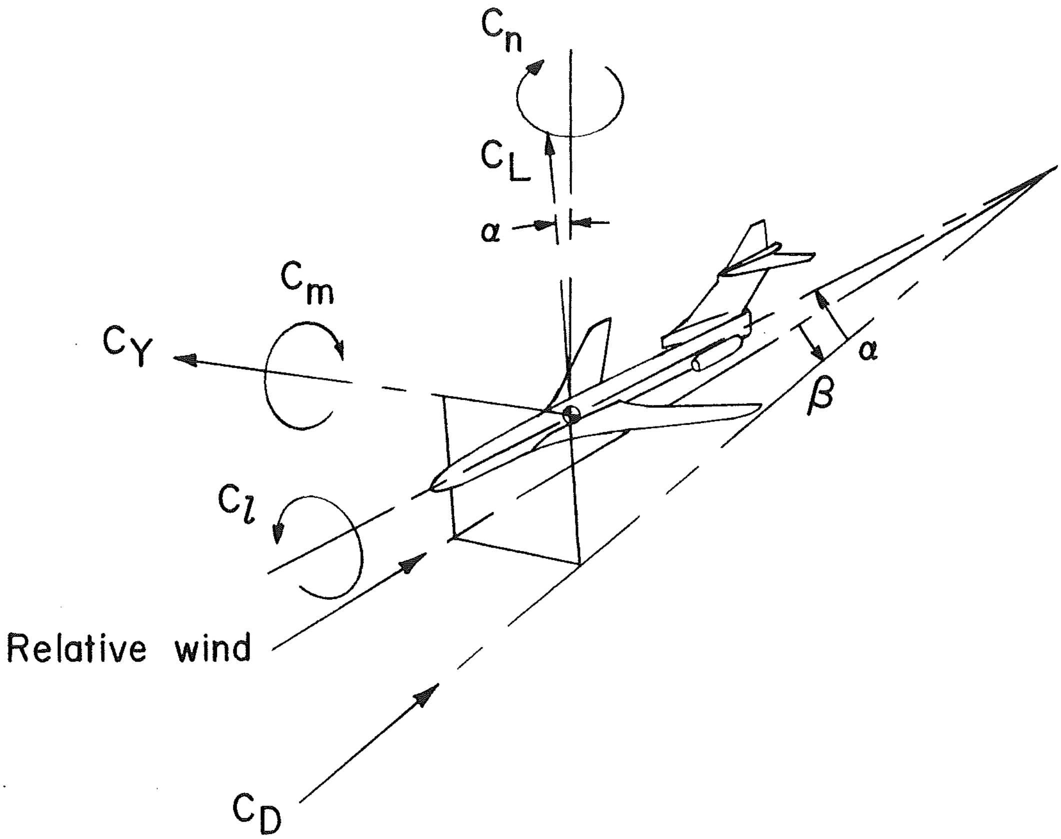

(a) Axis system. Positive values of forces, moments, and angles are indicated by arrows. Origin of stability axes has been displaced from moment reference center, for clarity.

Figure 1.- Axis system, model, tunnel geometry, and support-sting details. Dimensions are in centimeters, inches in parentheses.

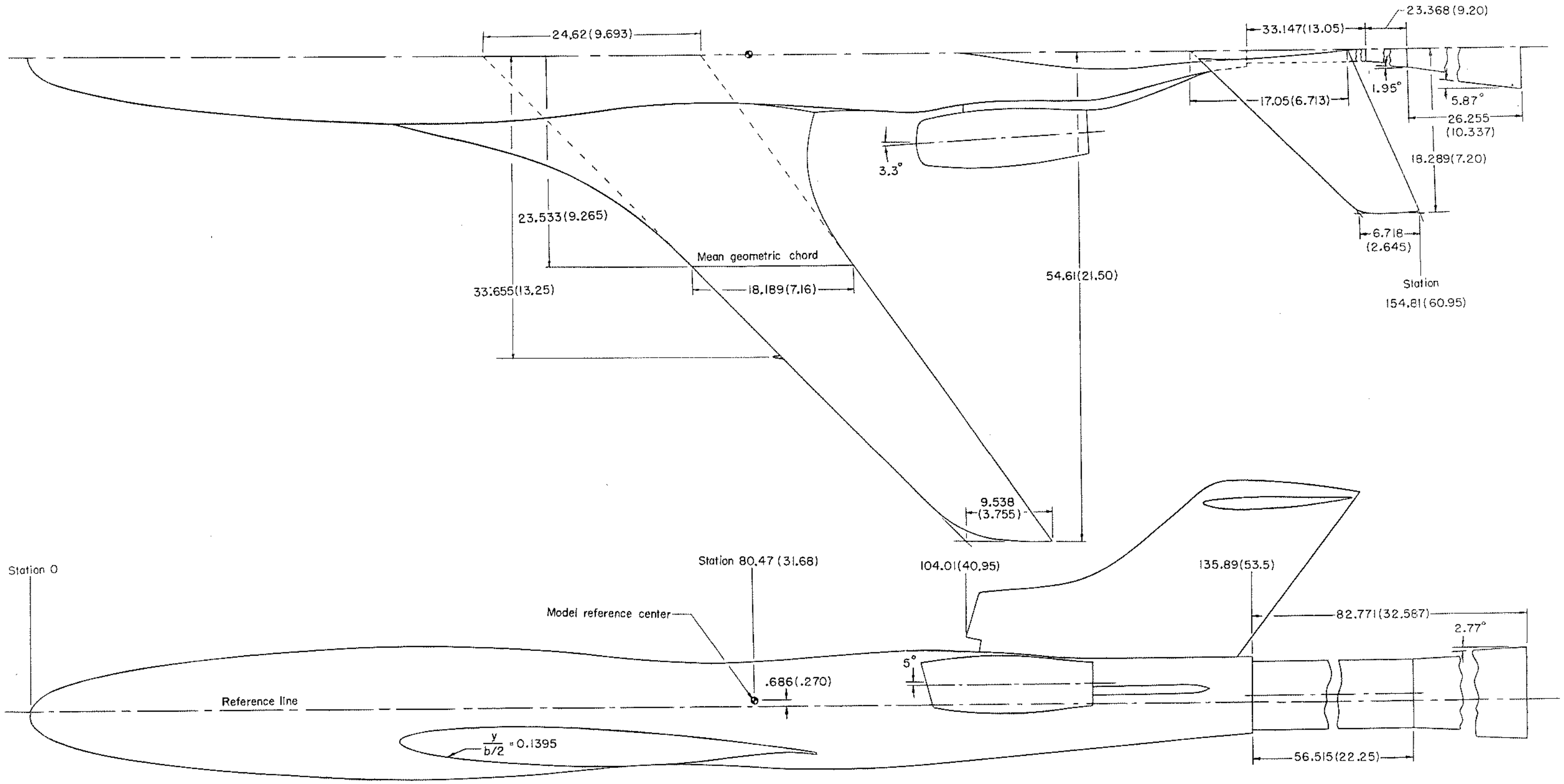

(b) General arrangement of model.

Figure 1.- Continued.

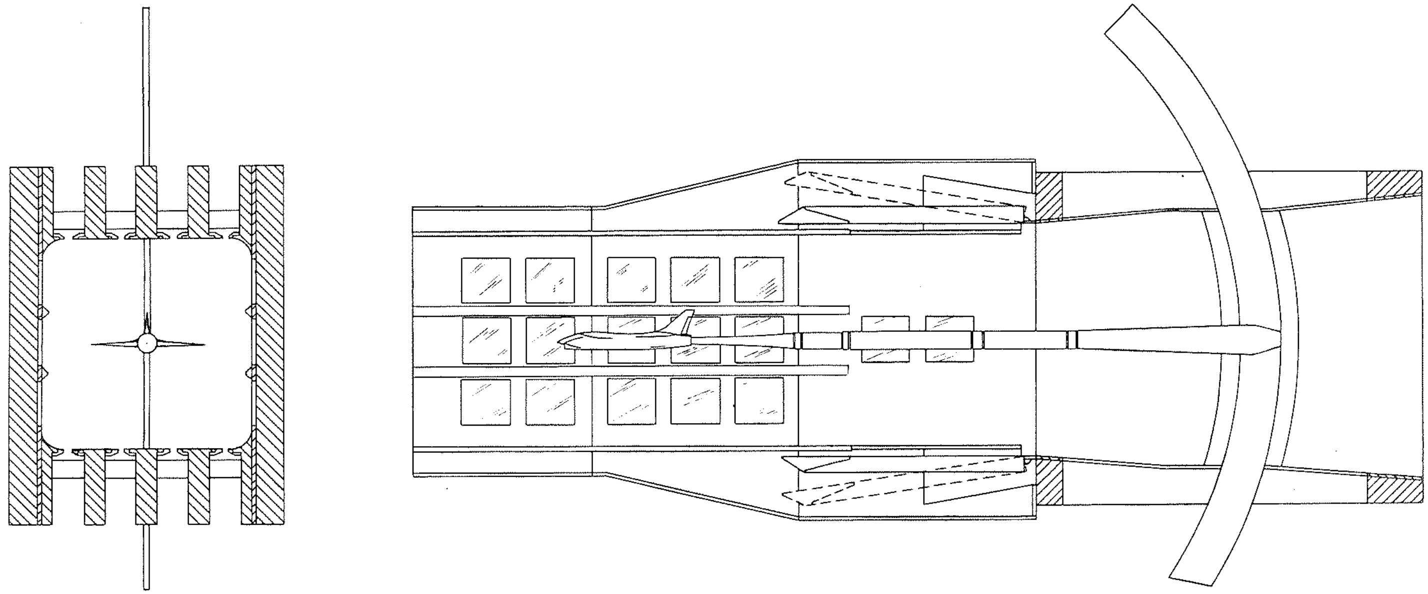

(c) Sketch illustrating tunnel wall inserts.

Figure 1.- Continued.

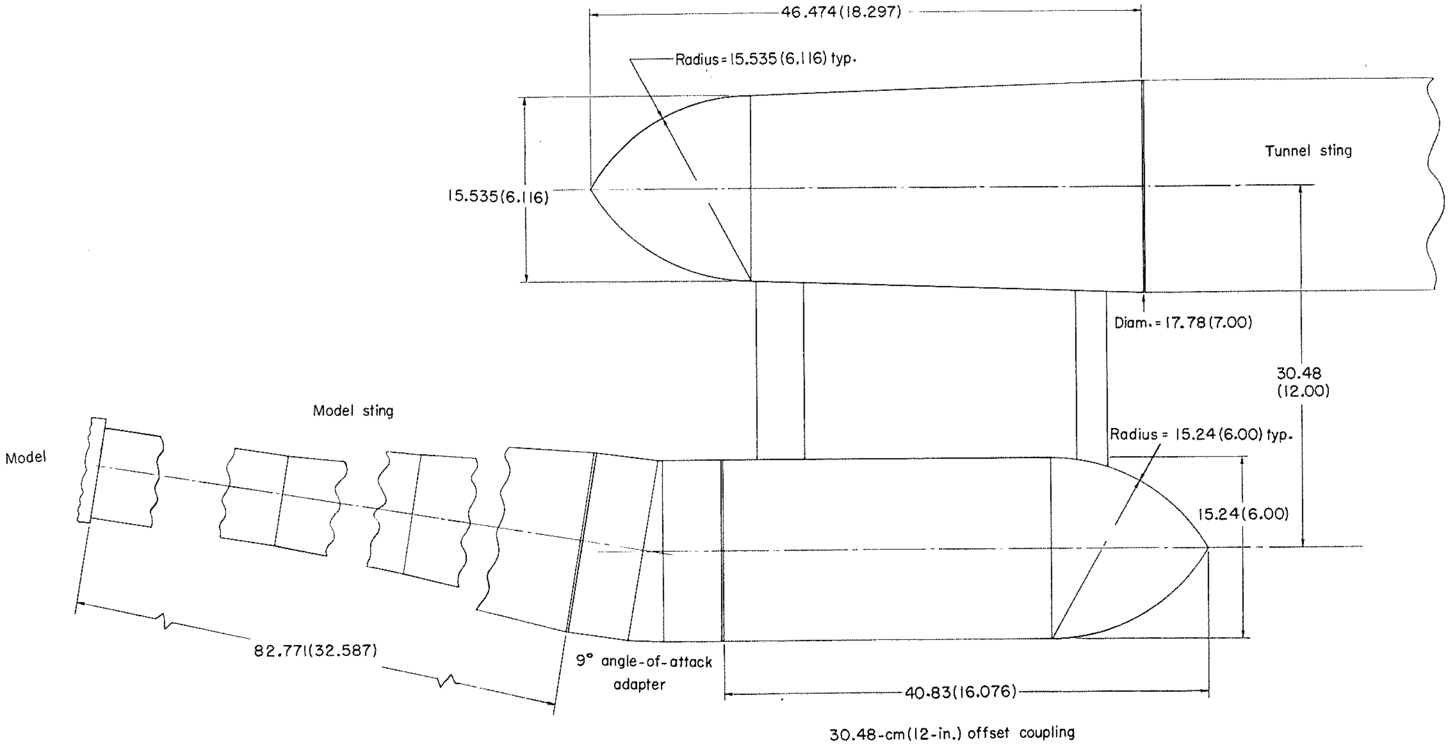

(d) Offset sting arrangement.

Figure 1.- Concluded.

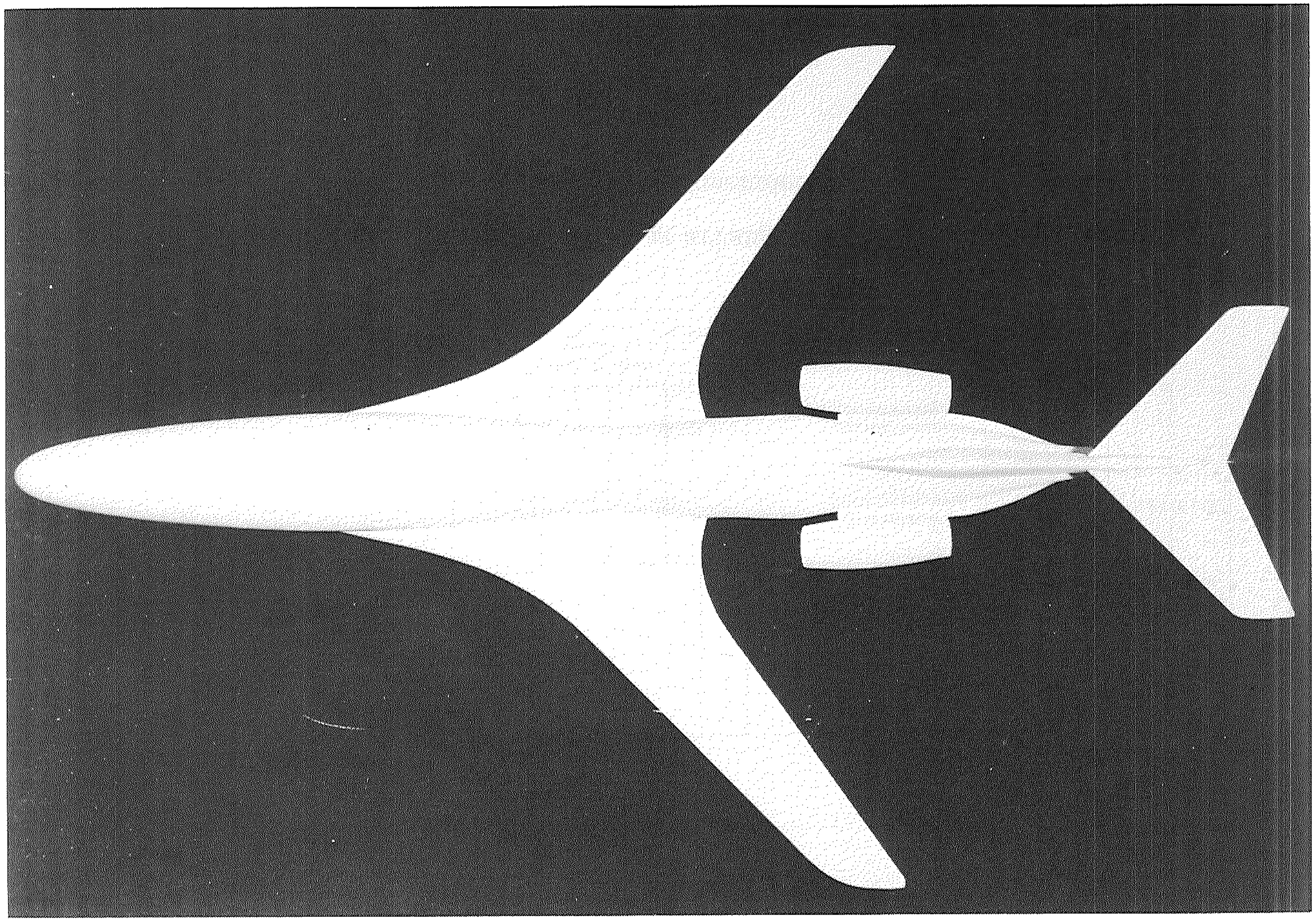

L-71-3328

(a) Top plan view.

Figure 2.- Views of model.

CONFIDENTIAL

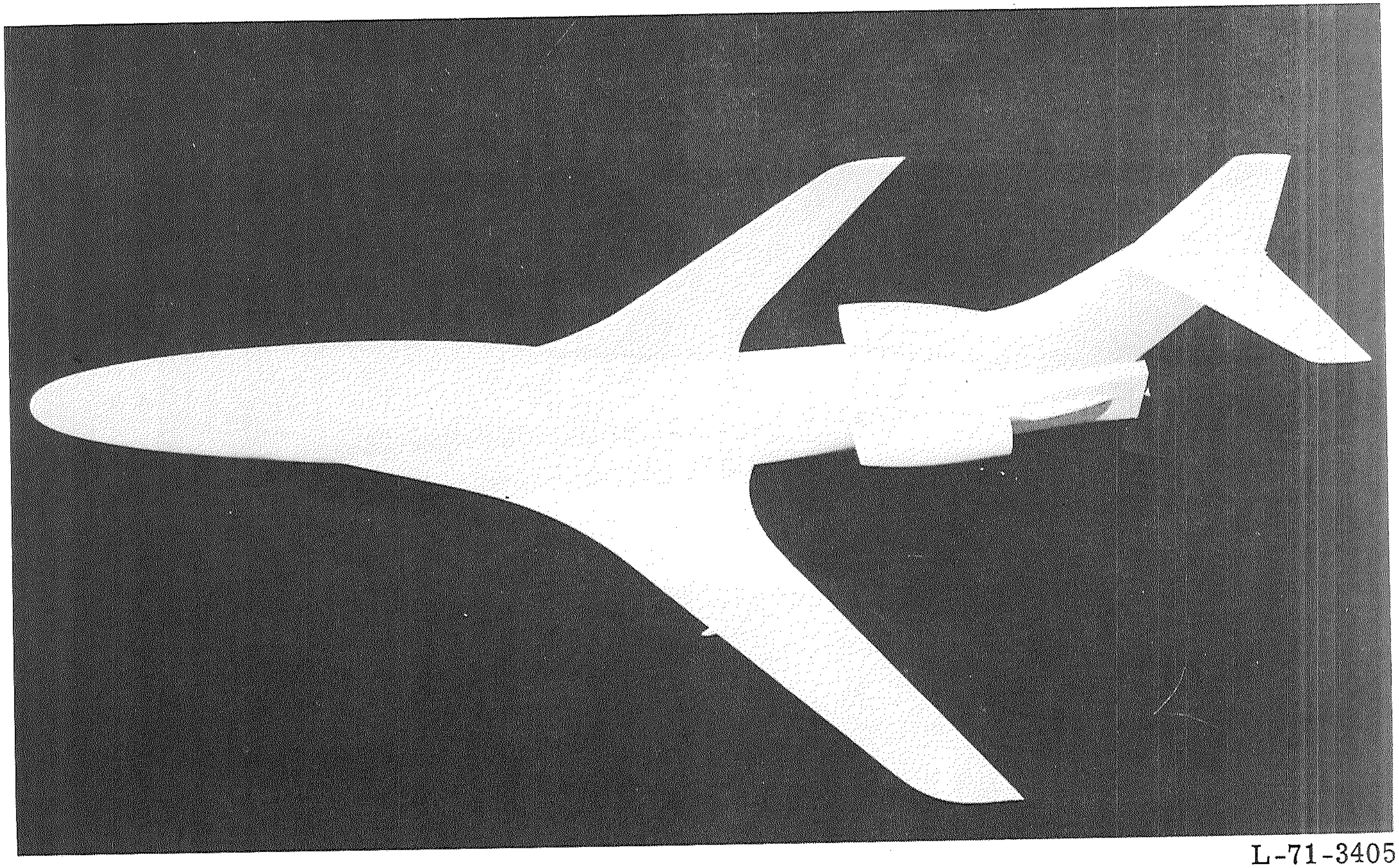

L-71-3405

(b) Top 45° view.

Figure 2.- Continued.

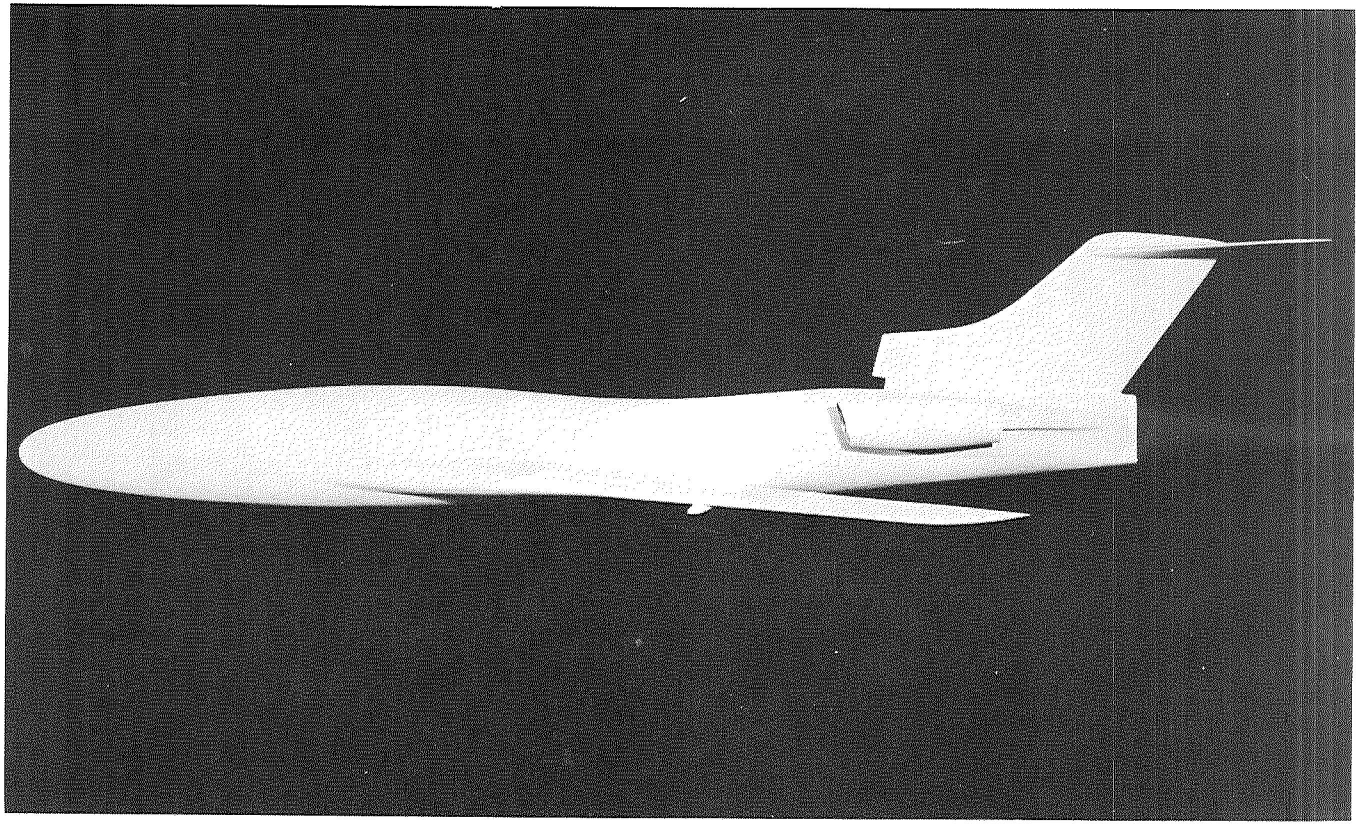

L-71-3327

(c) Side view.

Figure 2.- Continued.

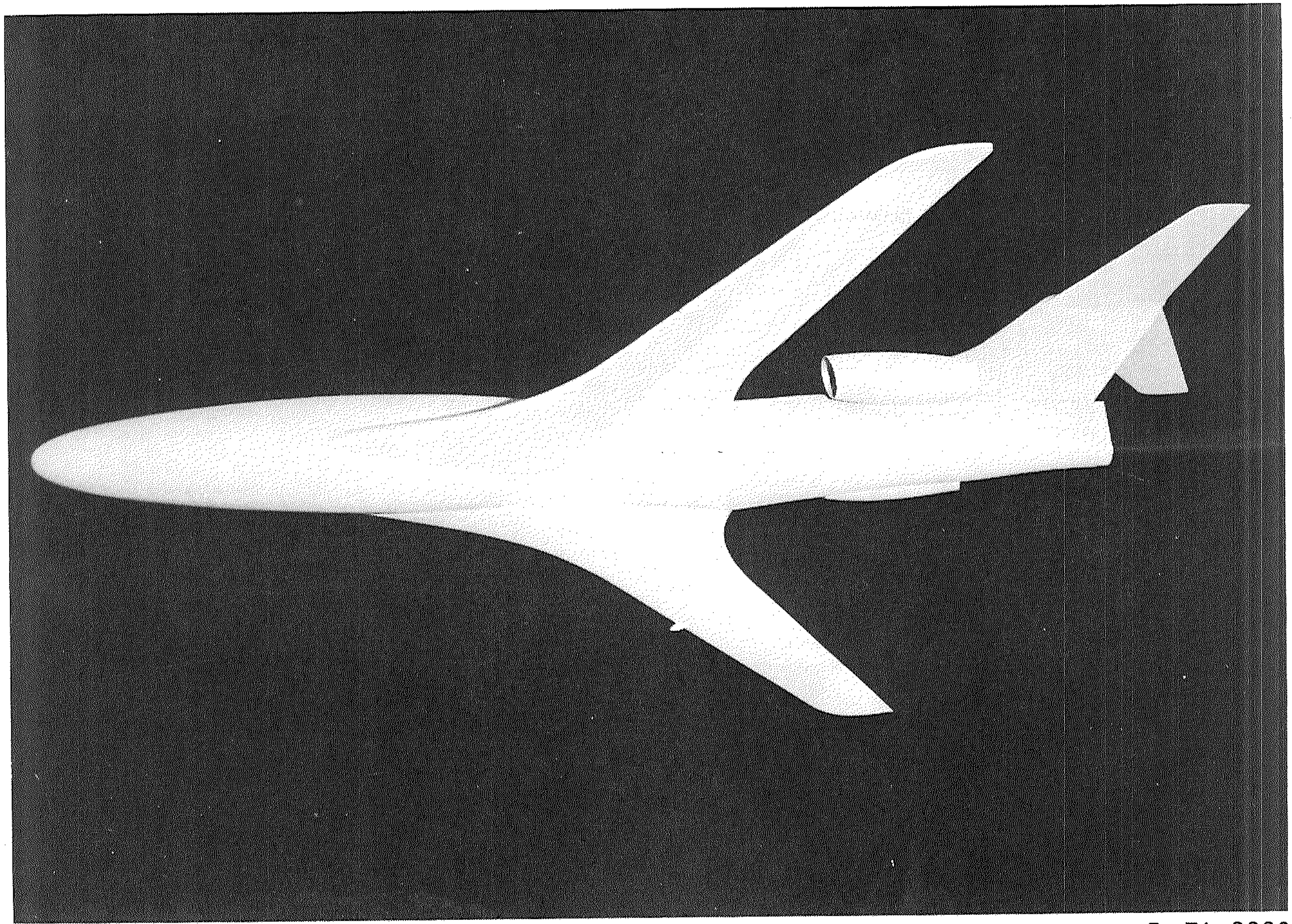

L-71-3330

(d) Bottom 45° view.

Figure 2.- Continued.

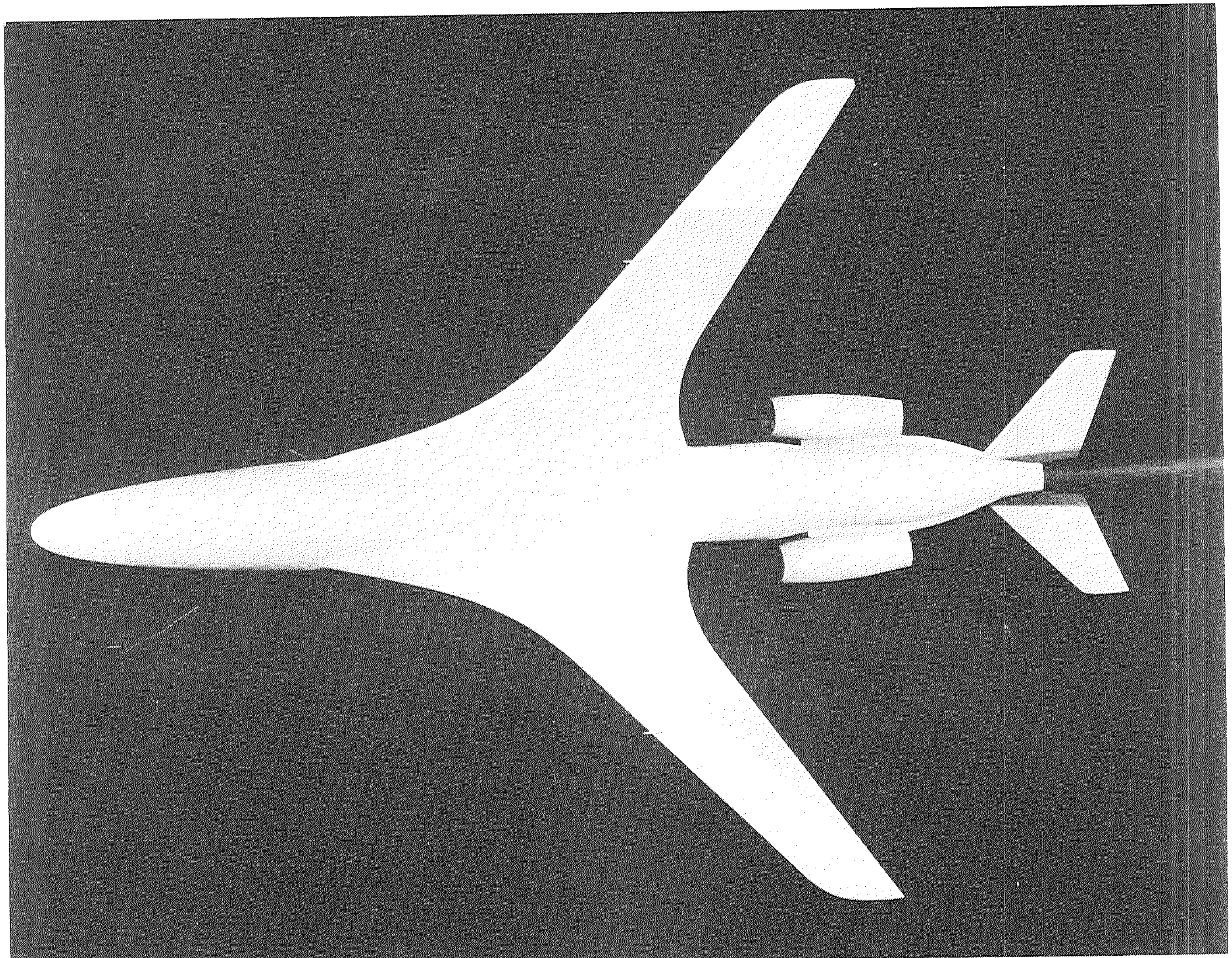

L-71-3329

(e) Bottom plan view.

Figure 2.- Concluded.

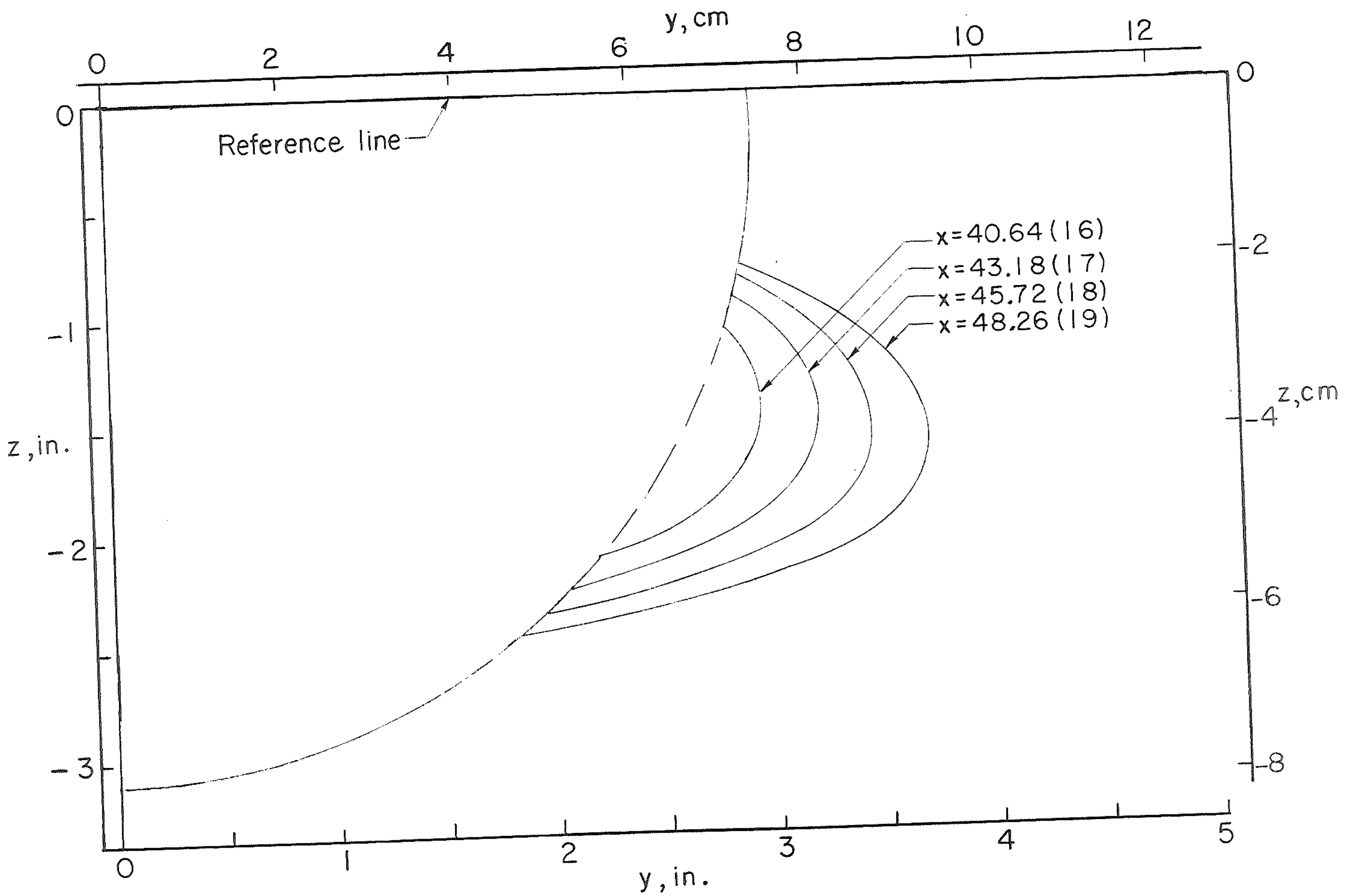

Figure 3.- Cross sections of model normal to longitudinal axis. (Dashed lines indicate divisions of areas shown in fig. 4.) Values of x are centimeters (in.) from fuselage apex.

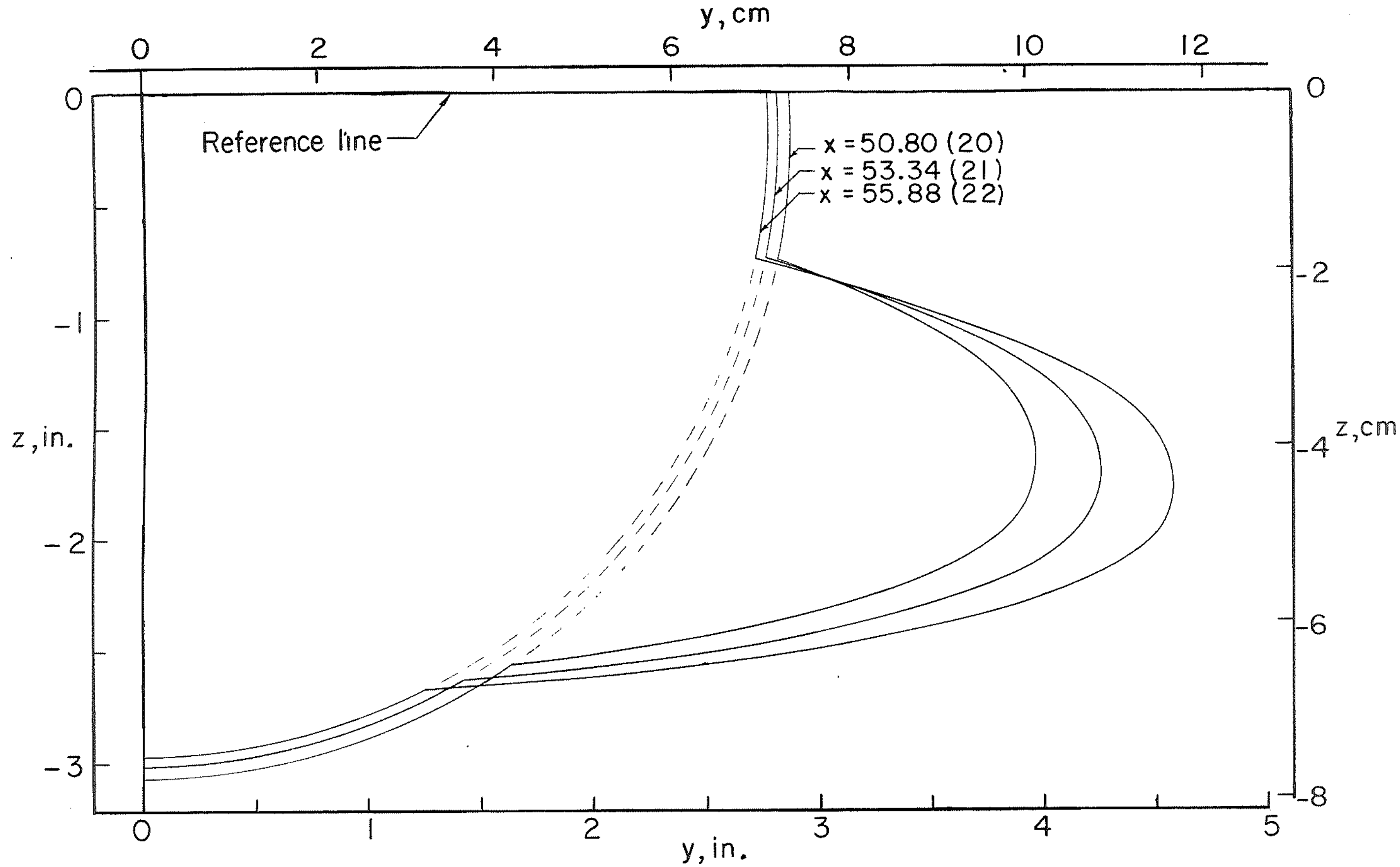

Figure 3.- Continued.

CONFIDENTIAL

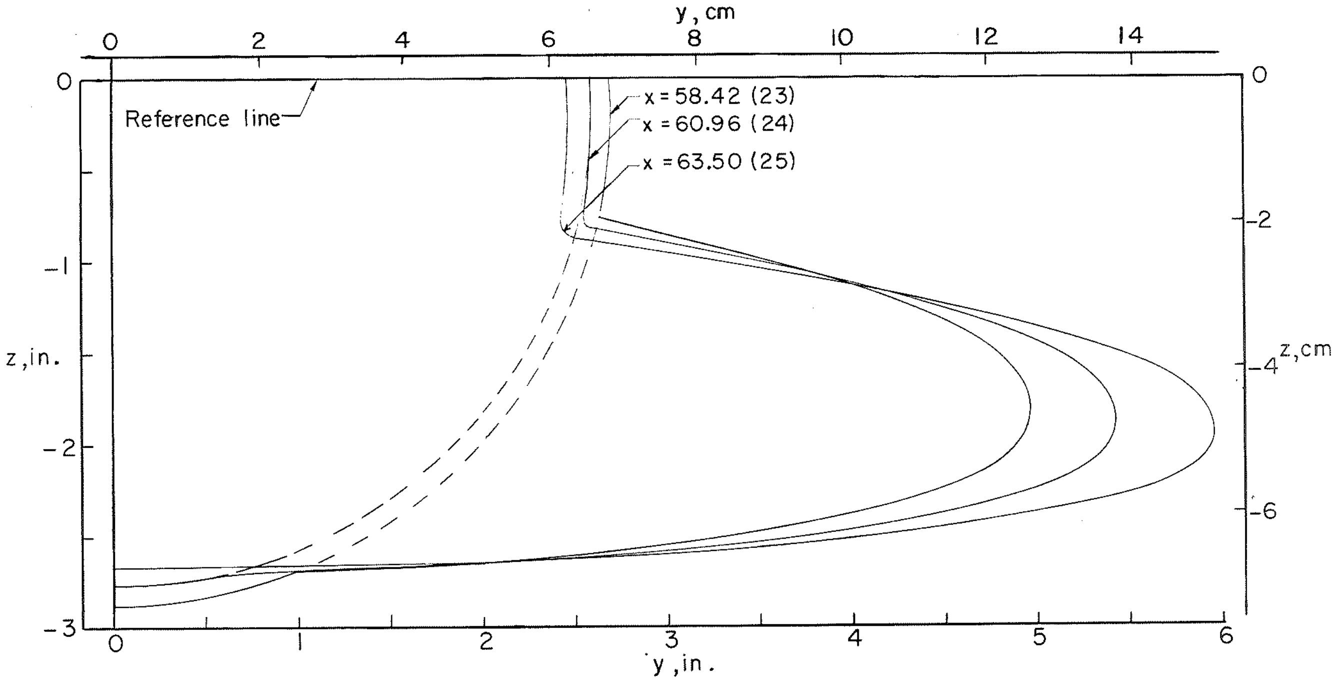

Figure 3.- Continued.

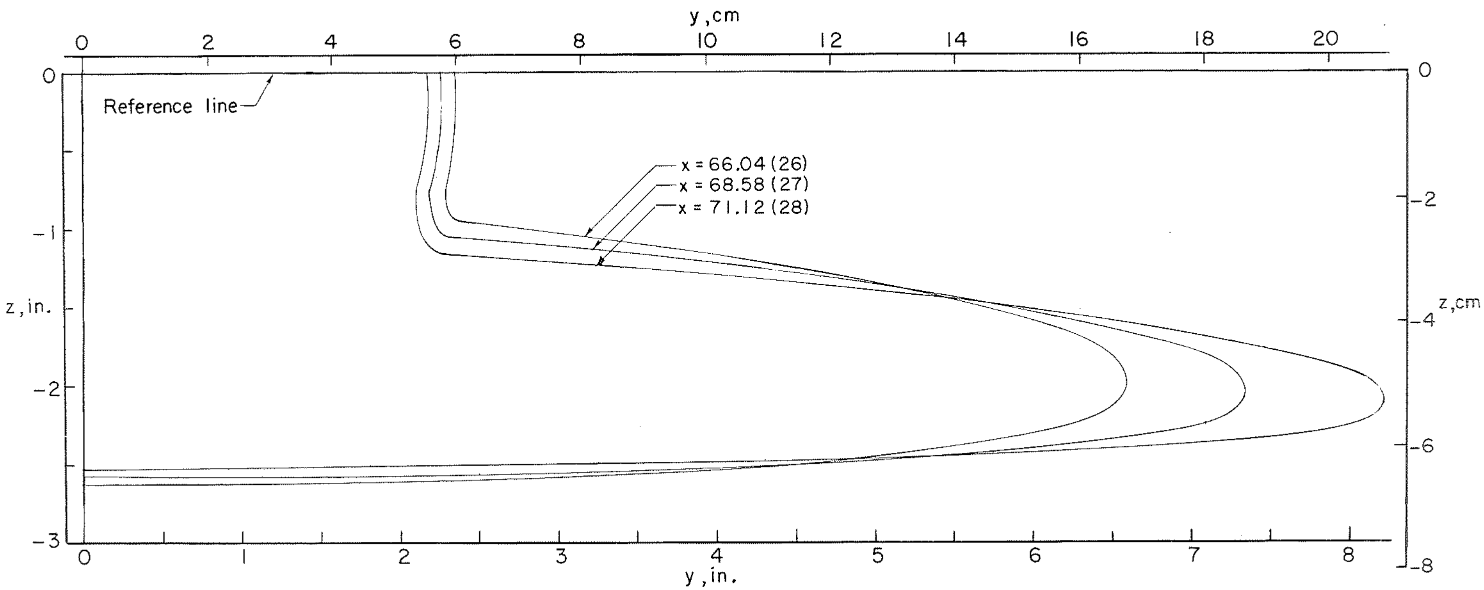

Figure 3.- Continued.

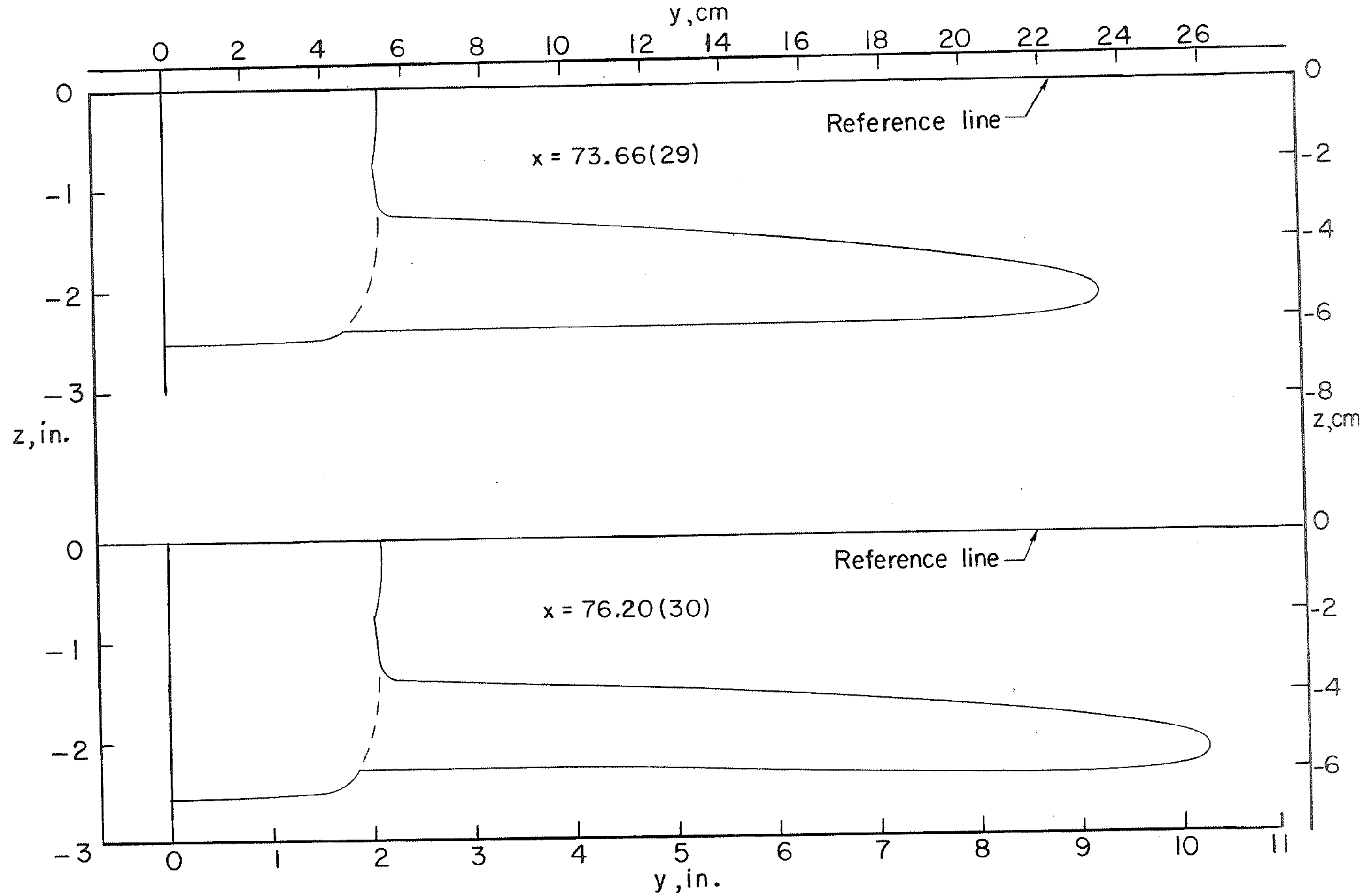

Figure 3.- Continued.

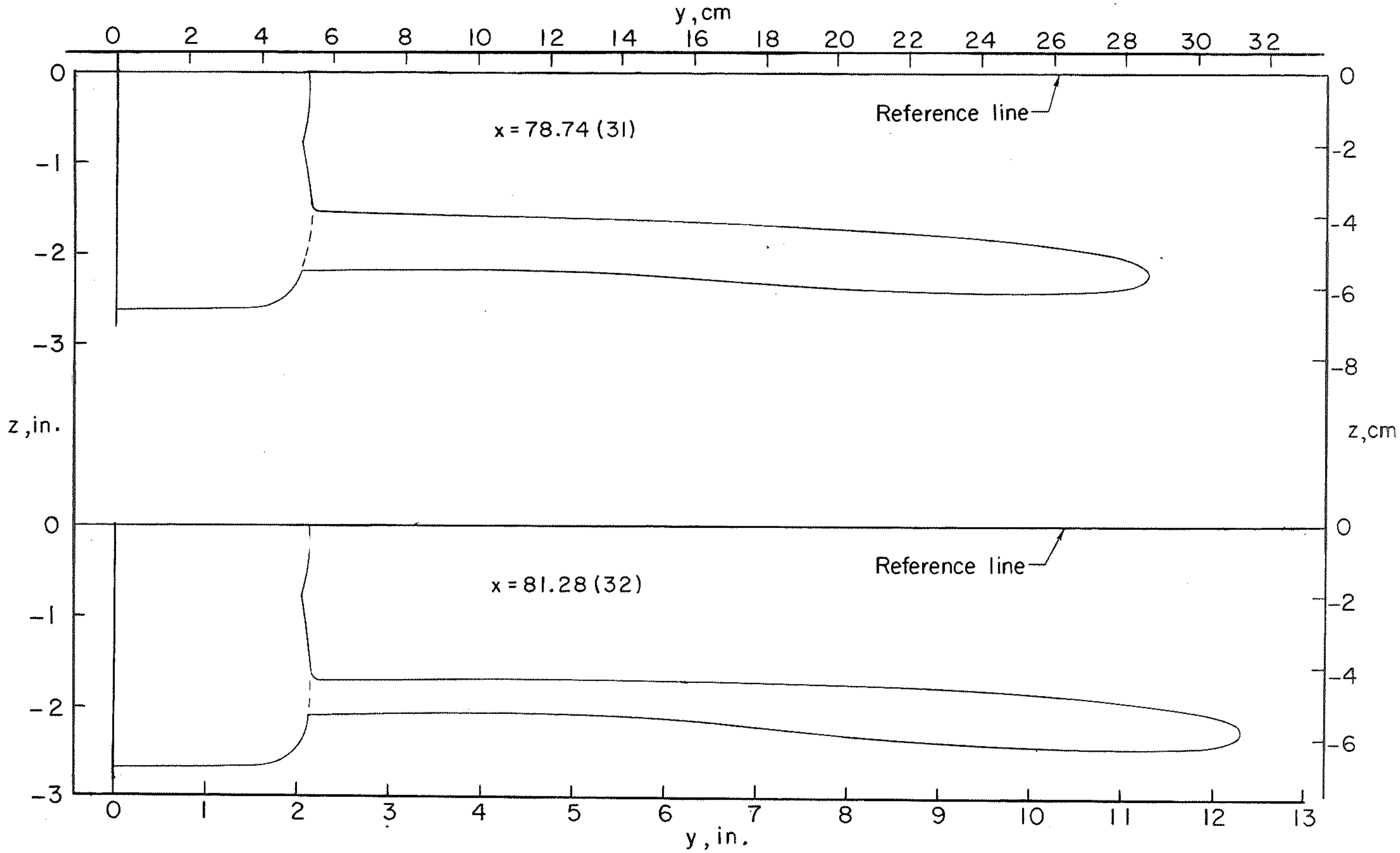

Figure 3.- Continued.

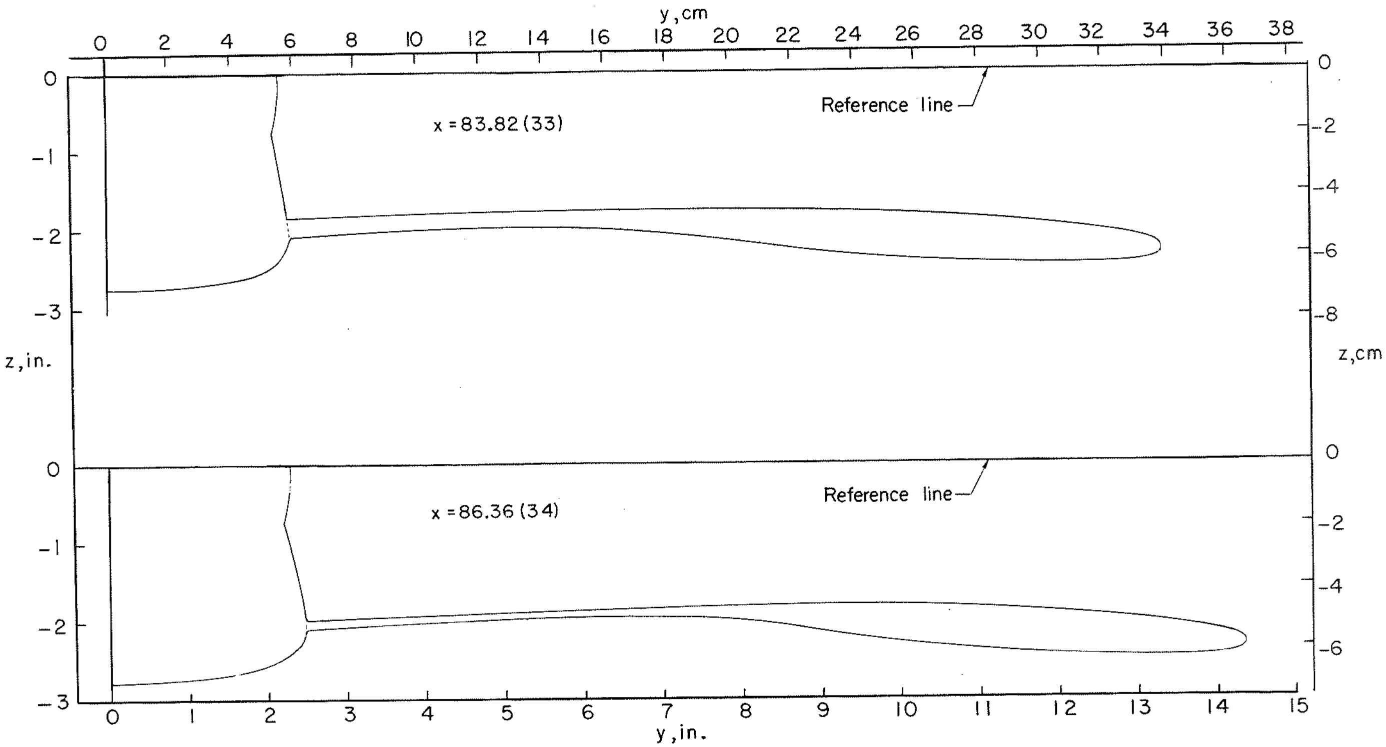

Figure 3.- Continued.

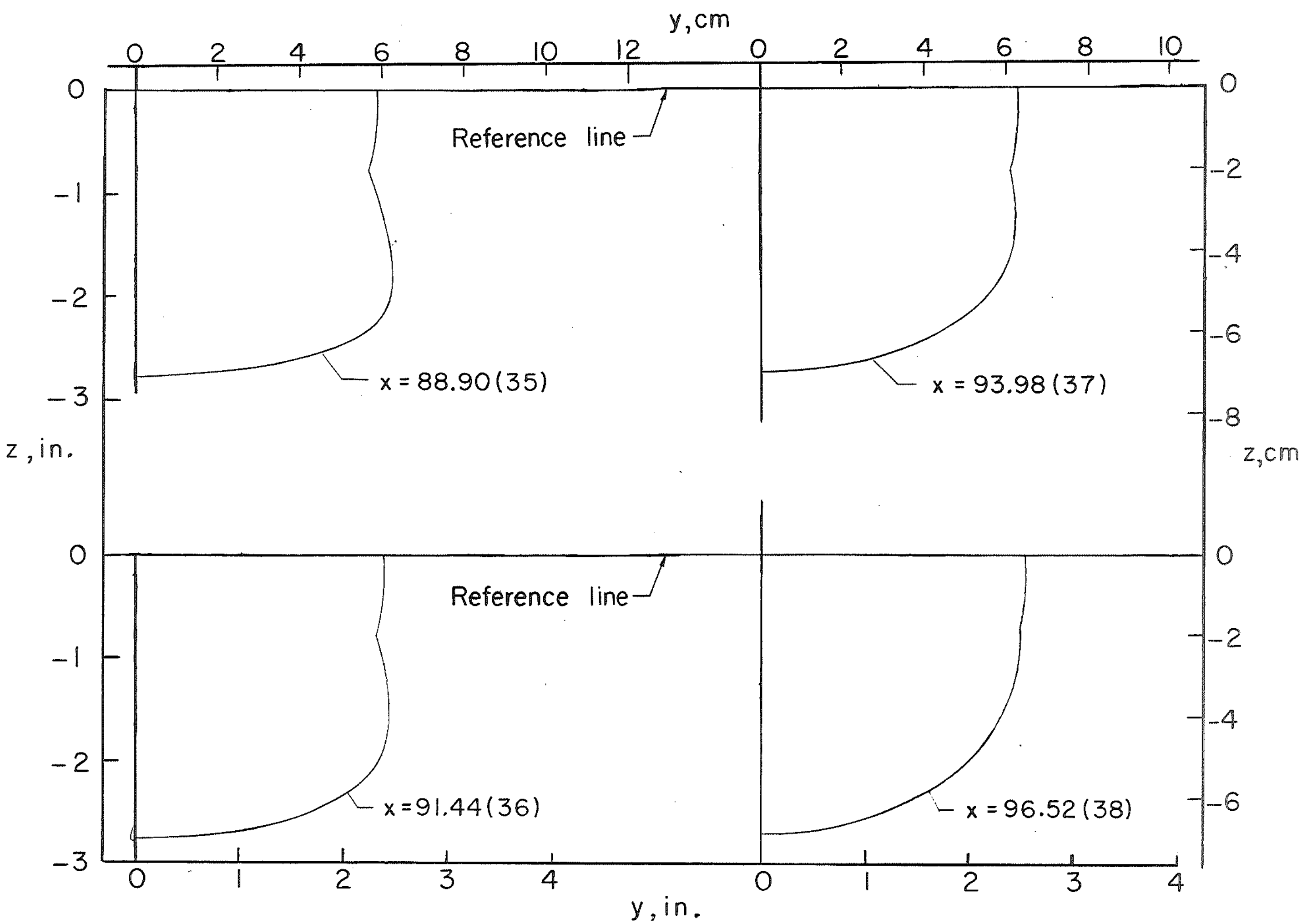

Figure 3.- Continued.

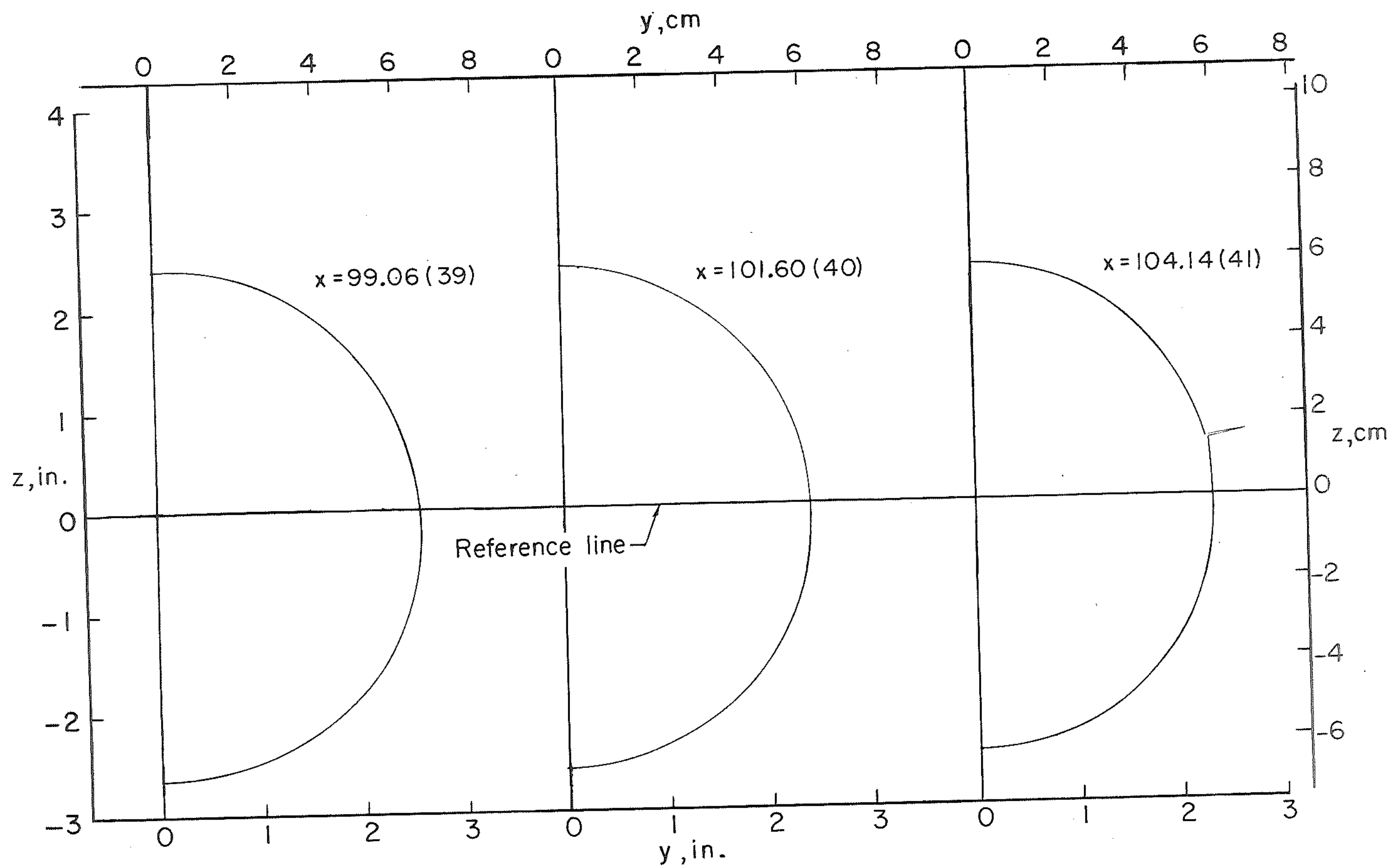

Figure 3.- Continued.

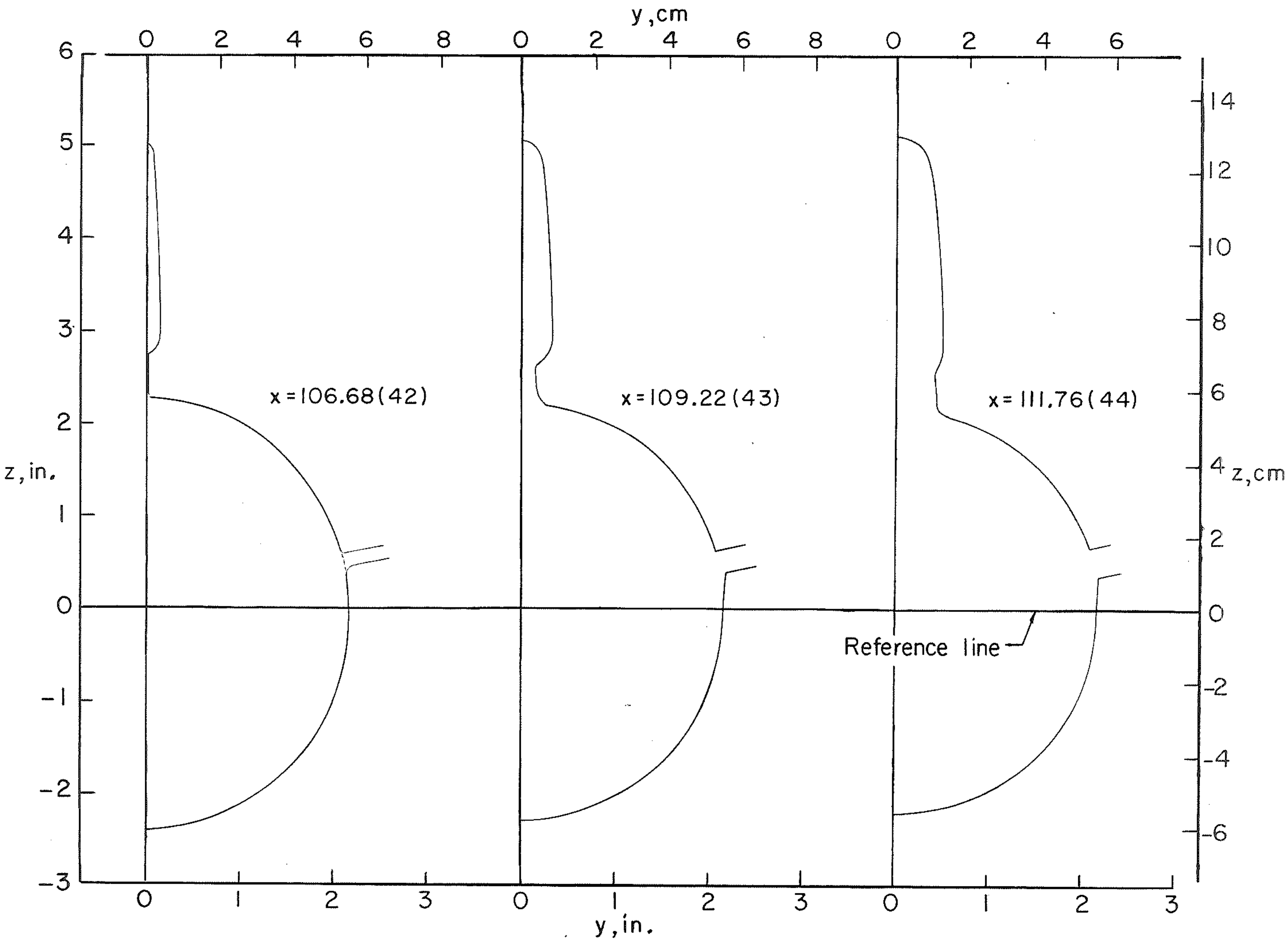

Figure 3.- Continued.

CONFIDENTIAL

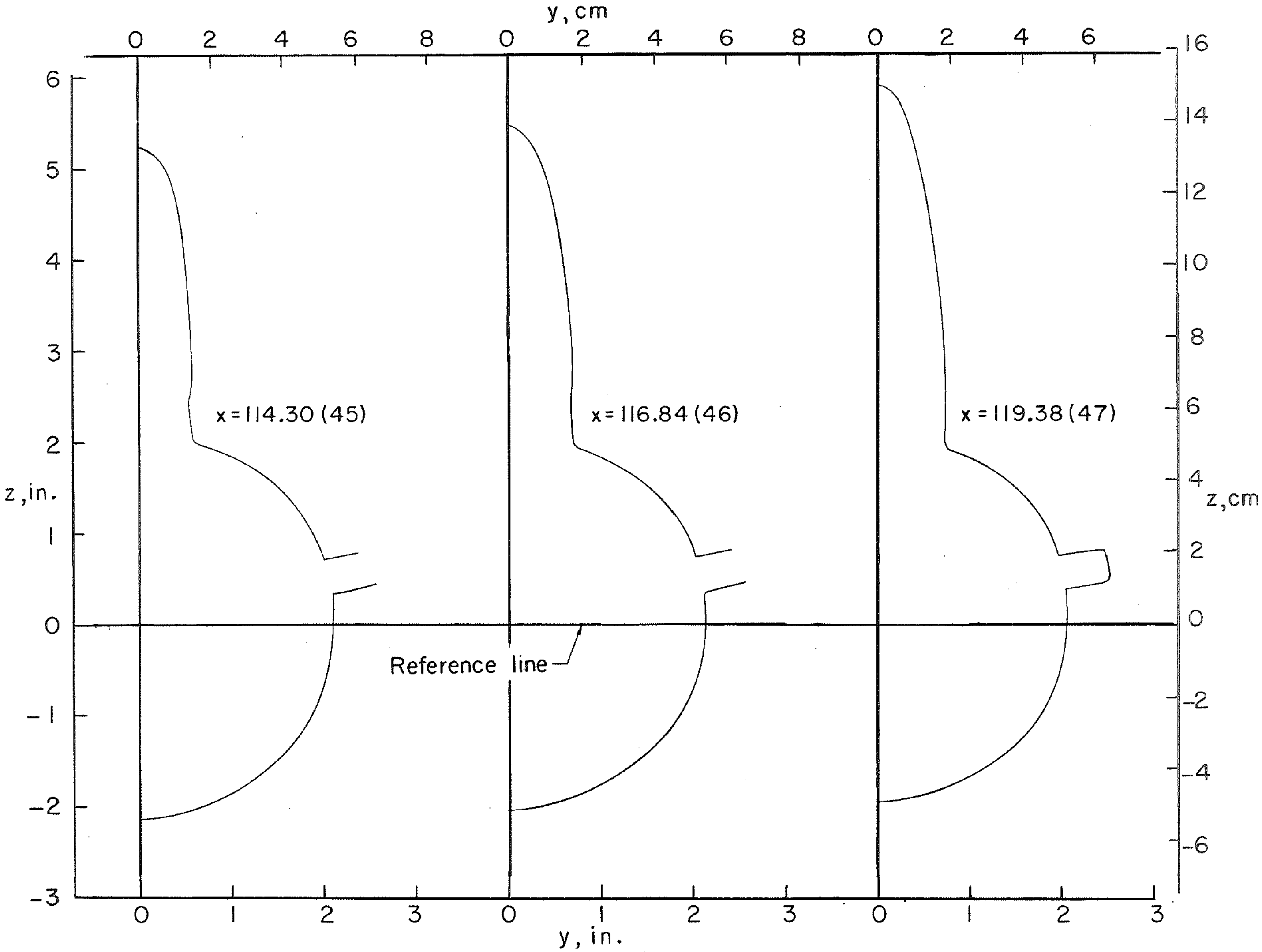

Figure 3.- Continued.

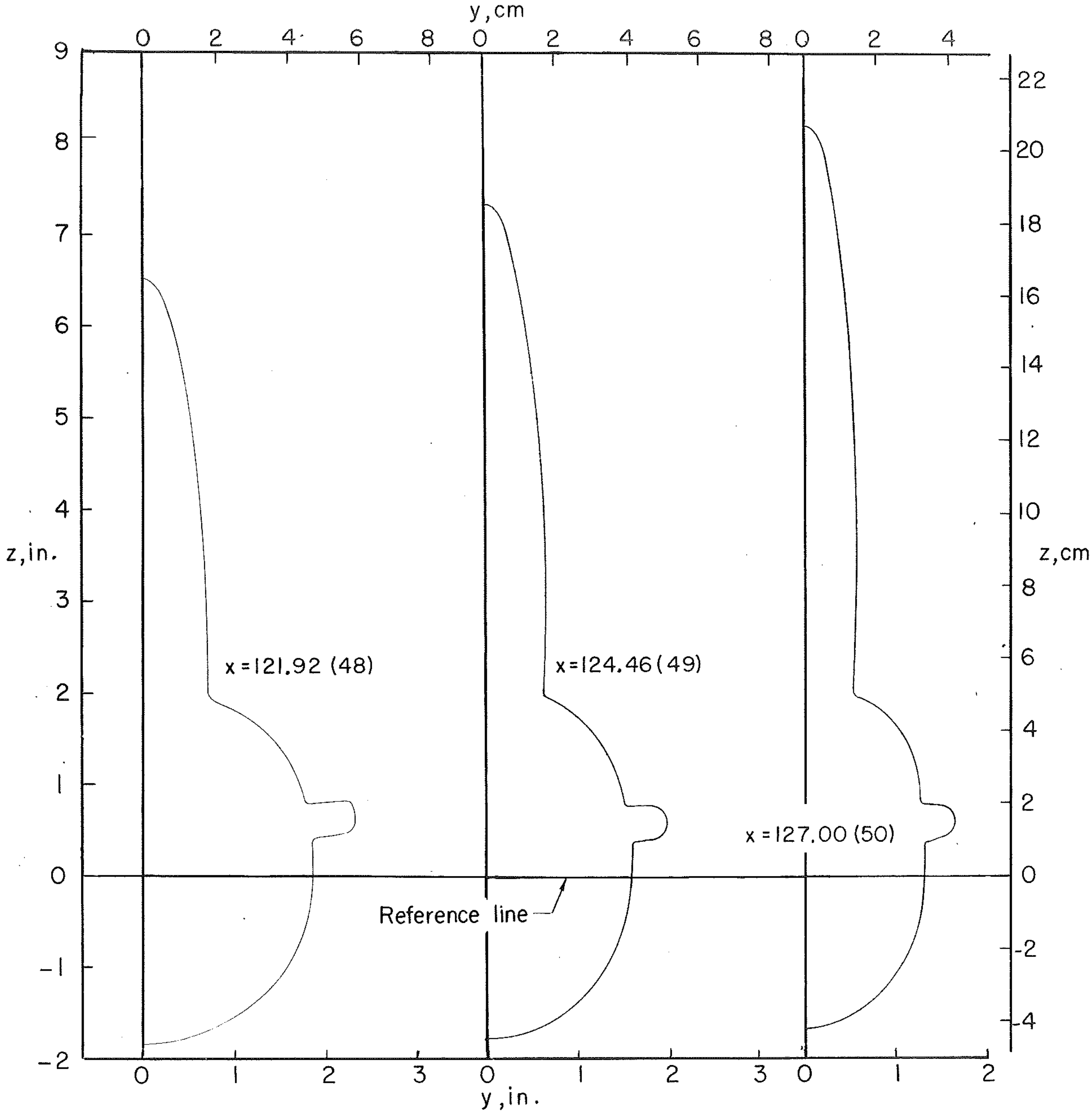

Figure 3.- Continued.

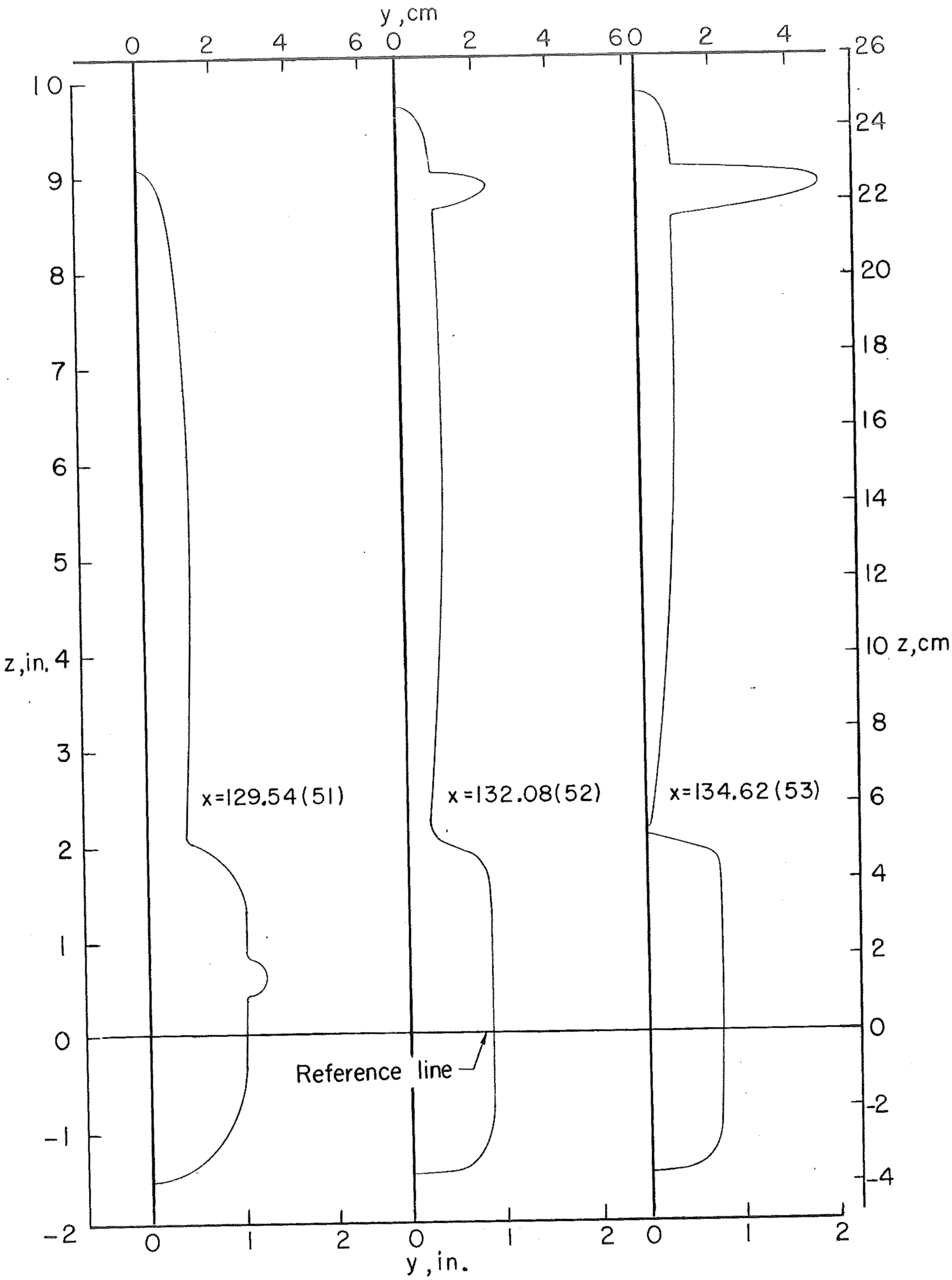

Figure 3.- Continued.

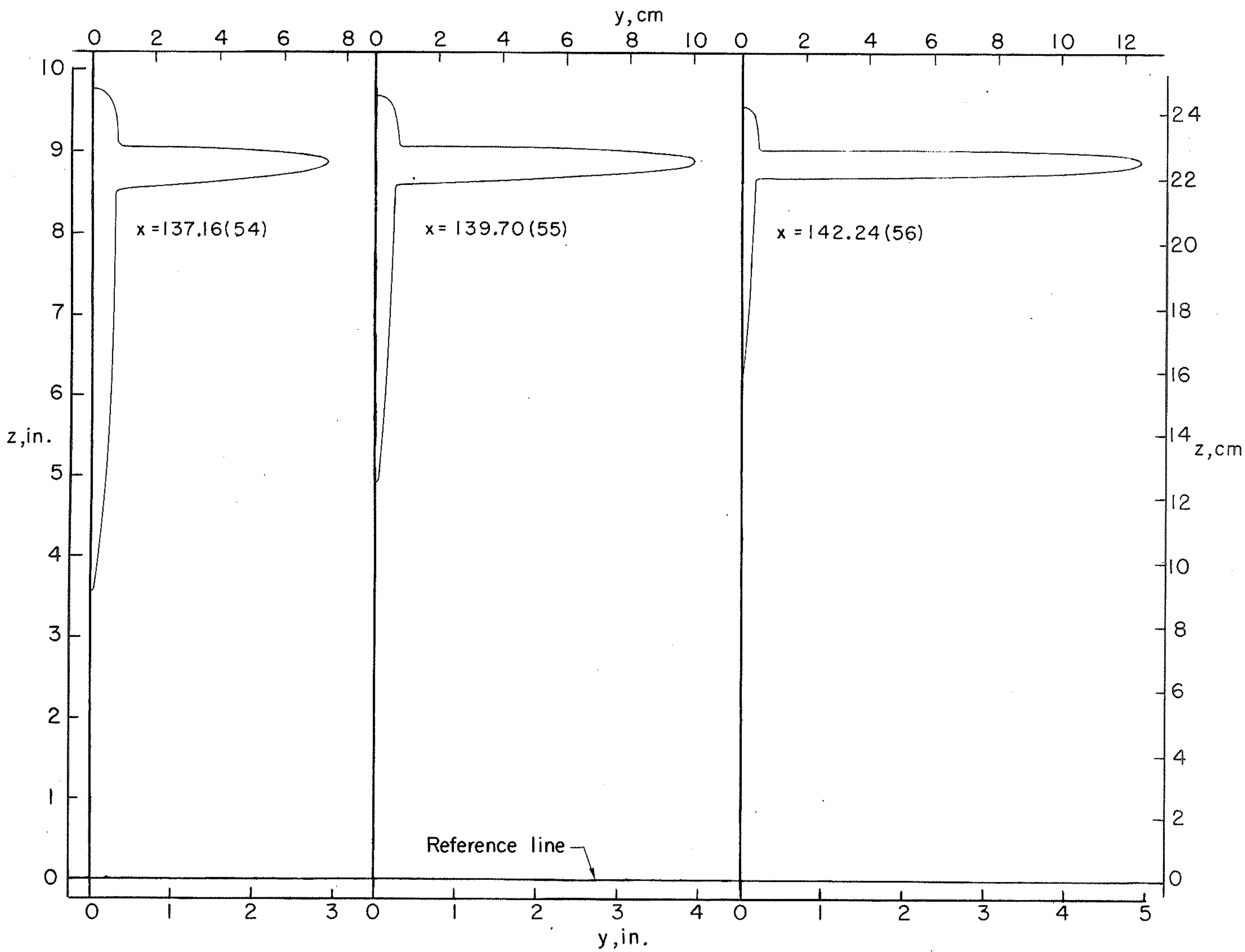

Figure 3.- Continued.

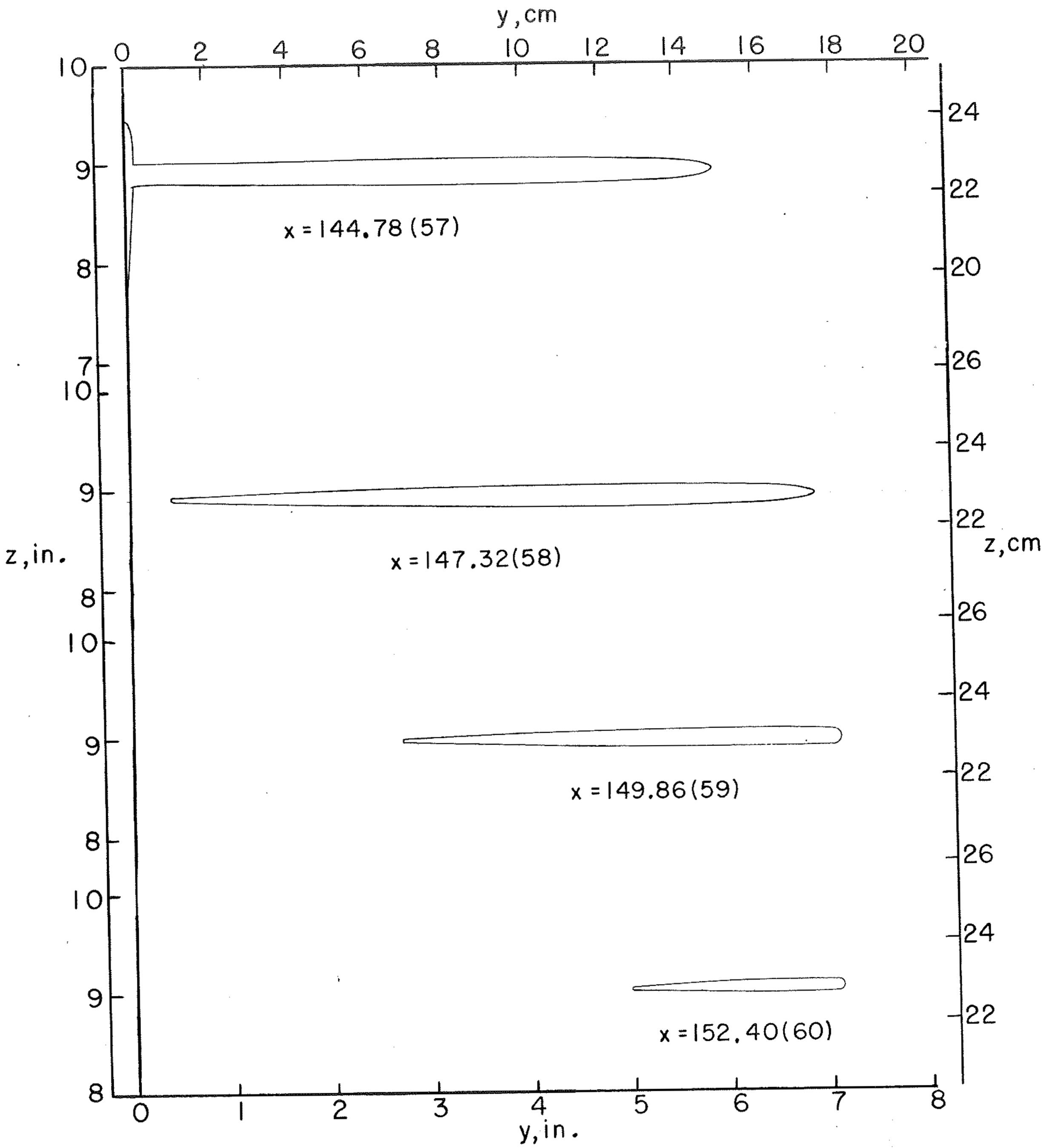

Figure 3.- Concluded.

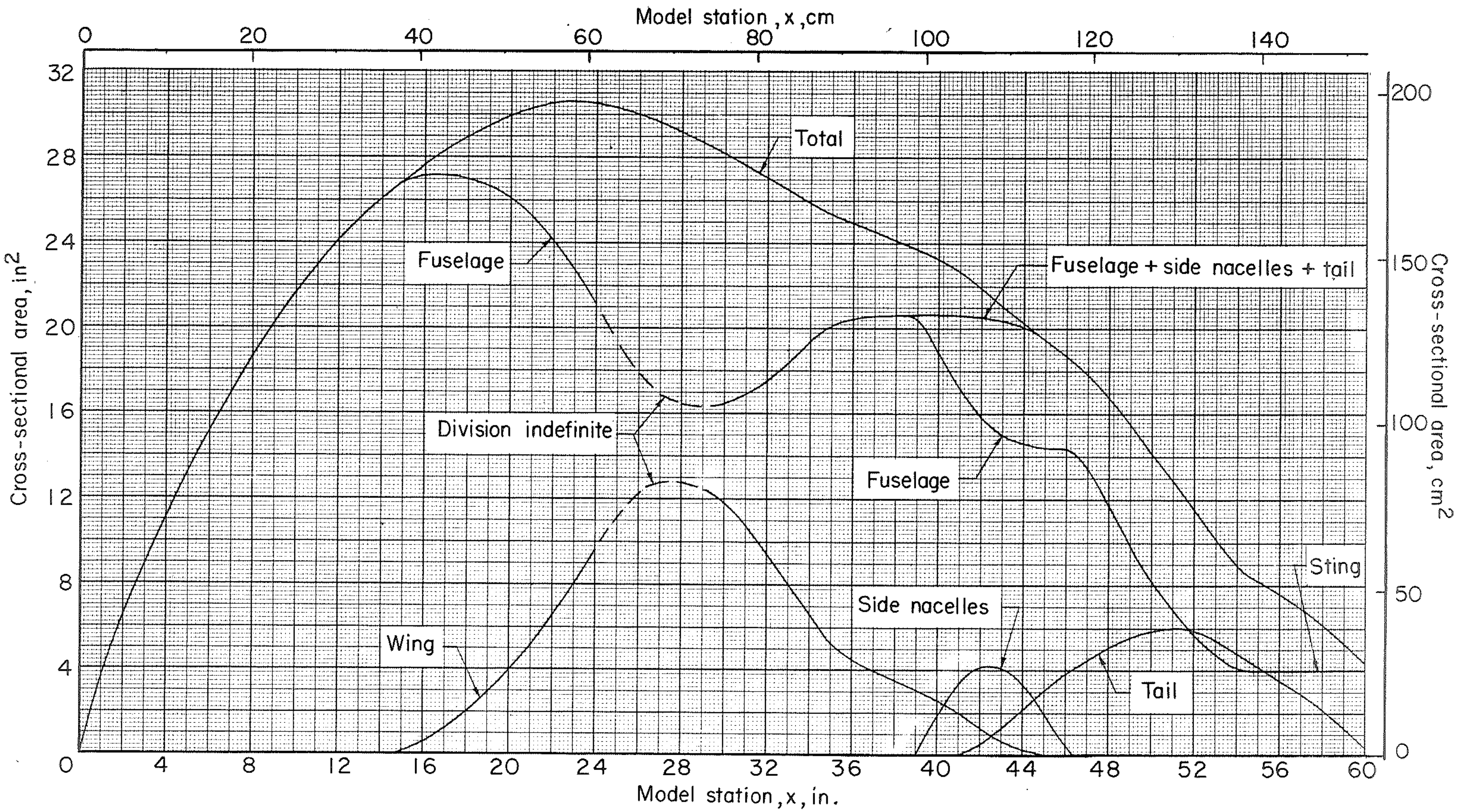

(a) Geometric areas.

Figure 4.- Longitudinal variations of cross-sectional areas.

CONFIDENTIAL

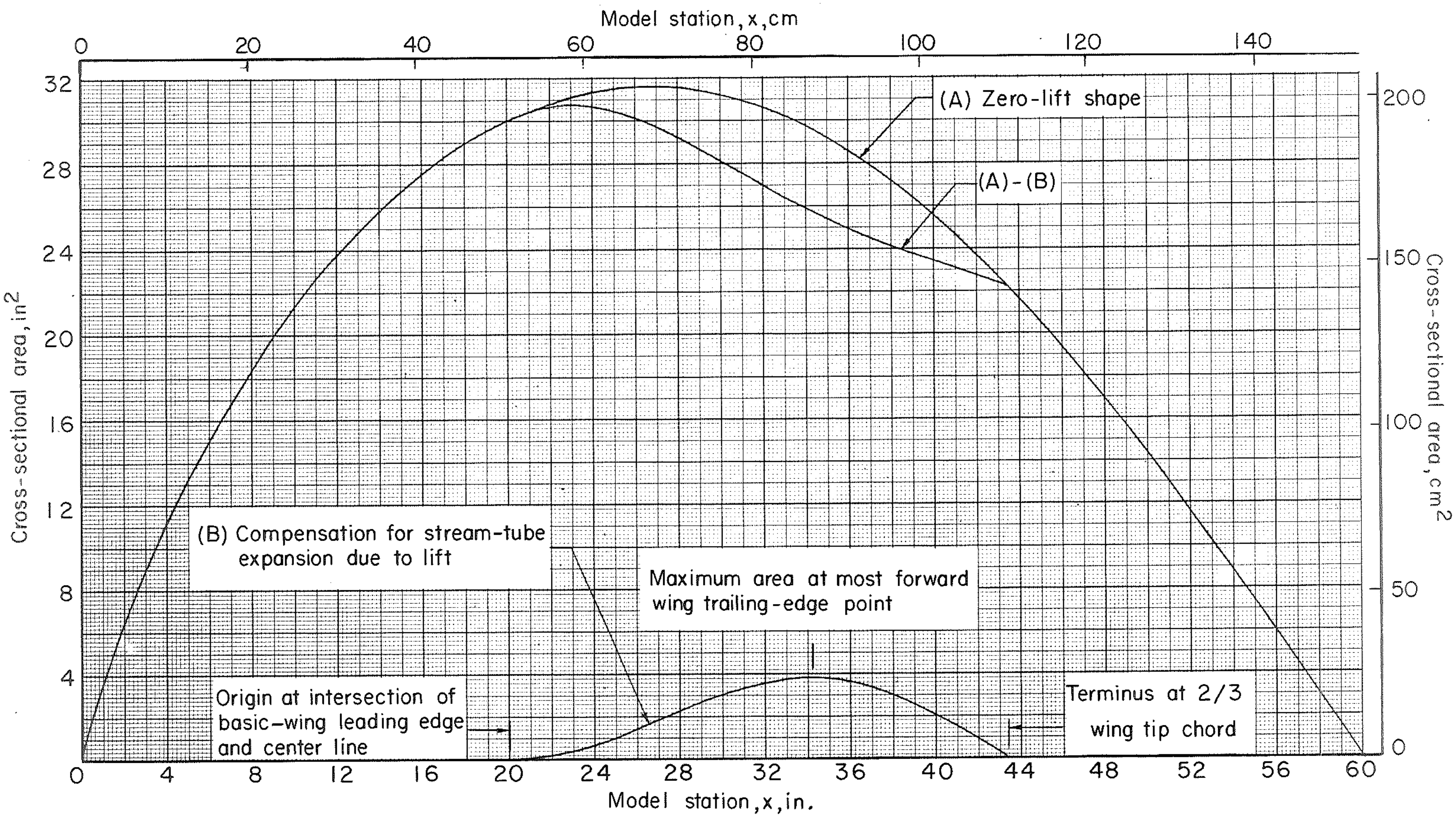

(b) Definition of design envelope. M = 0.99.

Figure 4.- Concluded.

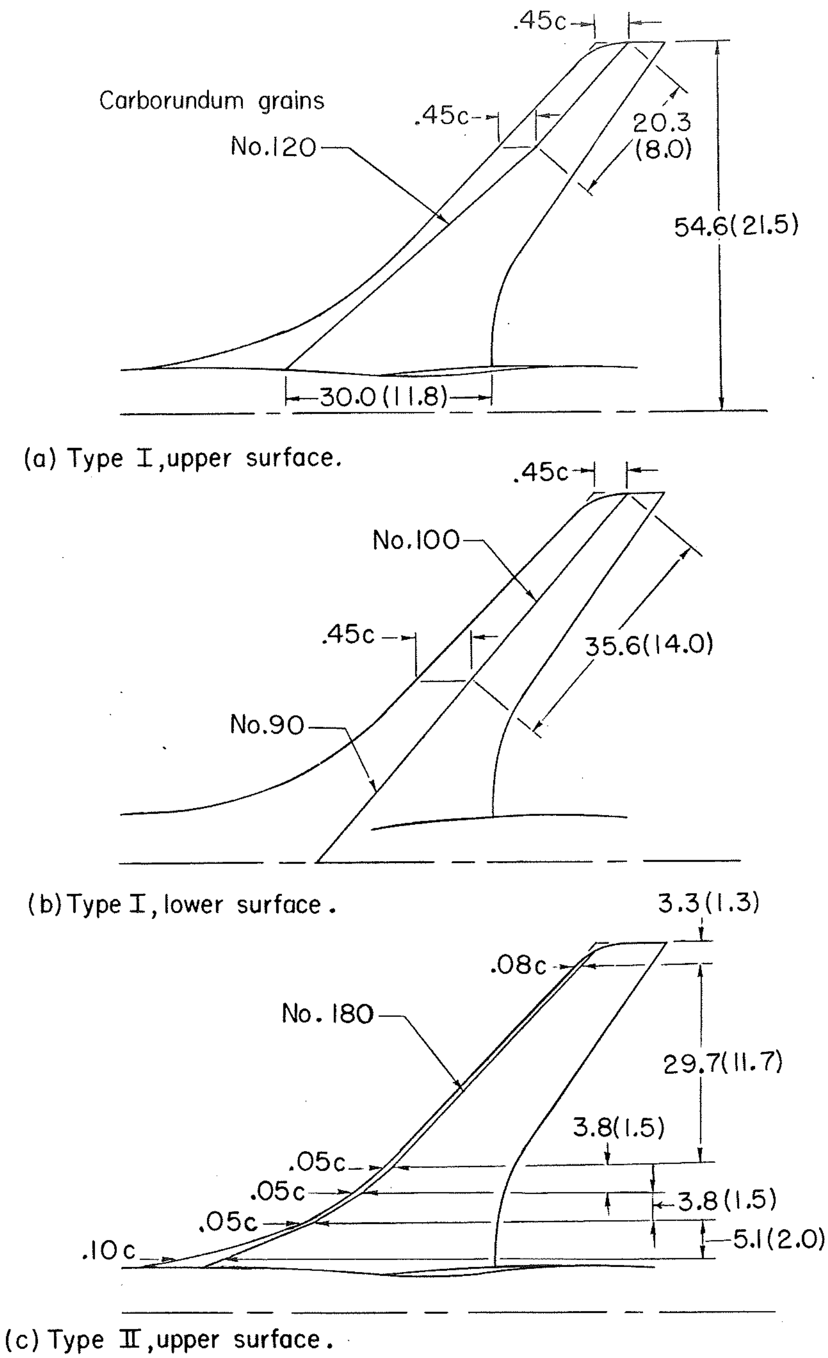

Figure 5.- Locations of transition strips. Dimensions are in centimeters, inches in parentheses.

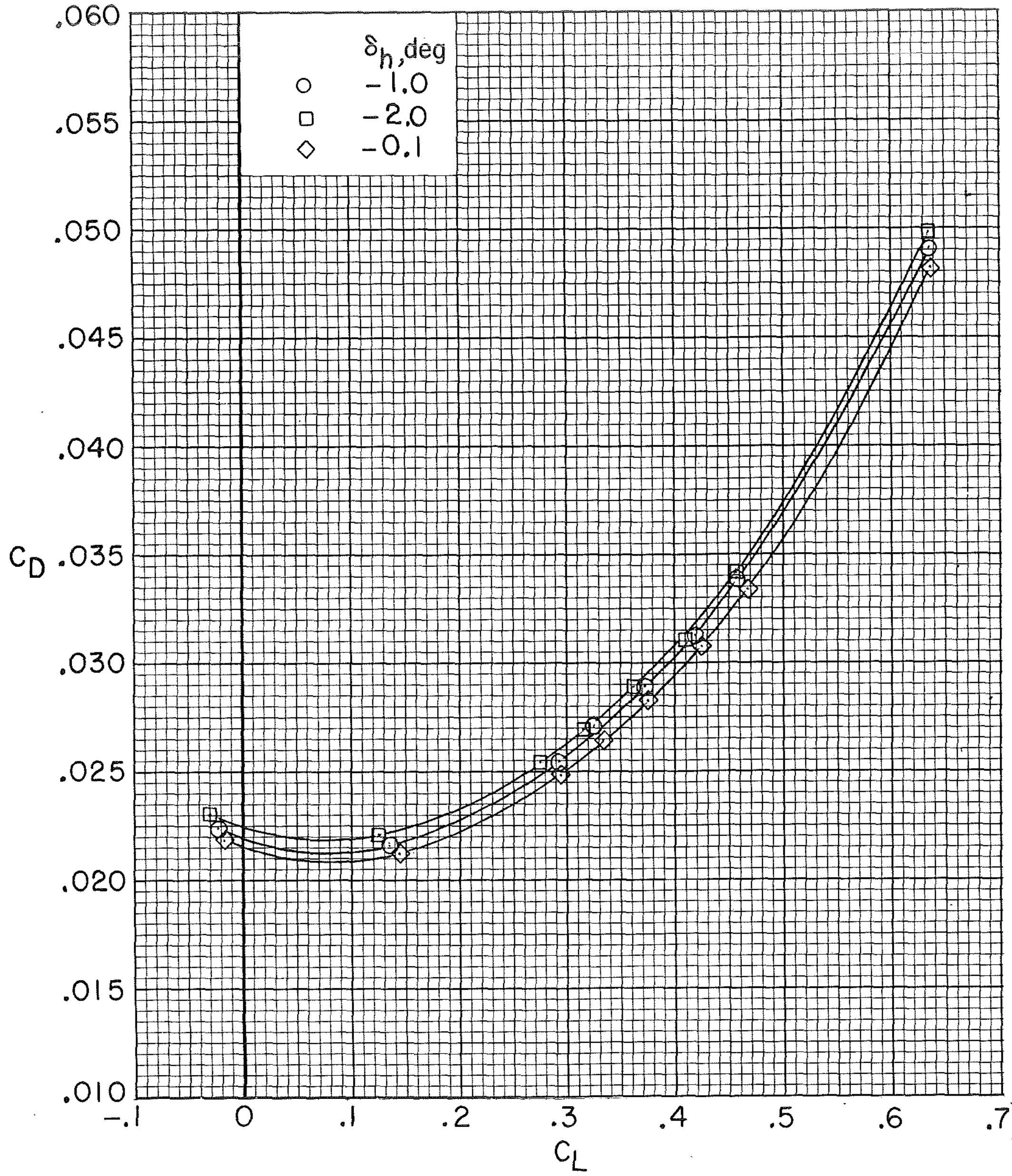

(a) M = 0.950.

Figure 6.- Longitudinal aerodynamic characteristics with type I transition. $\beta = 0^{\circ}$.

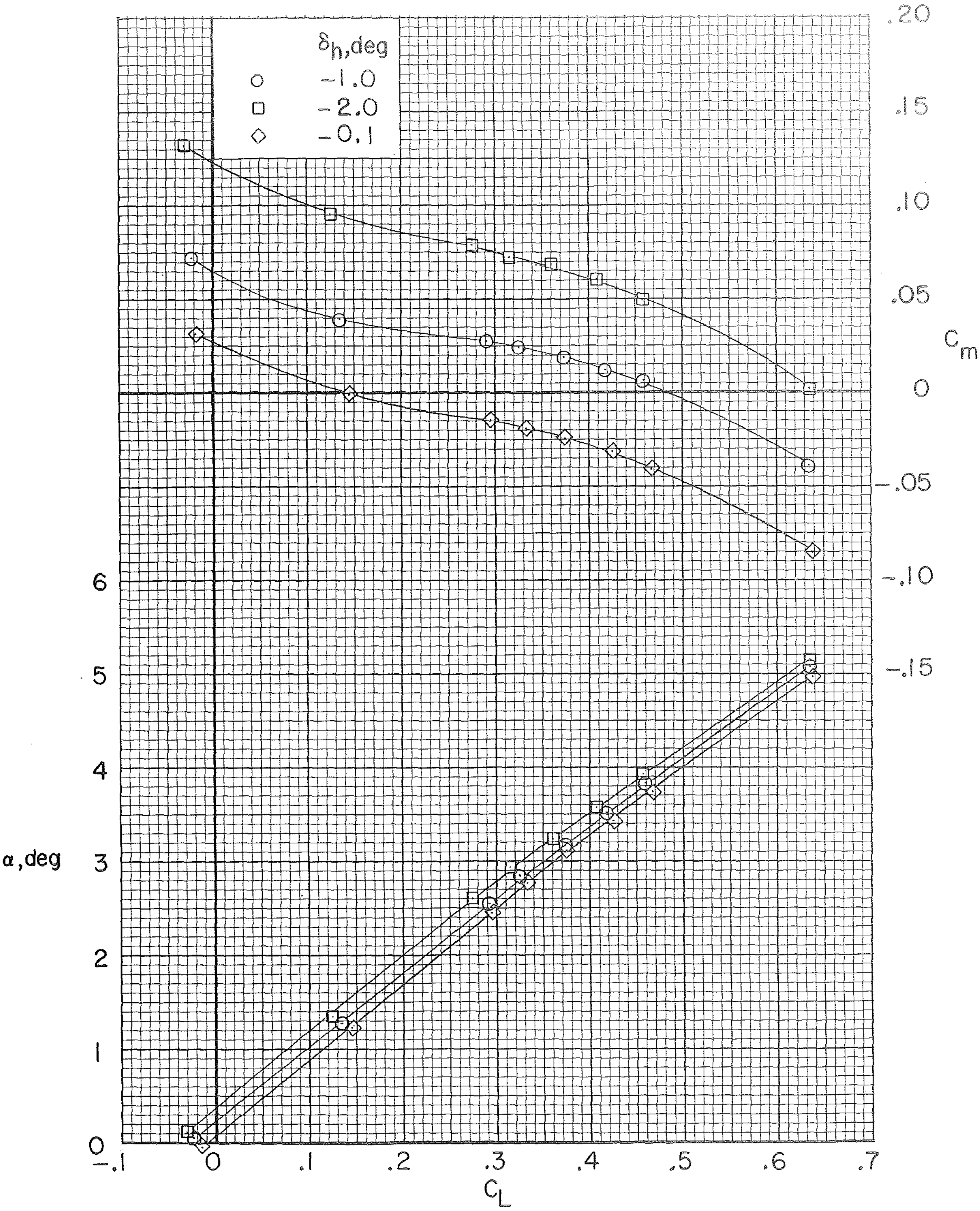

(a) M = 0.950. Concluded.

Figure 6.- Continued.

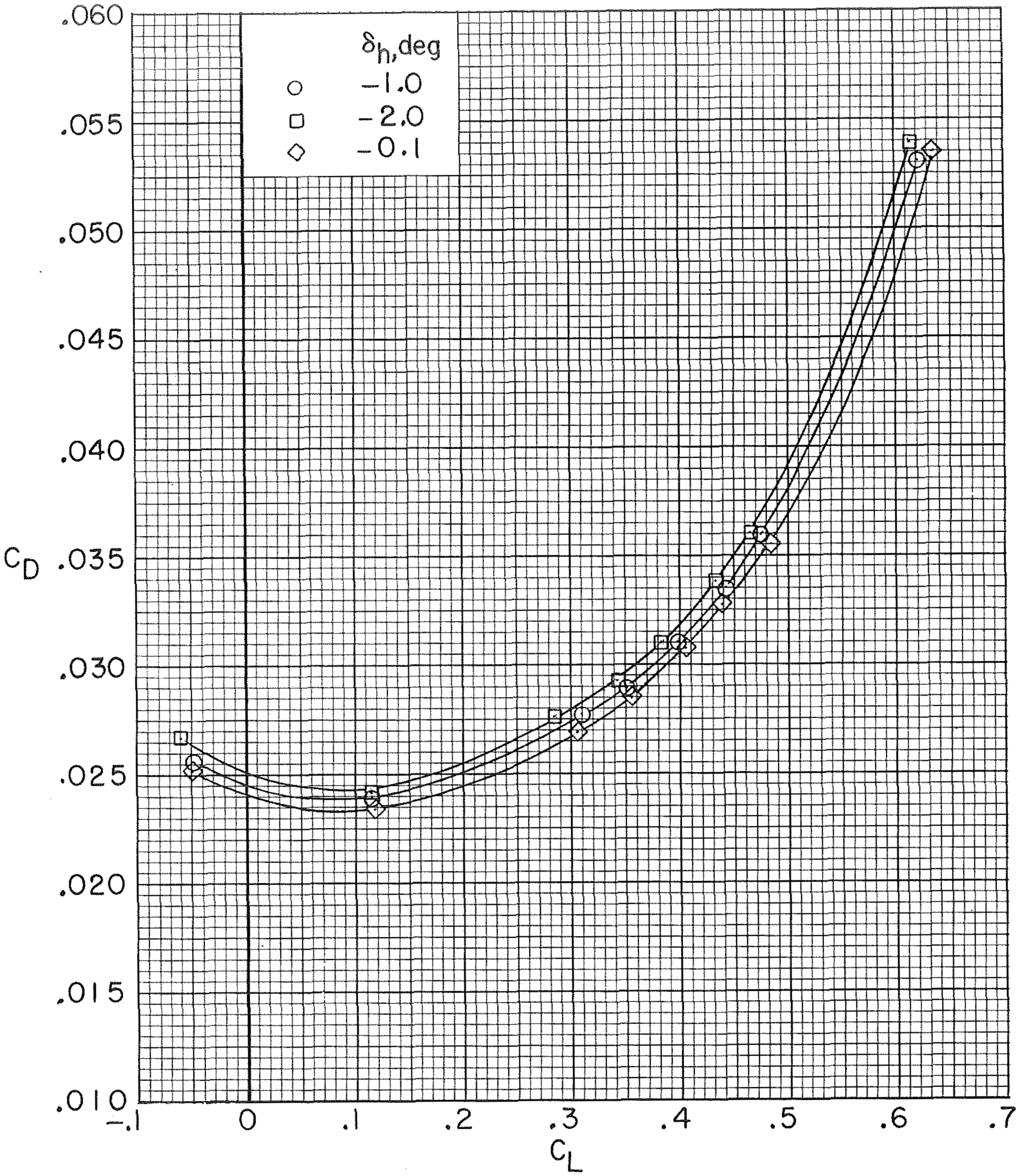

(b) M = 0.980.

Figure 6.- Continued.

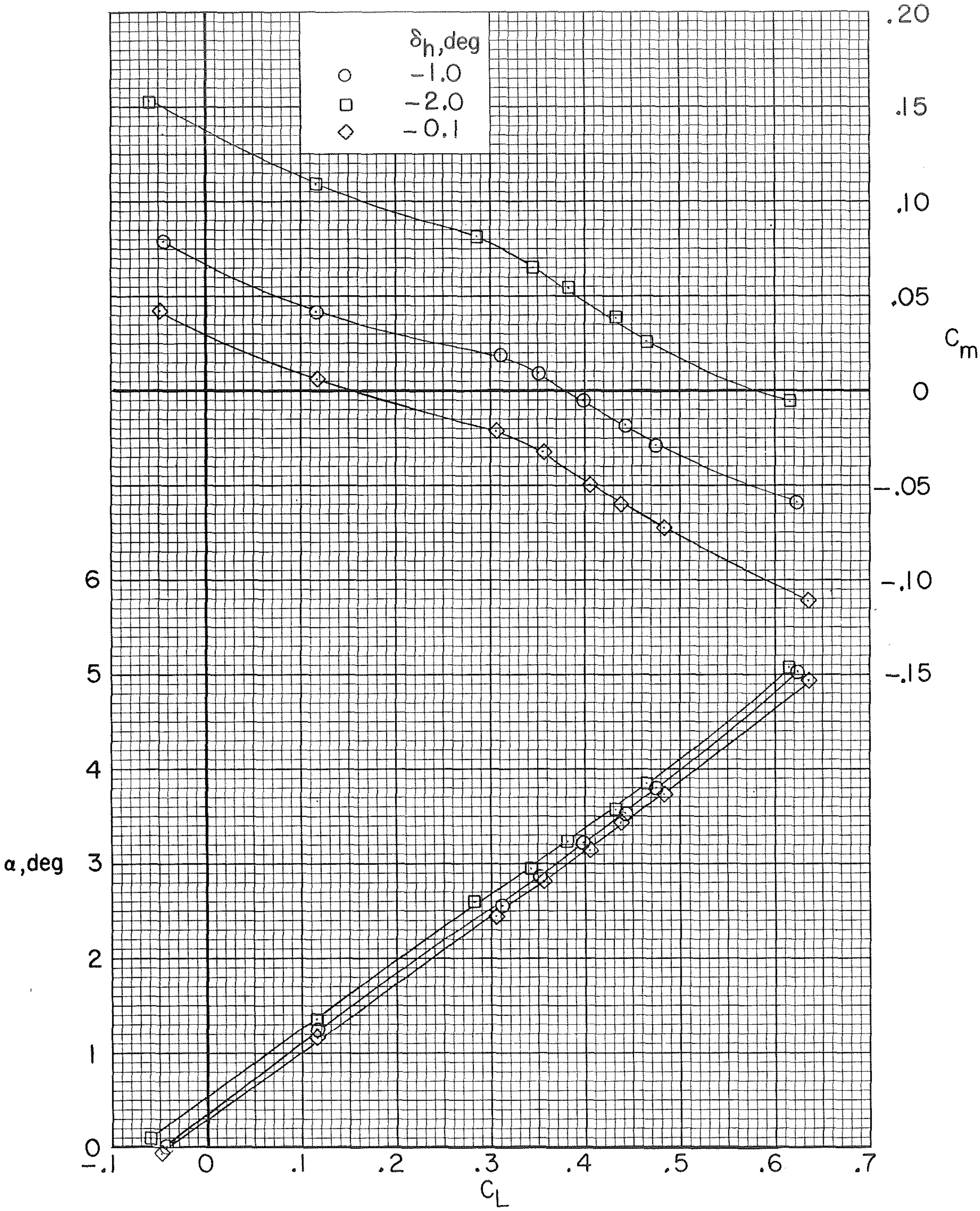

(b) M = 0.980. Concluded.

Figure 6.- Continued.

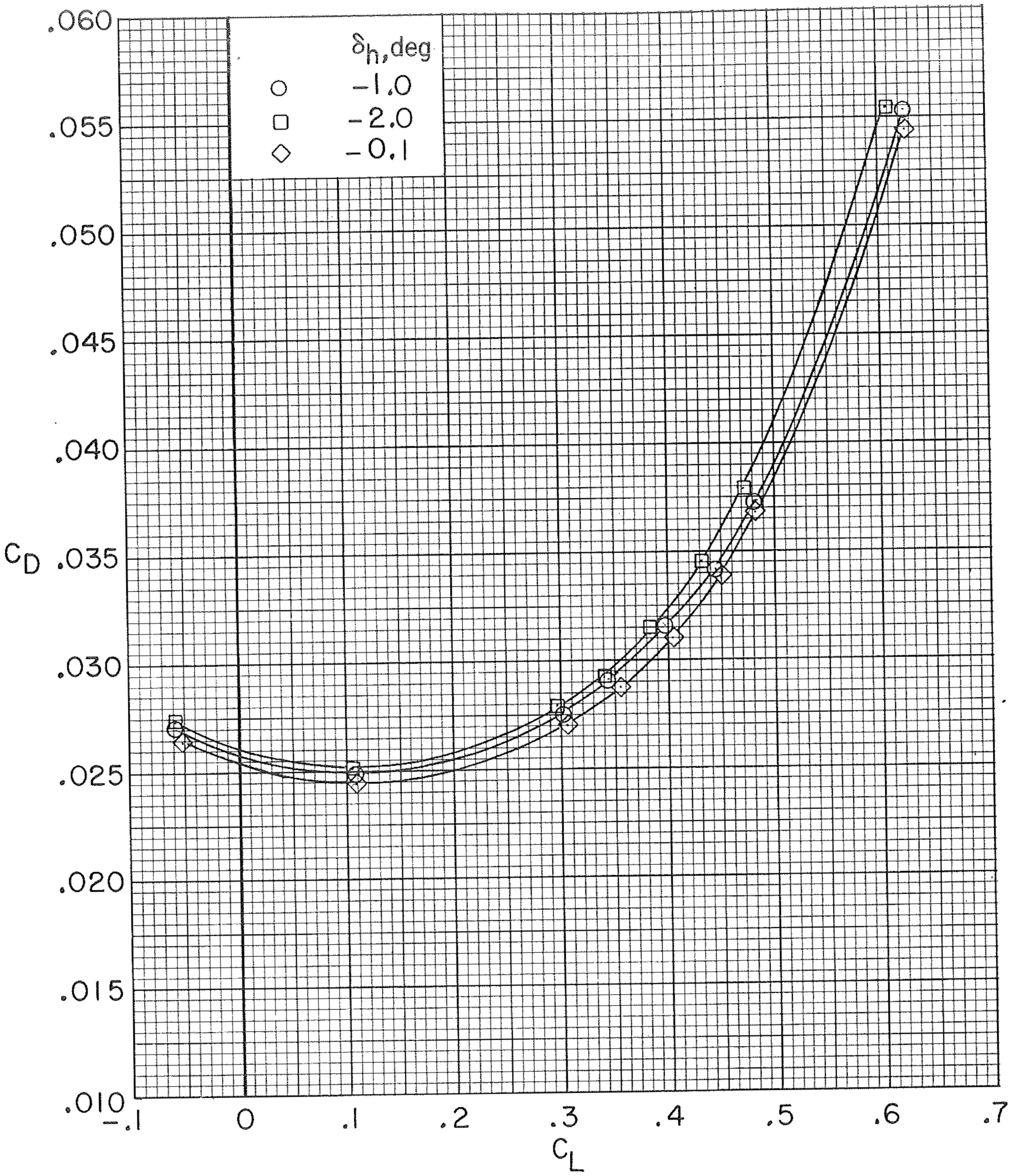

(c) M = 0.990.

Figure 6.- Continued.

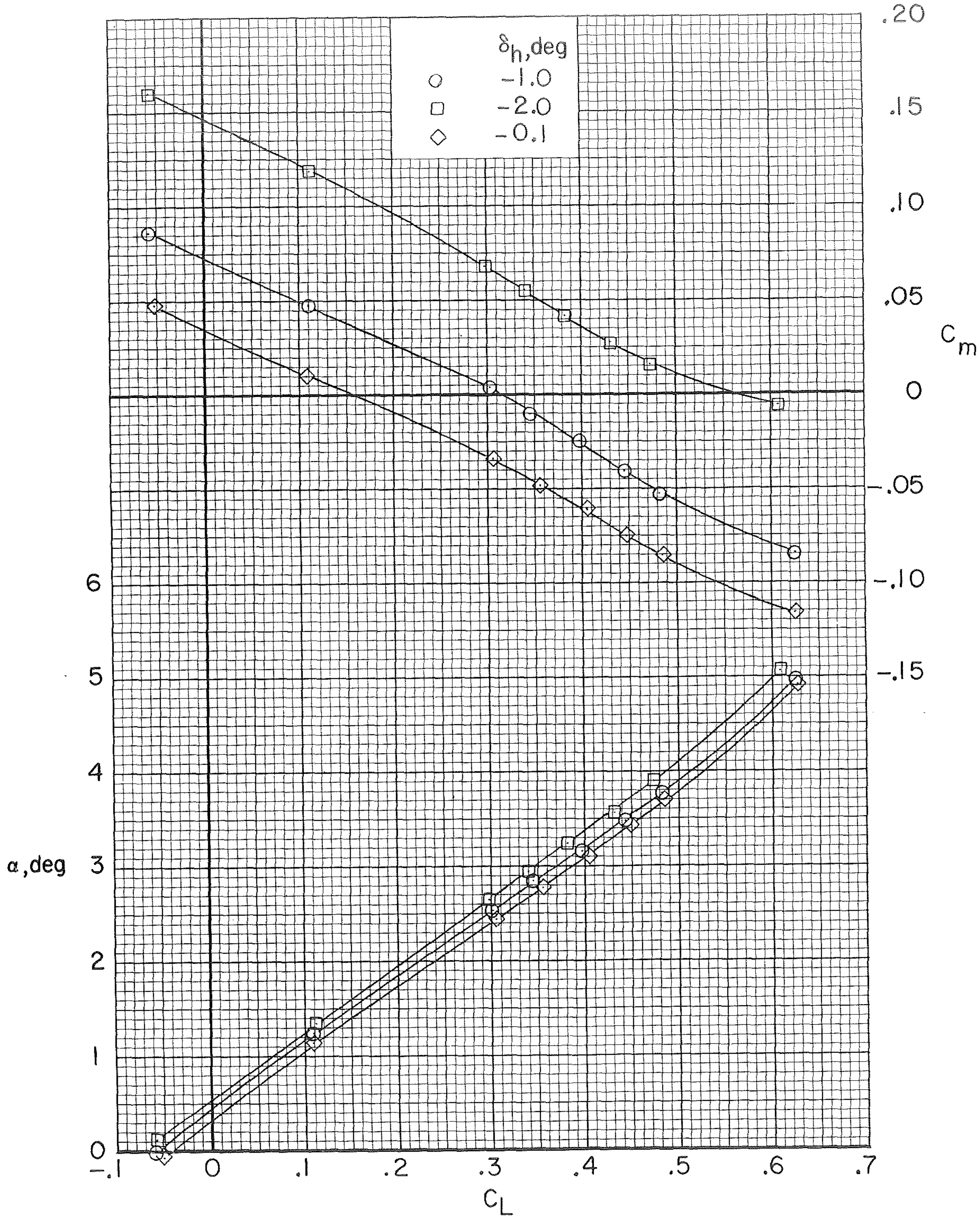

(c) M = 0.990. Concluded.

Figure 6.- Continued.

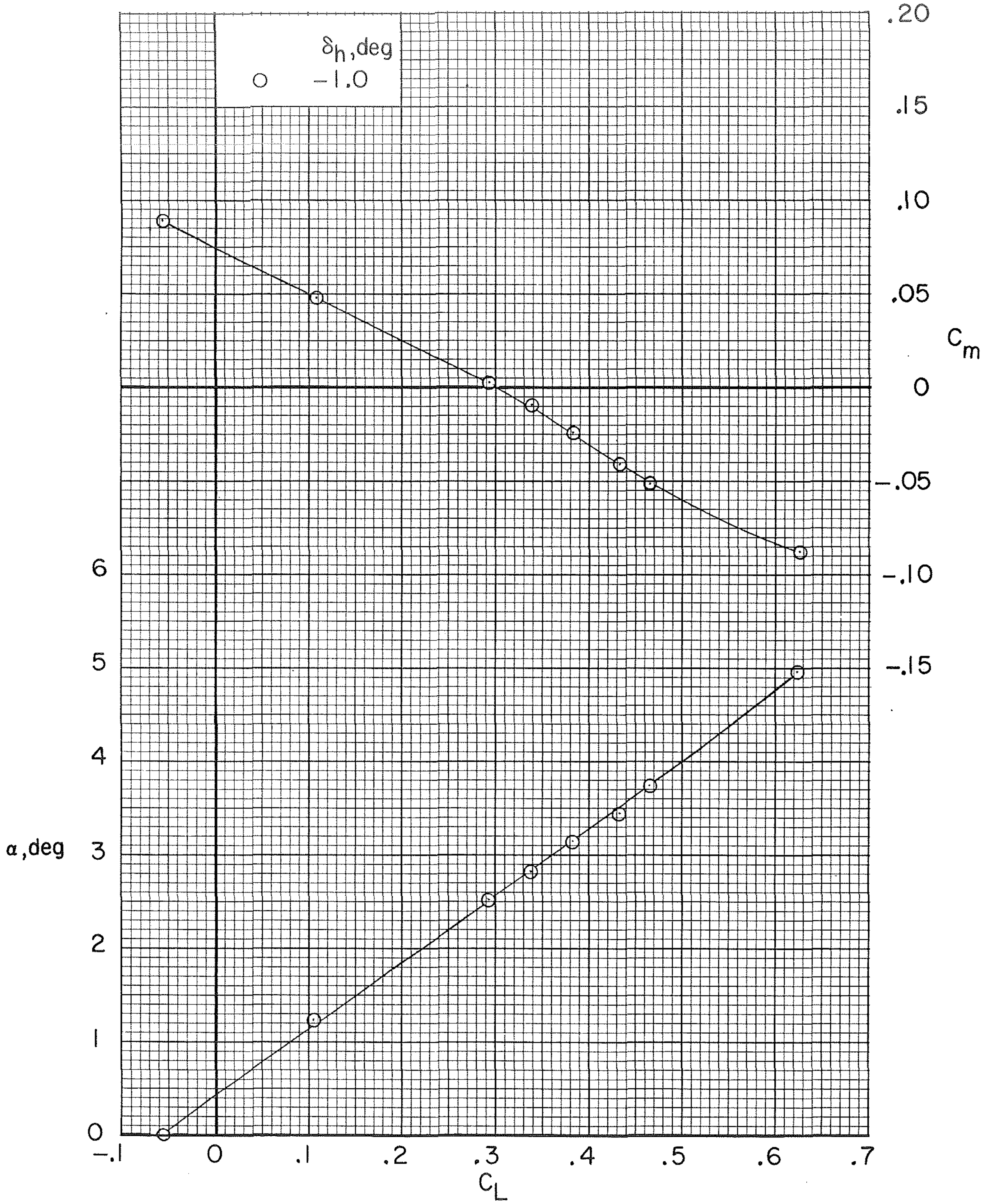

(d) M = 0.995.

Figure 6.- Continued.

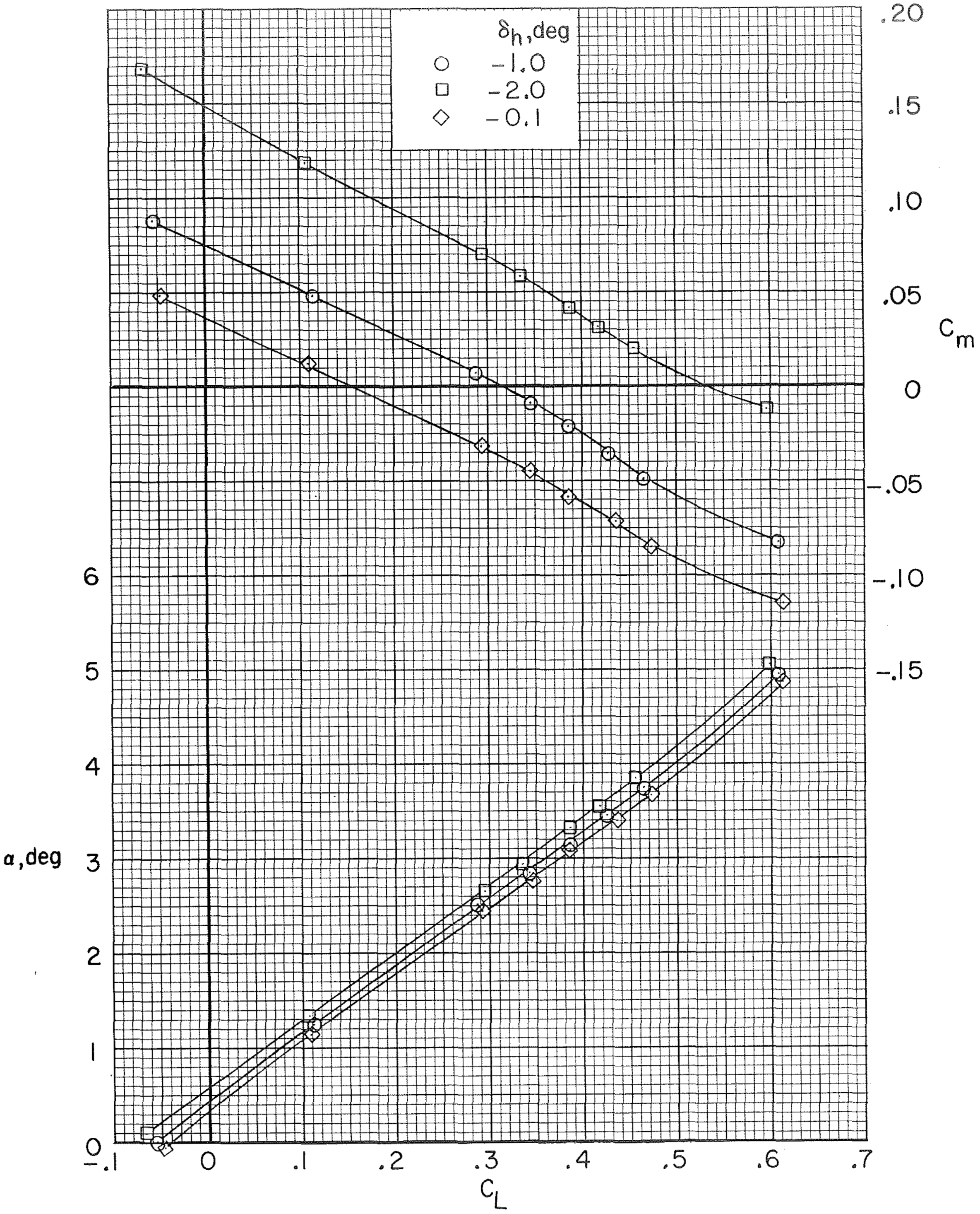

(e) M = 1.000.

Figure 6.- Continued.

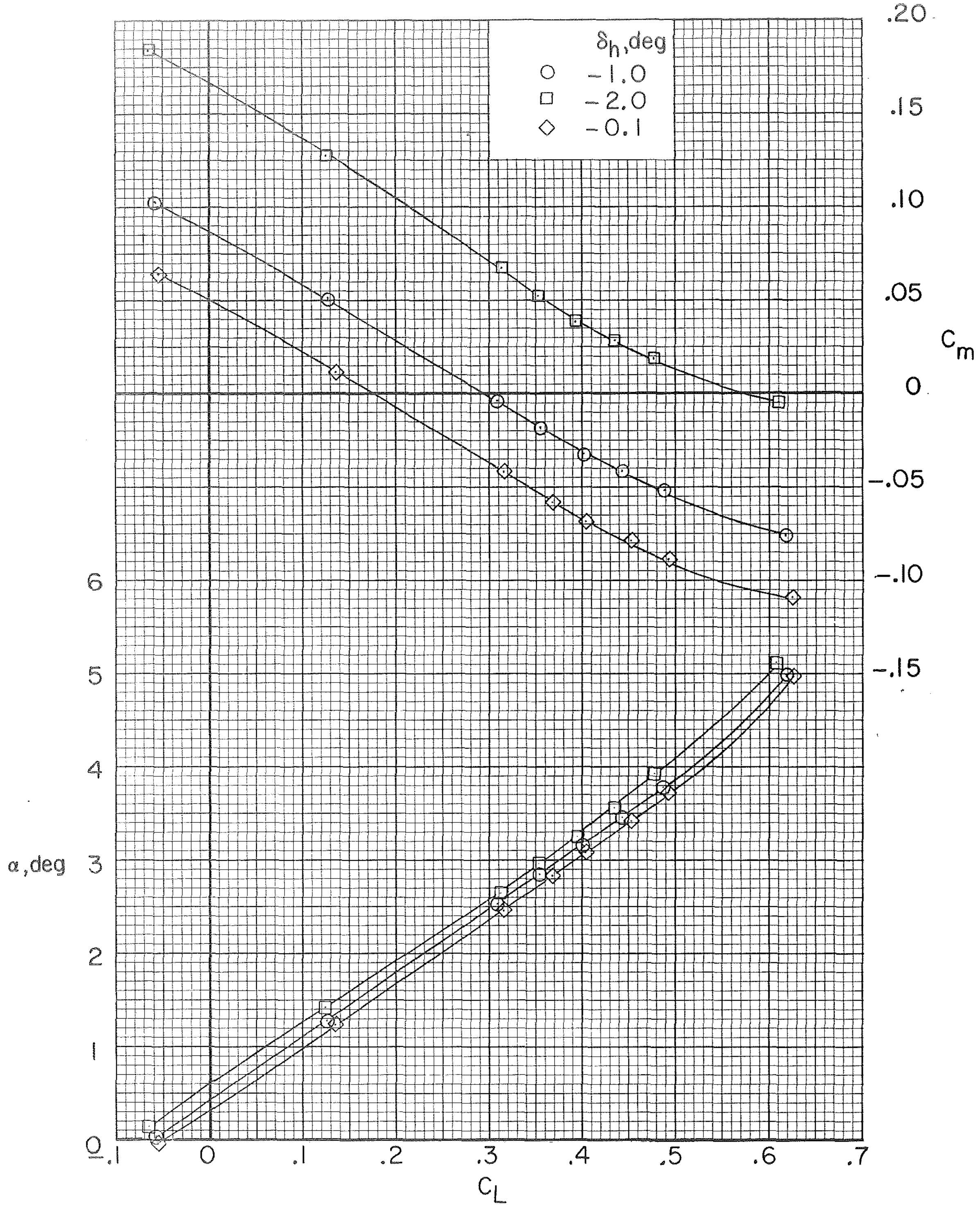

(f) M = 1.010.

Figure 6.- Concluded.

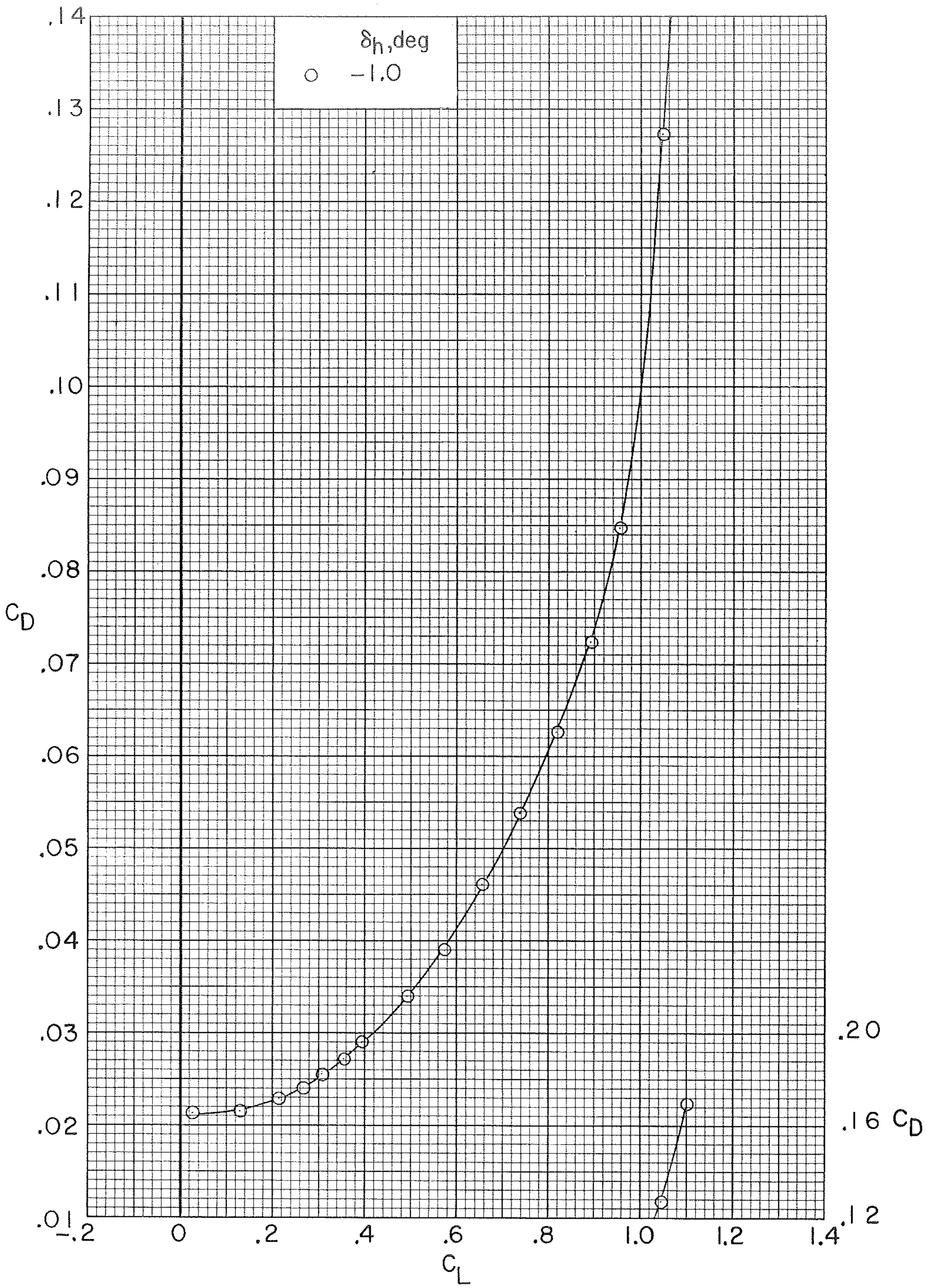

(a) M = 0.250.

Figure 7.- Longitudinal aerodynamic characteristics with type II transition, except for flagged symbols, which are for type I transition. $\beta = 0^{\circ}$.

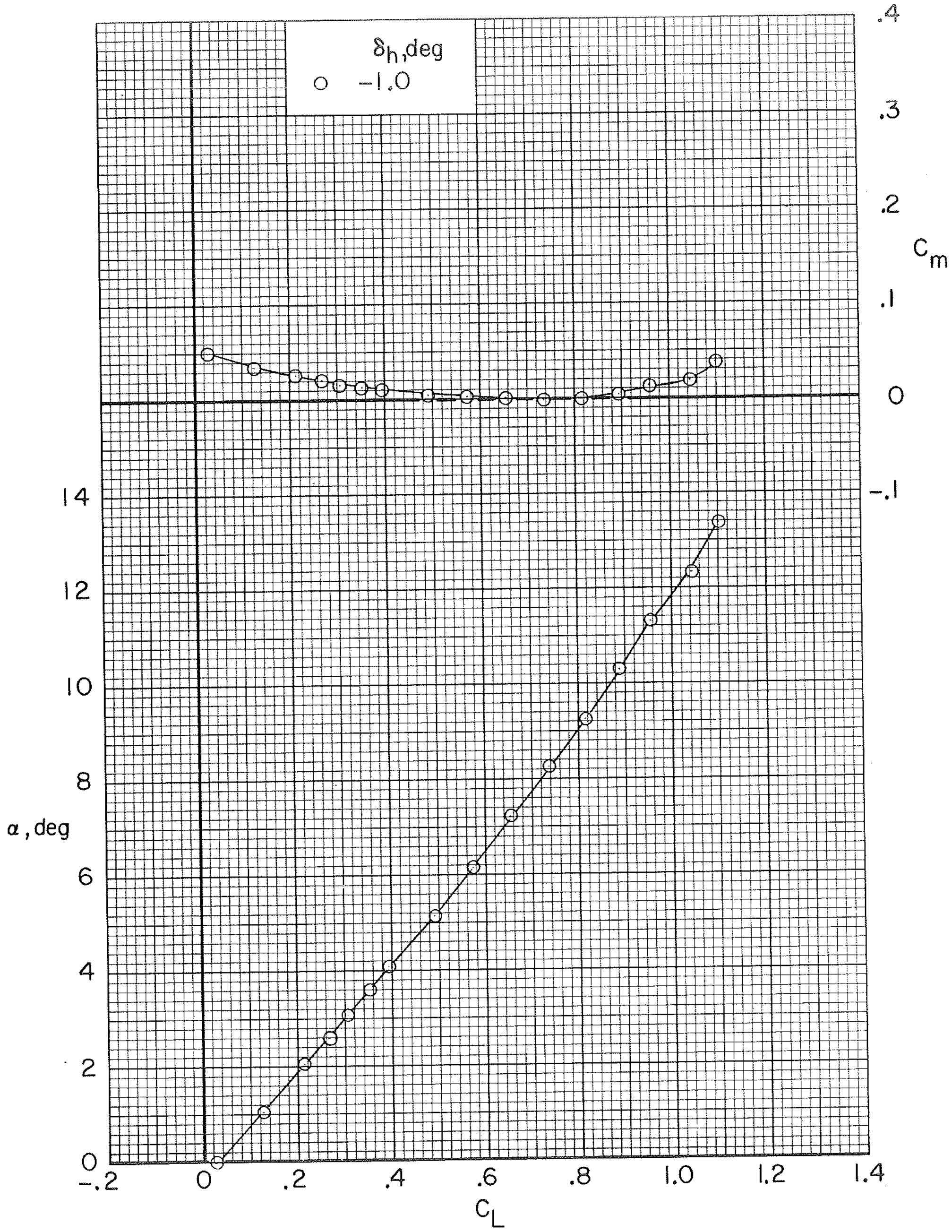

(a) M = 0.250. Concluded.

Figure 7.- Continued.

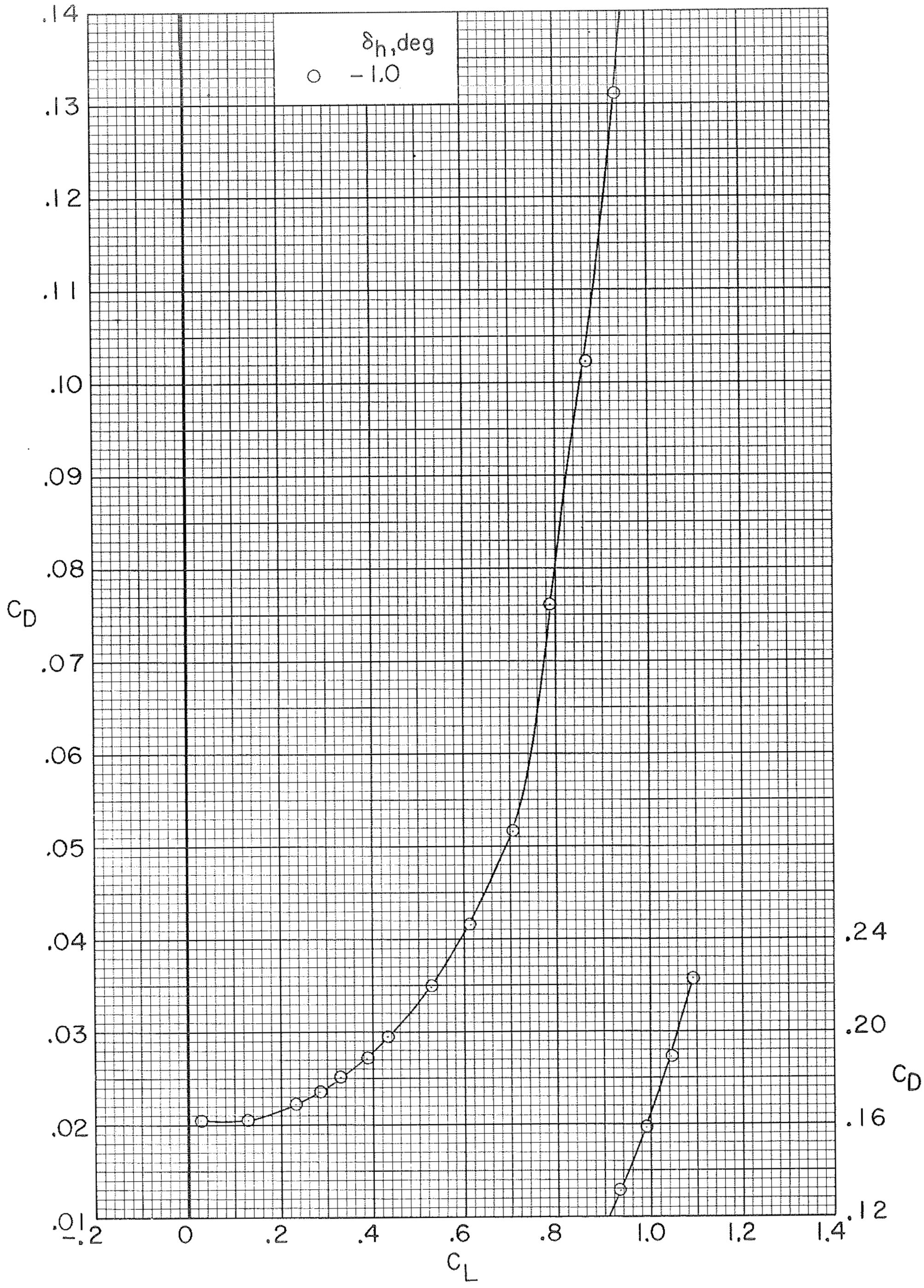

(b) M = 0.500.

Figure 7.- Continued.

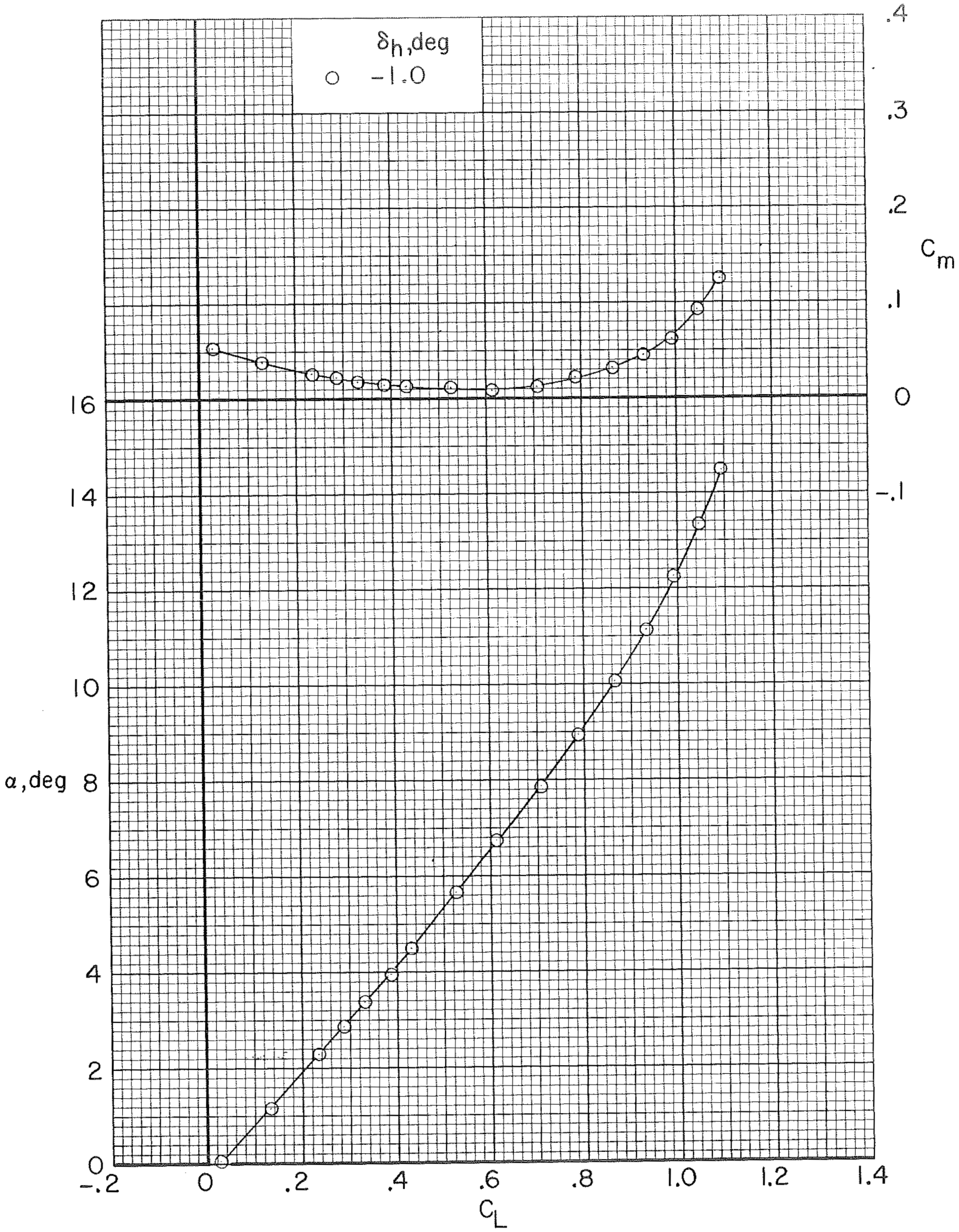

(b) M = 0.500. Concluded.

Figure 7.- Continued.

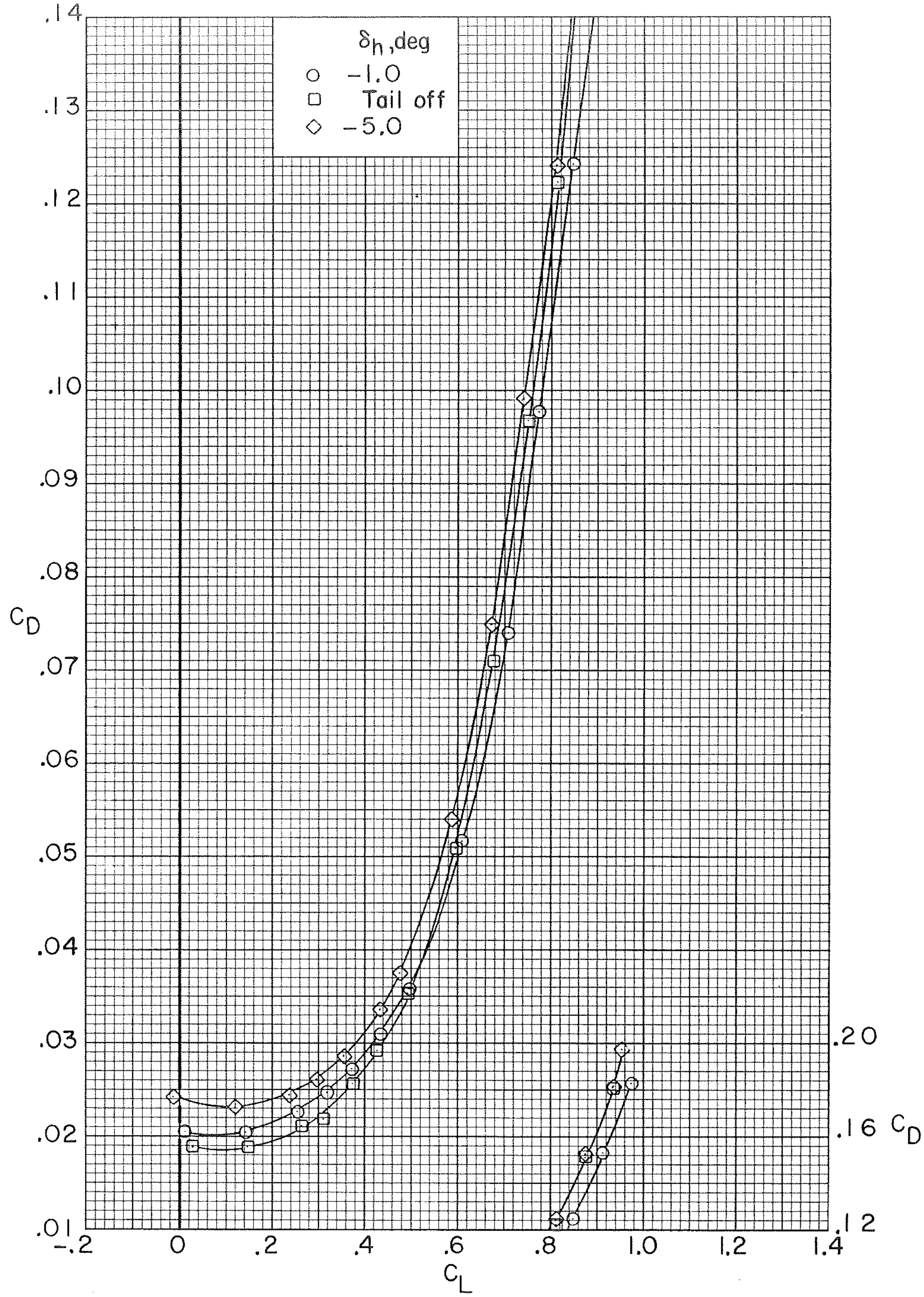

(c) M = 0.800.

Figure 7.- Continued.

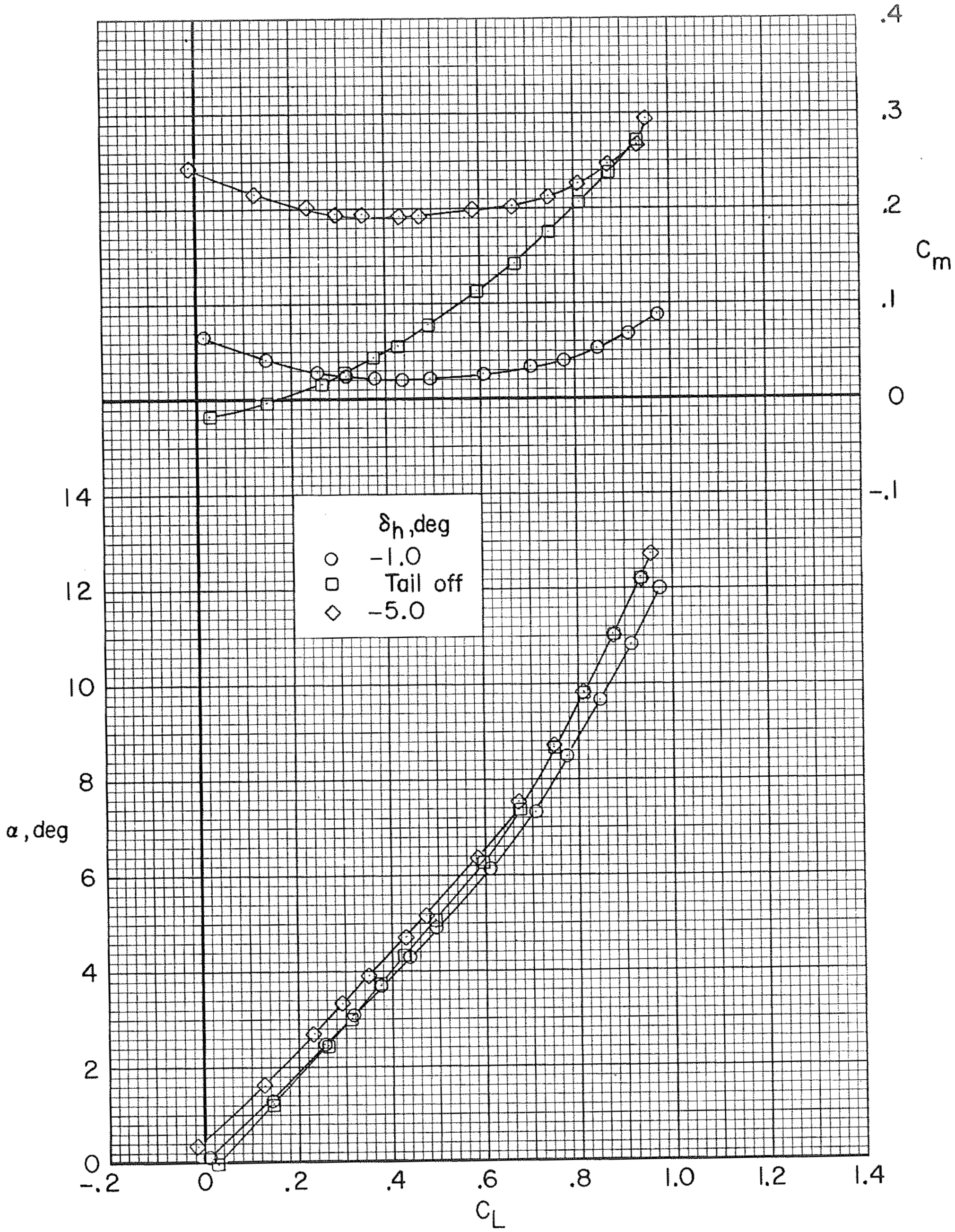

(c) M = 0.800. Concluded.

Figure 7.- Continued.

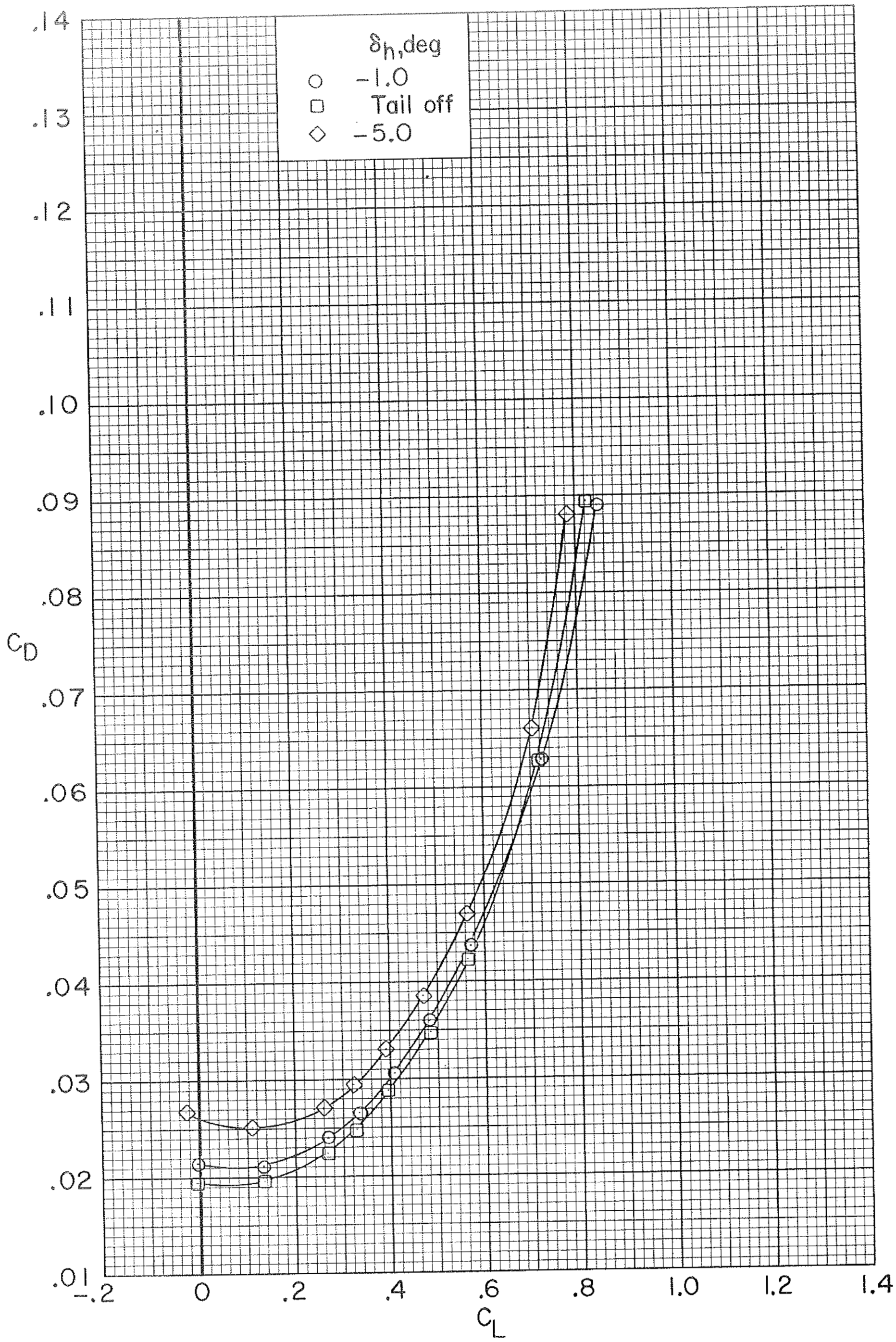

(d) M = 0.900.

Figure 7.- Continued.

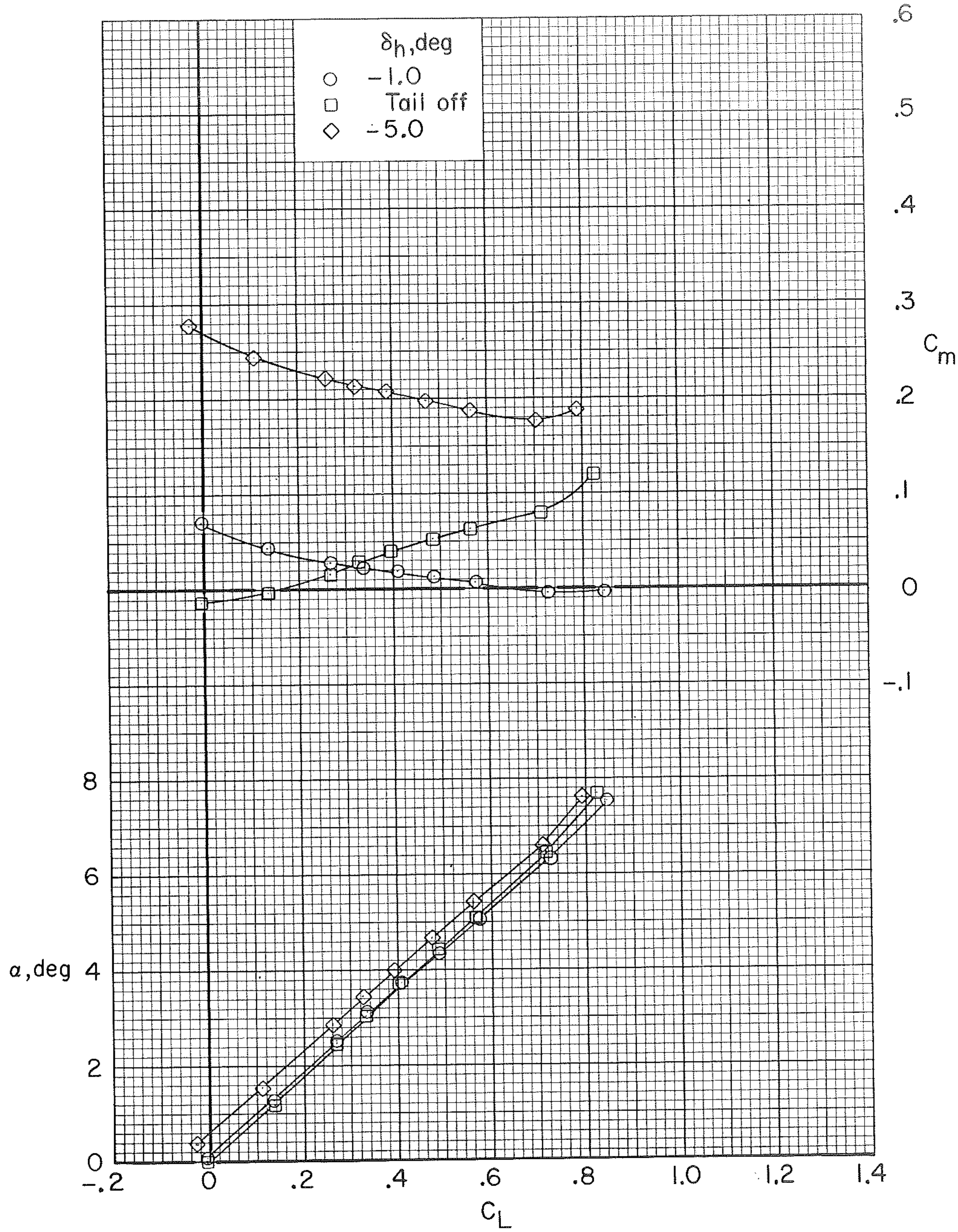

(d) M = 0.900. Concluded.

Figure 7.- Continued.

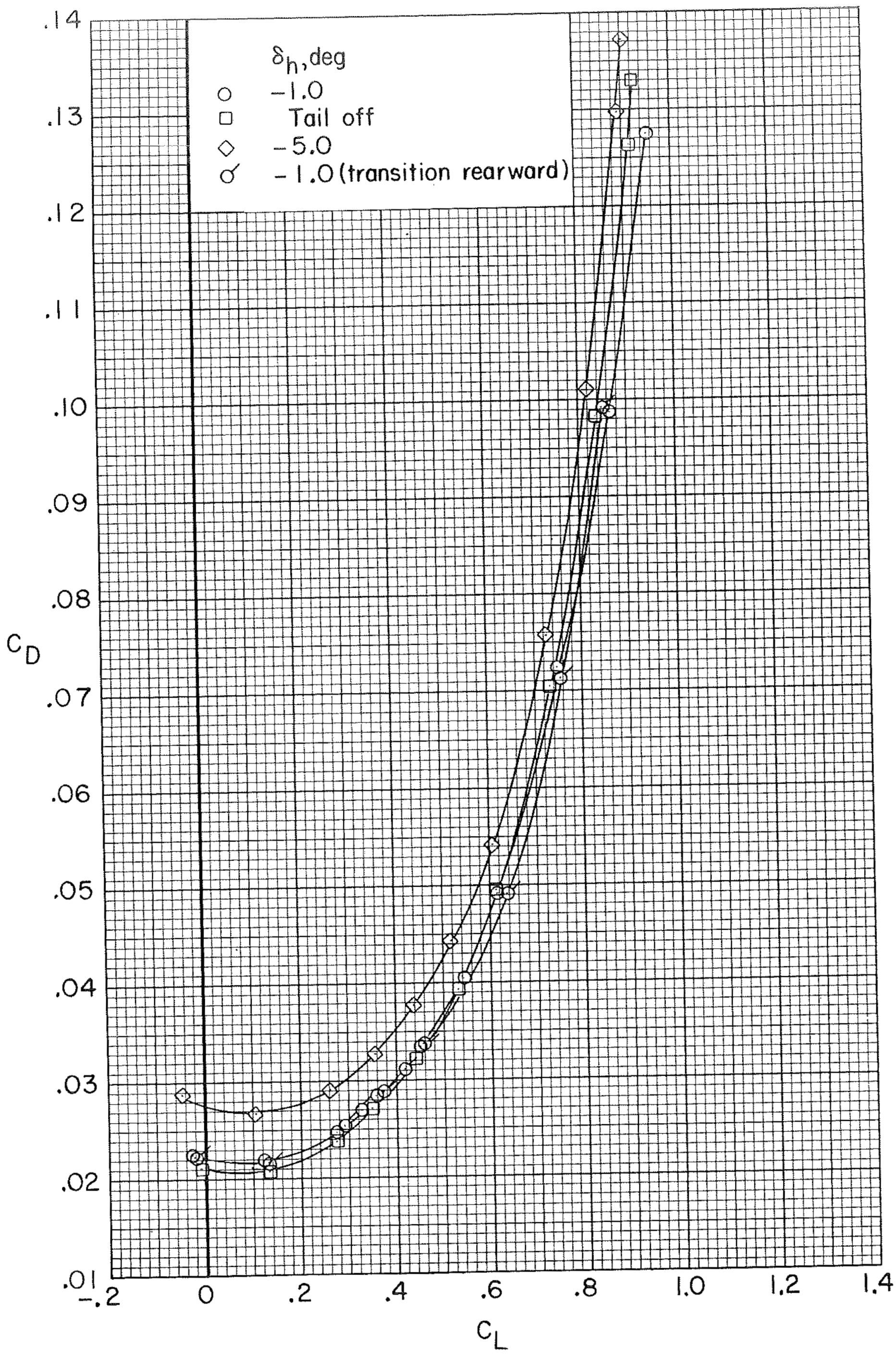

(e) $M = 0.950$.

Figure 7.- Continued.

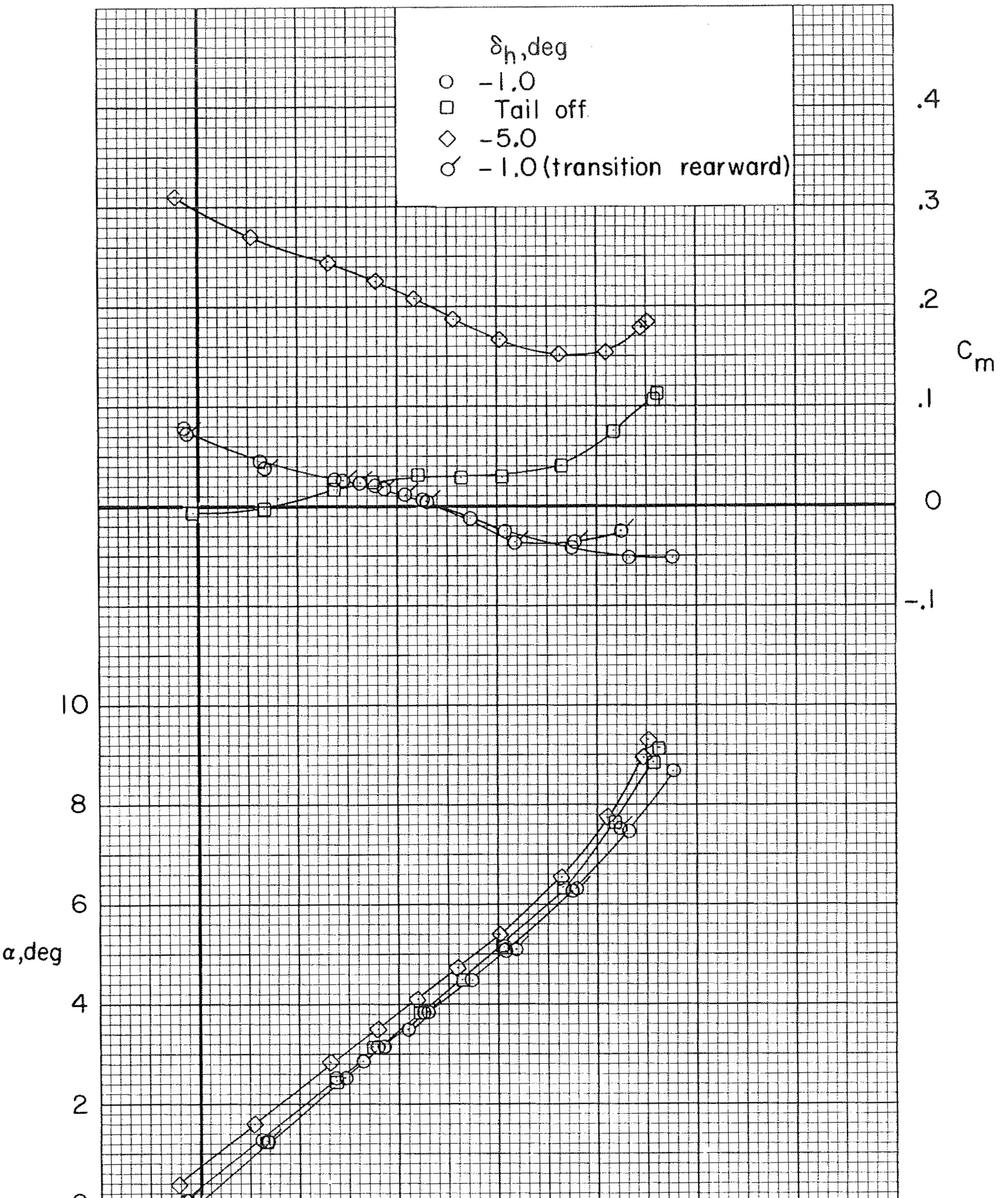

(e) M = 0.950. Concluded.

Figure 7.- Continued.

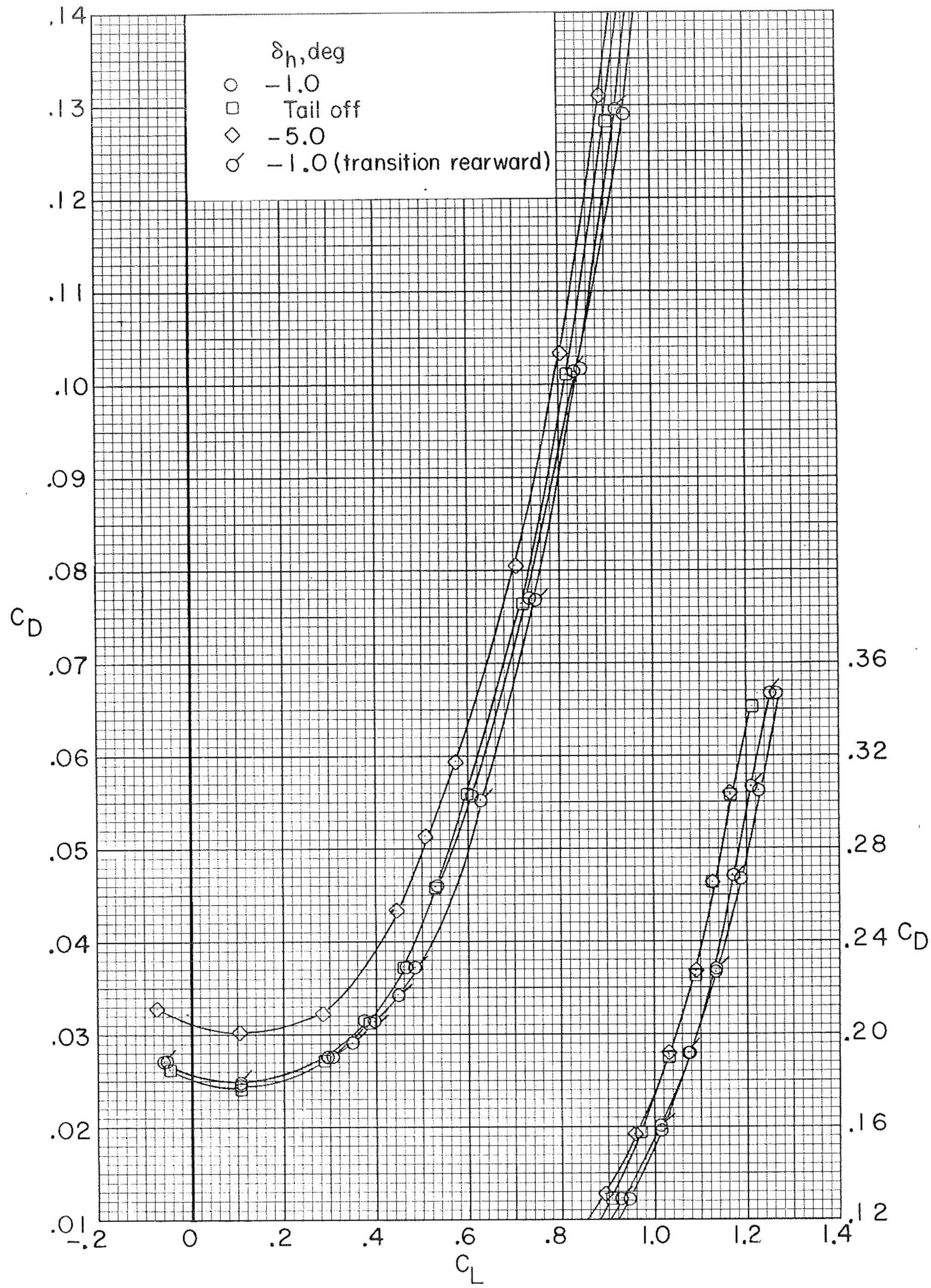

(f) M = 0.990.

Figure 7.- Continued.

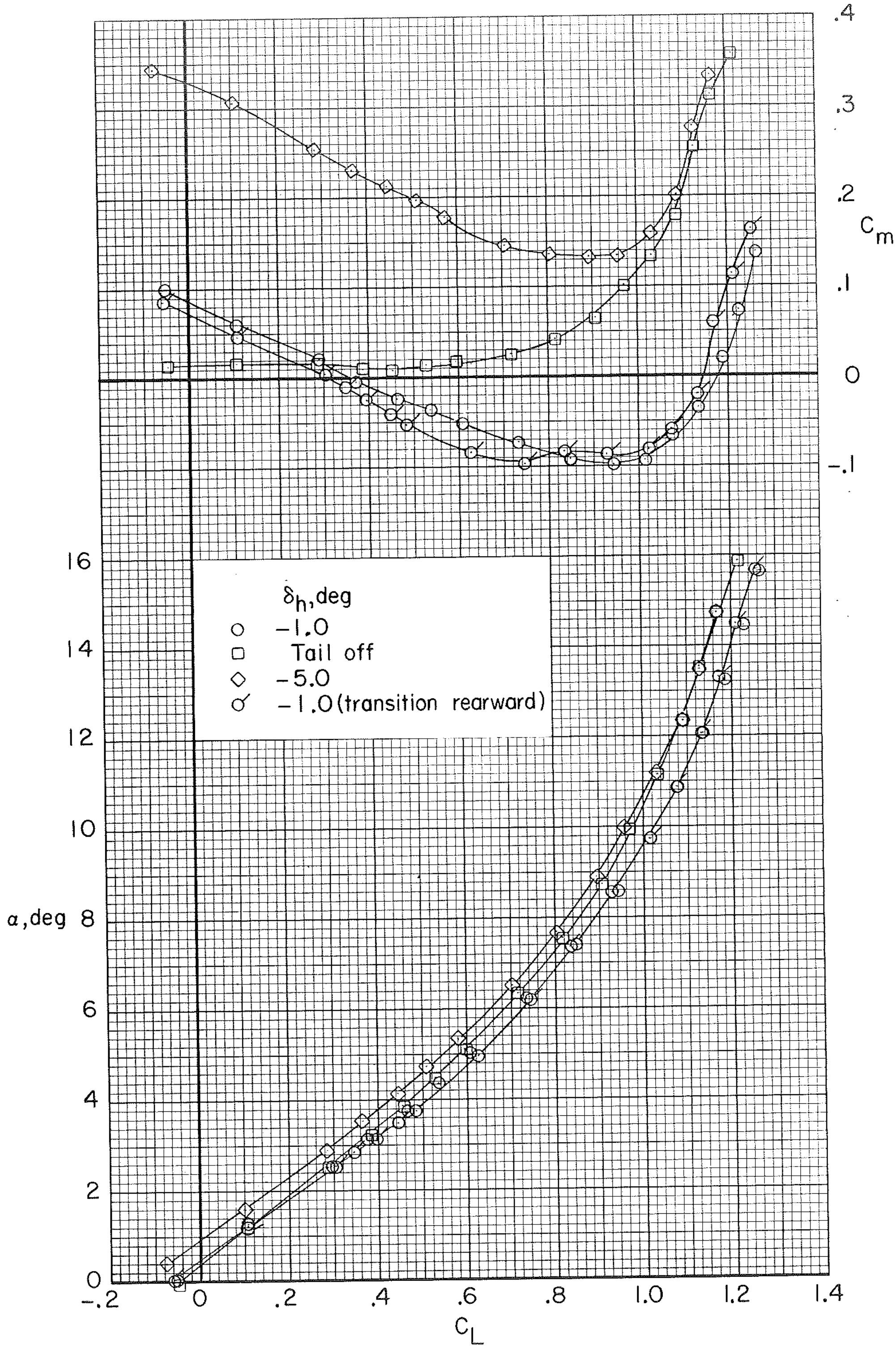

(f) M = 0.990. Concluded.

Figure 7.- Continued.

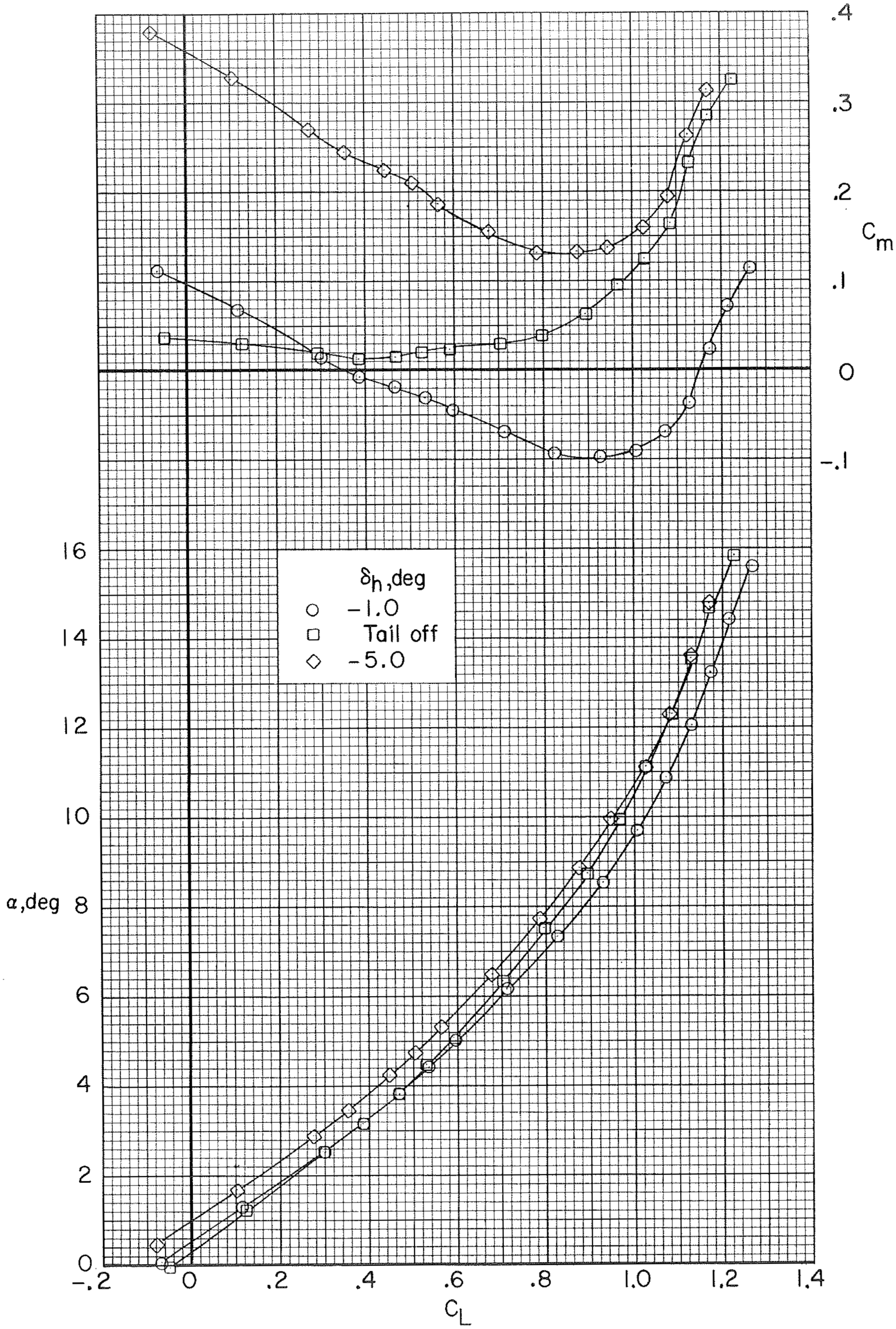

(g) M = 1.010.

Figure 7.- Concluded.

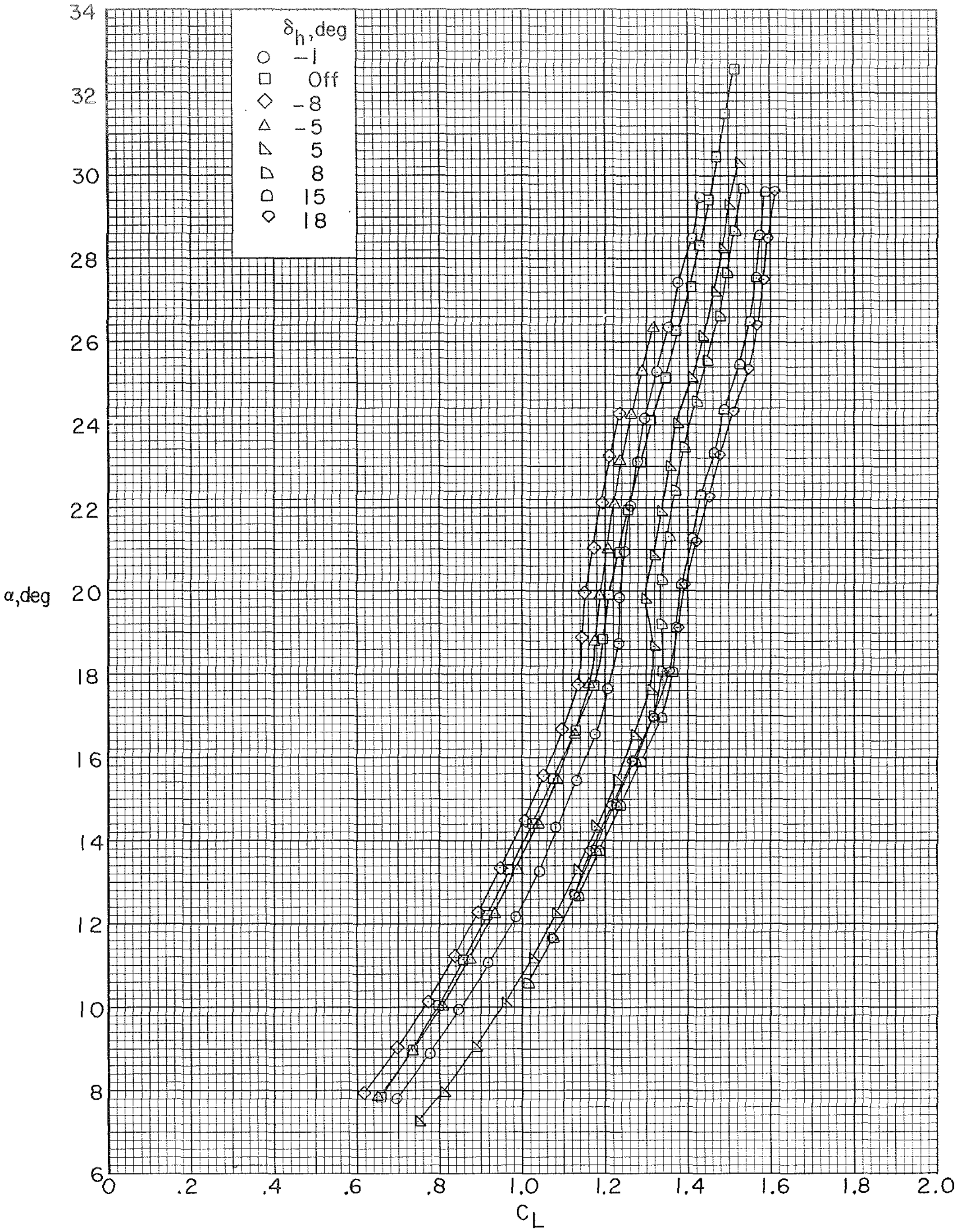

(a) M = 0.250.

Figure 8.- Effect of horizontal-tail deflections on longitudinal aerodynamic characteristics at high angles of attack. Transition type II; $\beta = 0^{\circ}$.

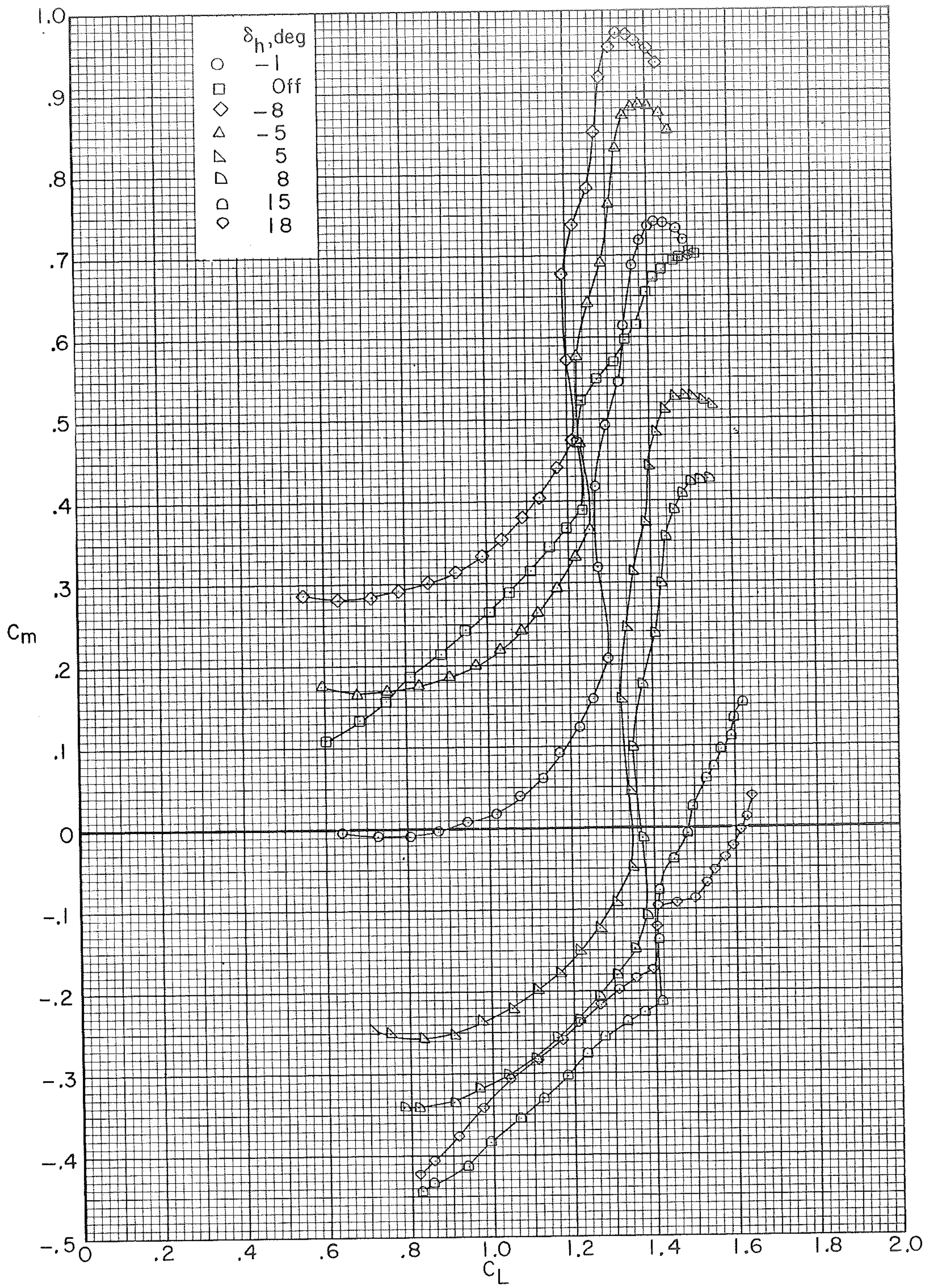

(a) M = 0.250. Concluded.

Figure 8.- Continued.

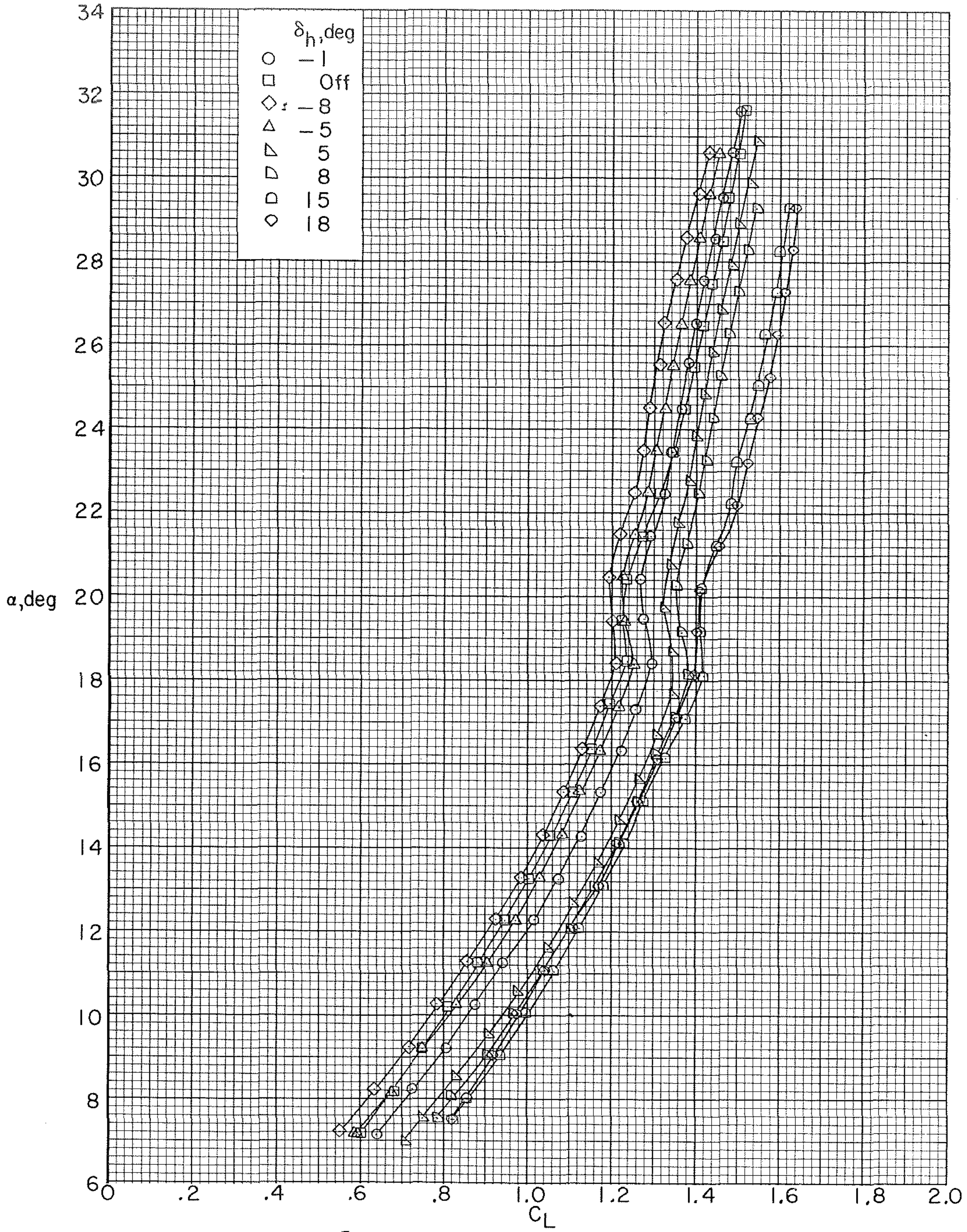

(b) M = 0.500.

Figure 8.- Continued.

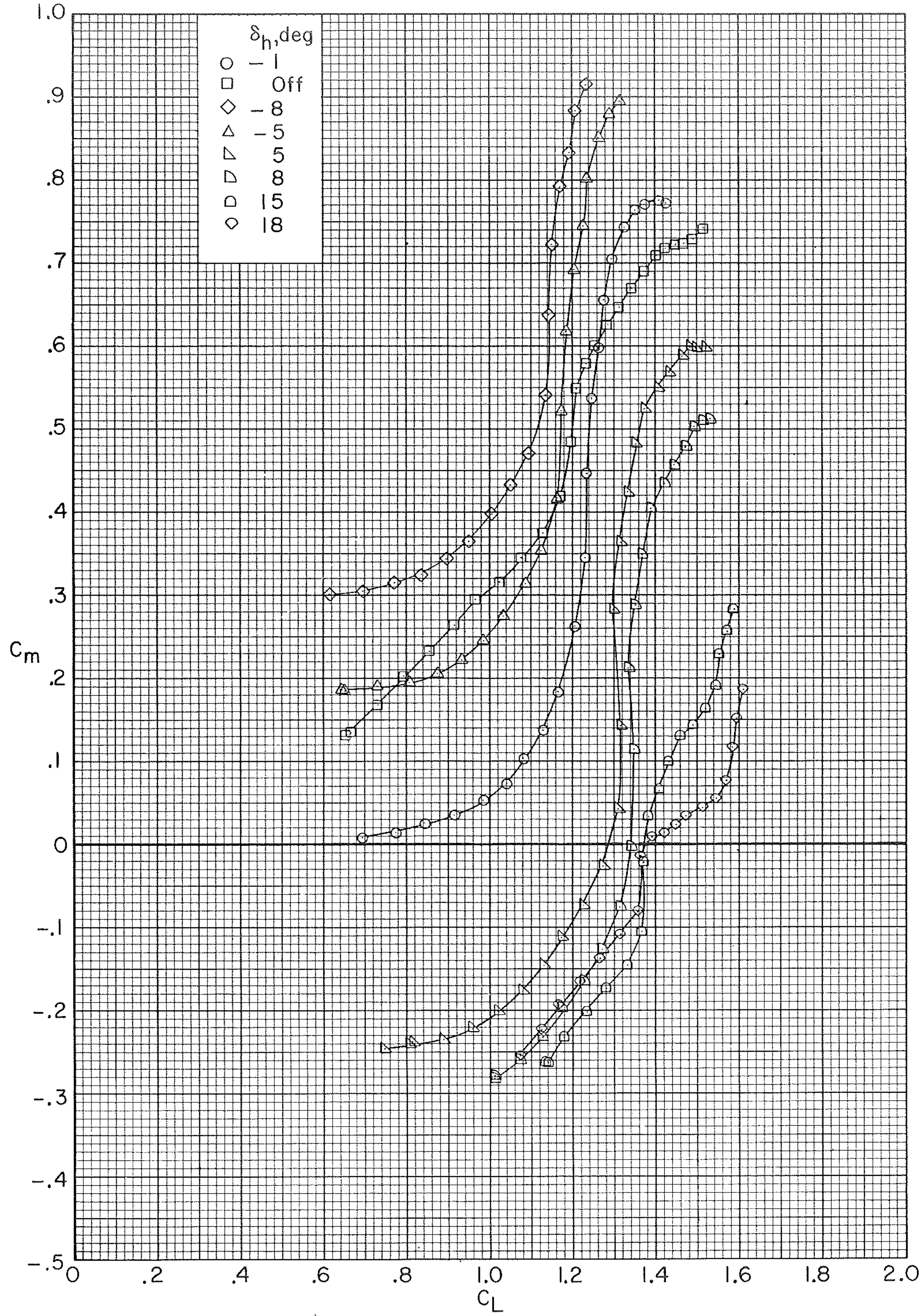

(b) M = 0.500. Concluded.

Figure 8.- Concluded.

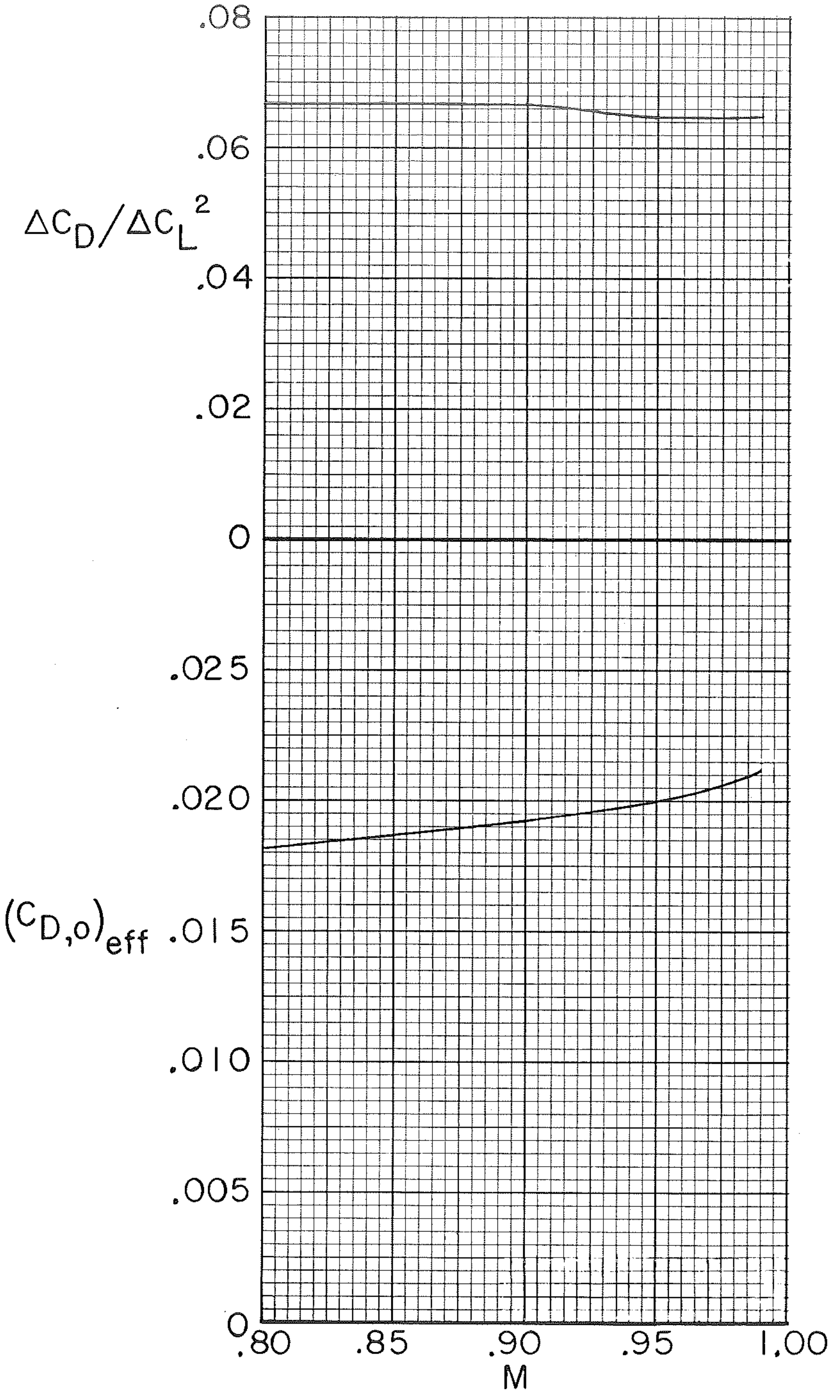

(a) Variation of drag-due-to-lift parameter and effective zero-lift drag with Mach number.

Figure 9.- Variation of longitudinal aerodynamic characteristics with Mach number. $\beta = 0^{\circ}$; $\delta_h = -1.0^{\circ}$.

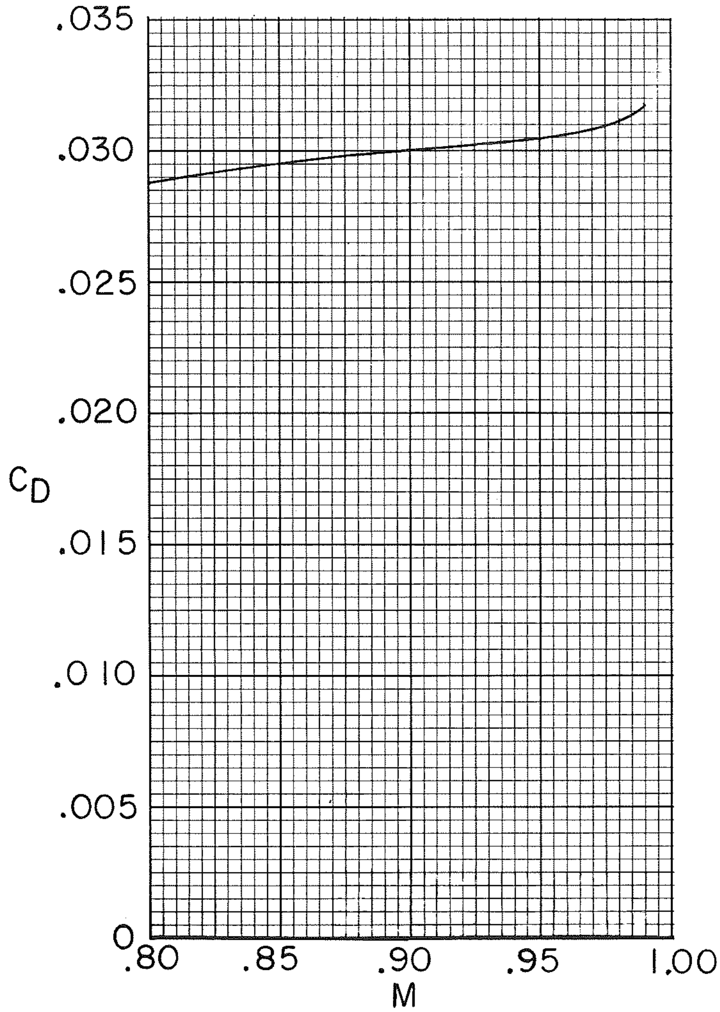

(b) Variation with Mach number of drag coefficient at a lift coefficient of 0.40.

Figure 9.- Continued.

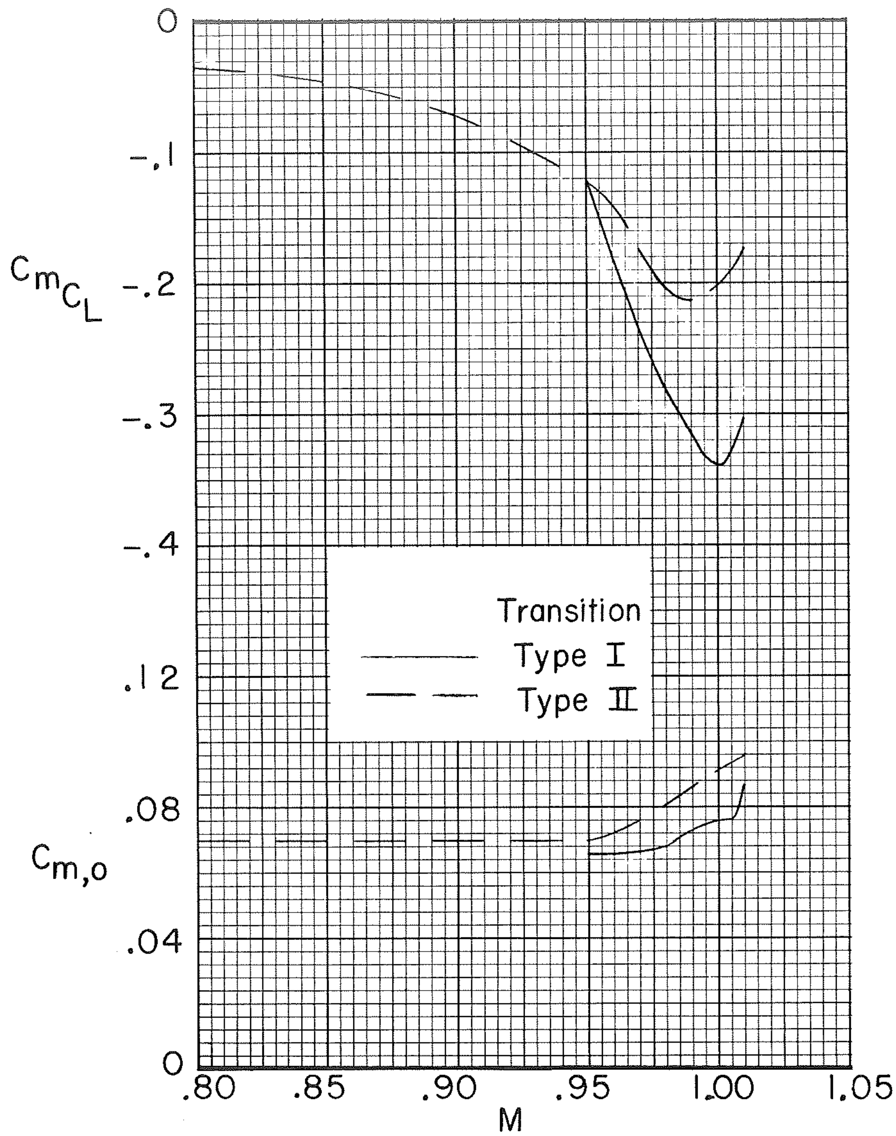

(c) Variation with Mach number of longitudinal stability parameter at lift coefficient of 0.40 and of pitching-moment coefficient at zero lift.

Figure 9.- Continued.

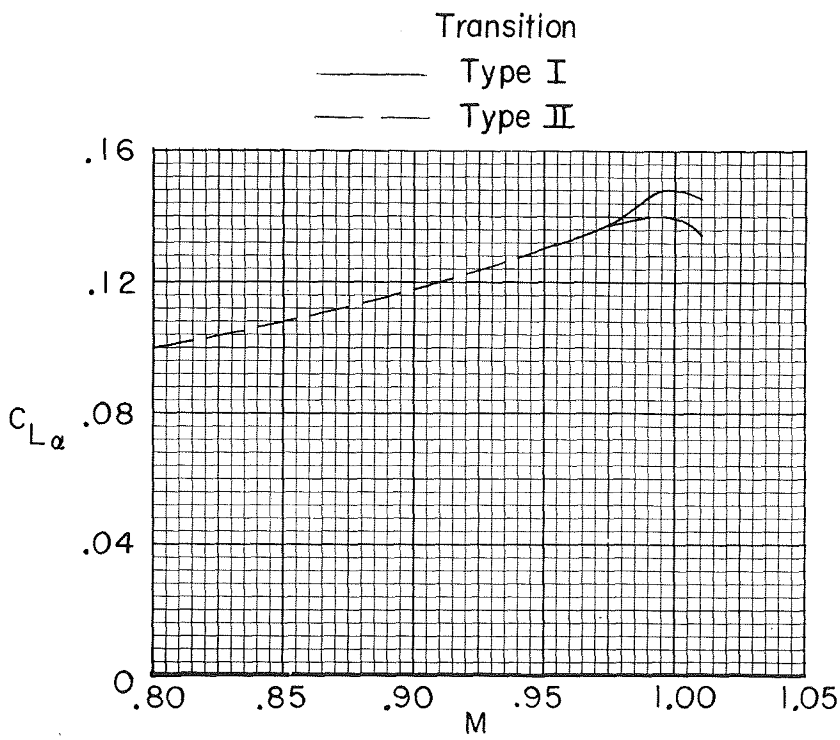

(d) Variation of lift-curve slope with Mach number at lift coefficient of 0.40.

Figure 9.- Concluded.

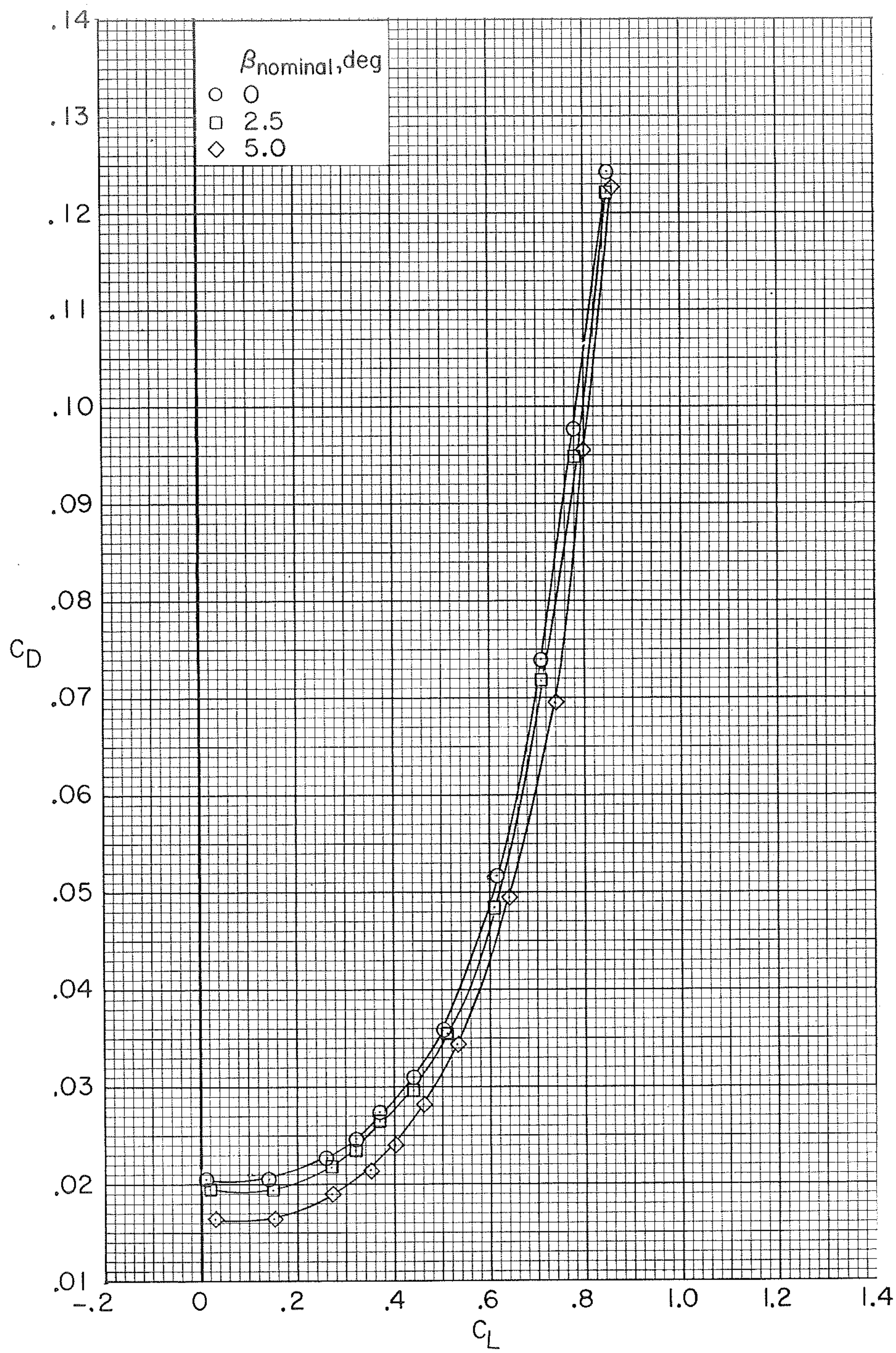

(a) M = 0.800.

Figure 10.- Effect of sideslip on longitudinal aerodynamic characteristics. Transition type I; $\delta_h = -1.0^\circ$.

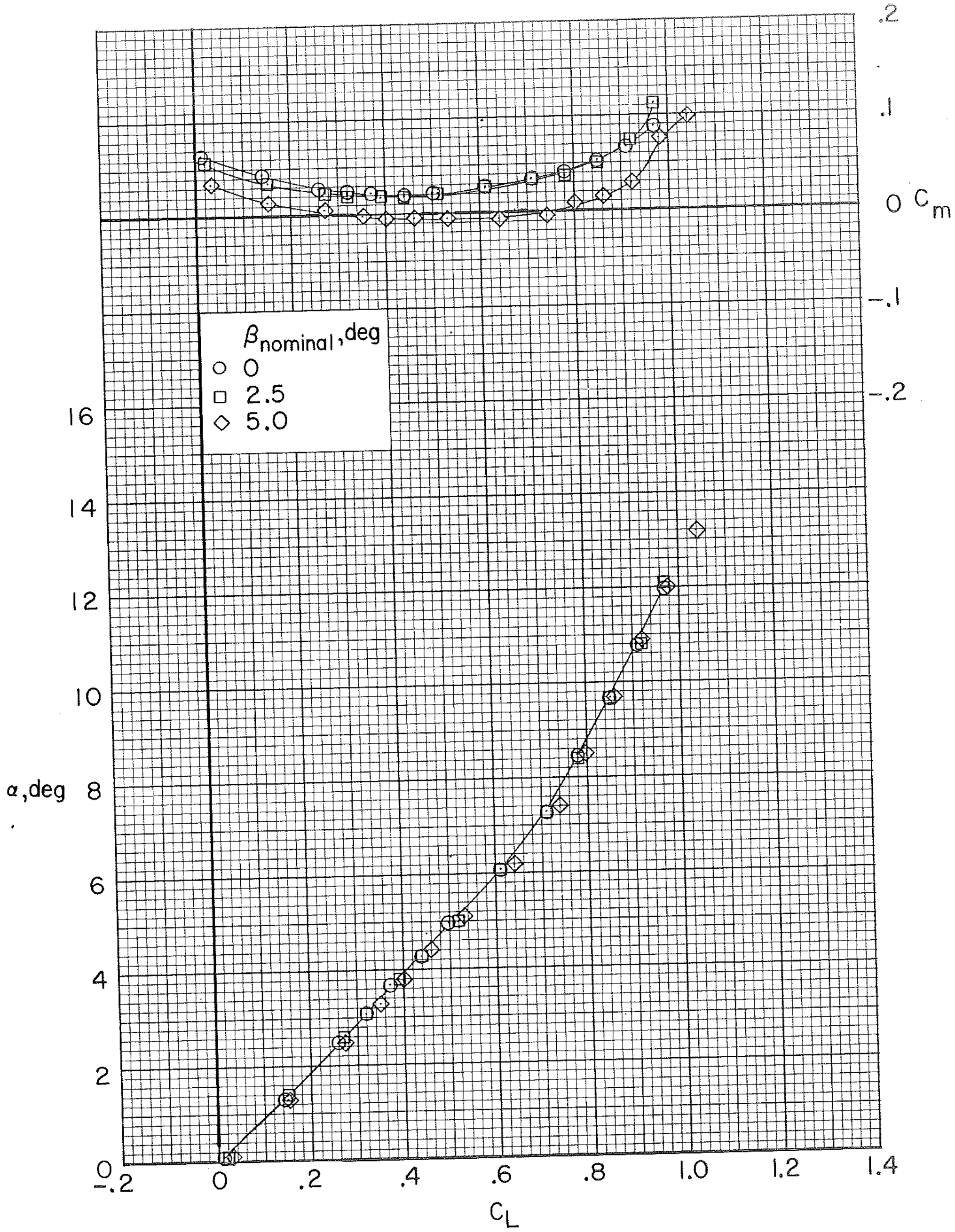

(a) M = 0.800. Concluded.

Figure 10.- Continued.

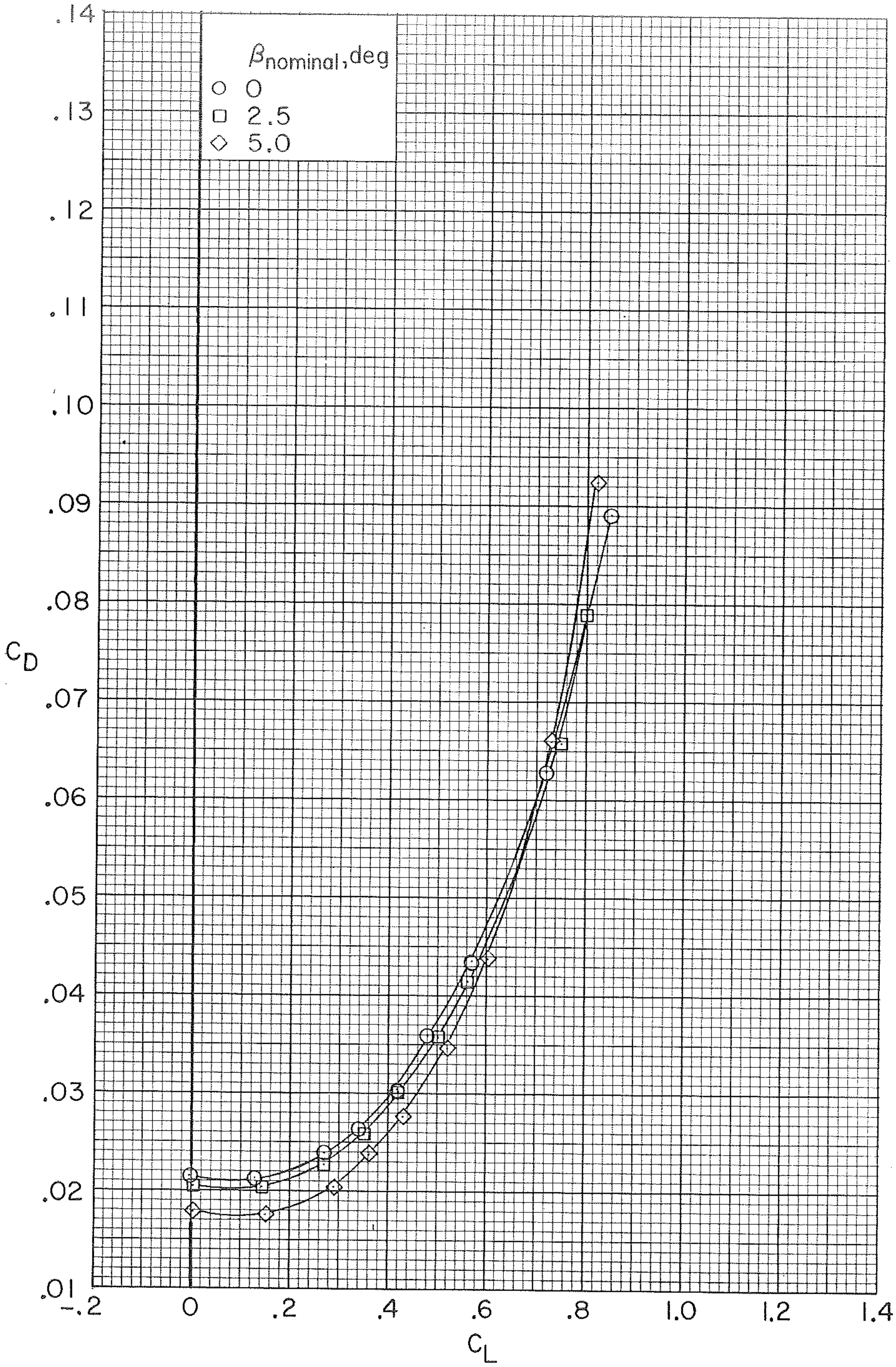

(b) M = 0.900.

Figure 10.- Continued.

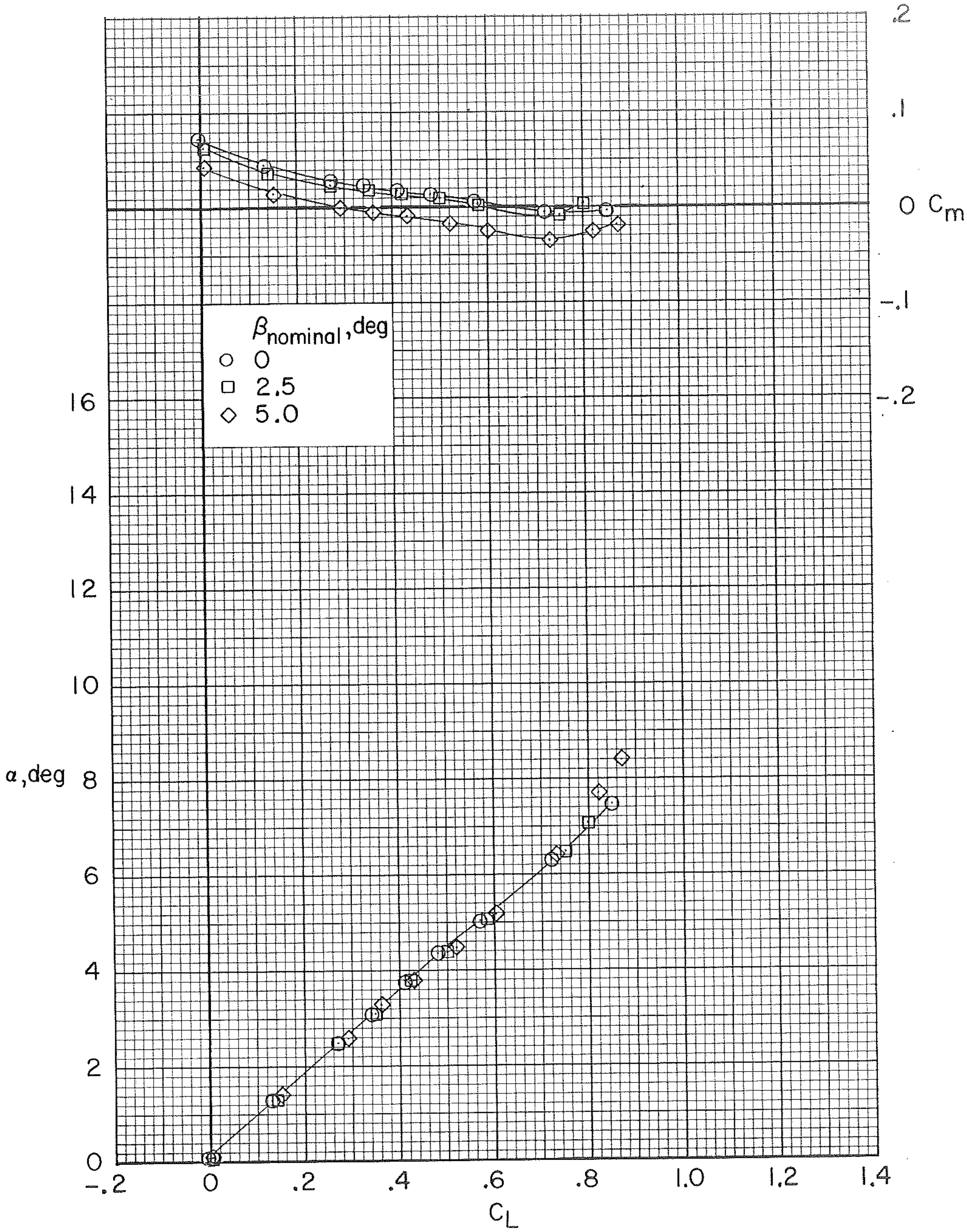

(b) M = 0.900. Concluded.

Figure 10.- Continued.

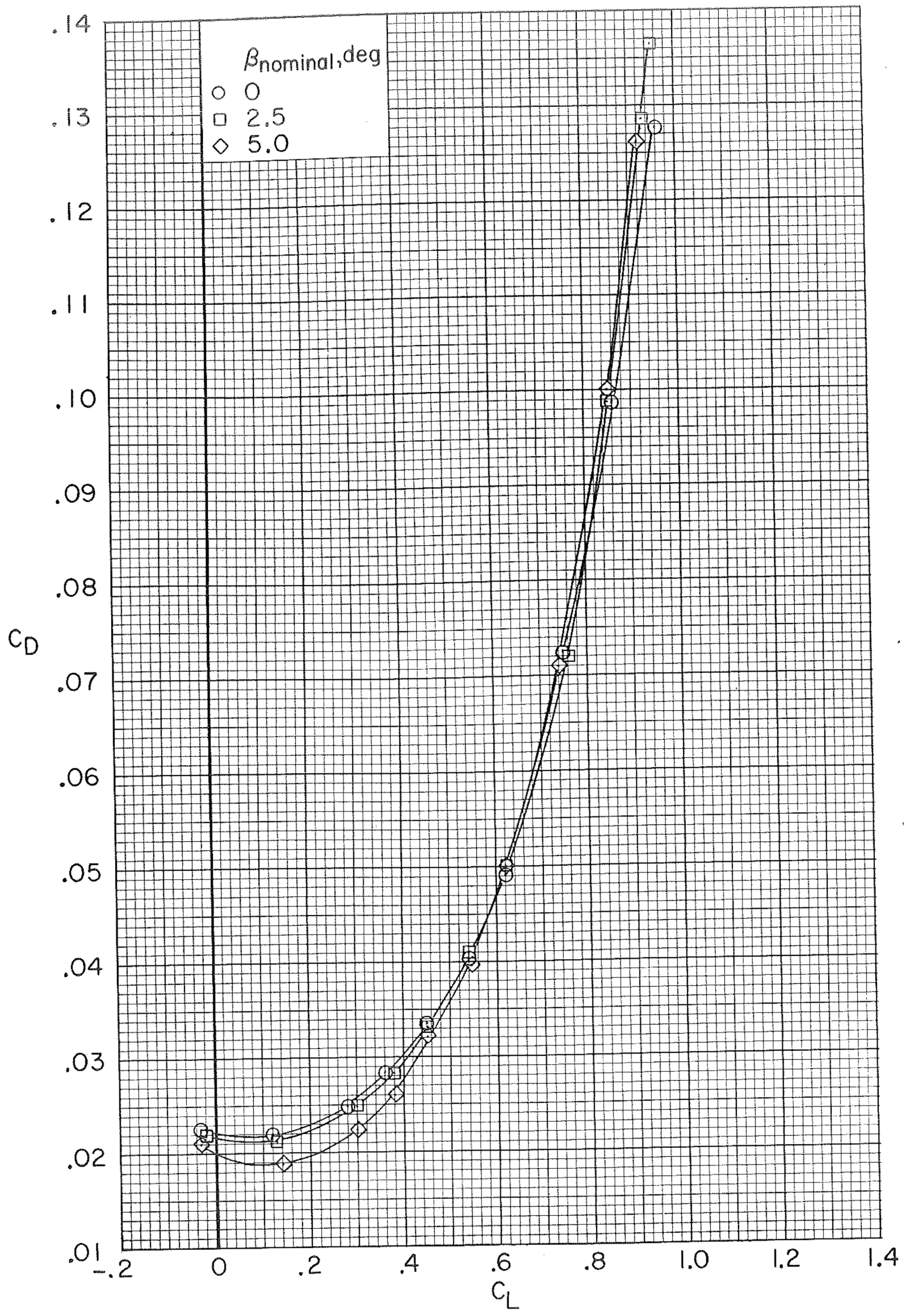

(c) M = 0.950.

Figure 10.- Continued.

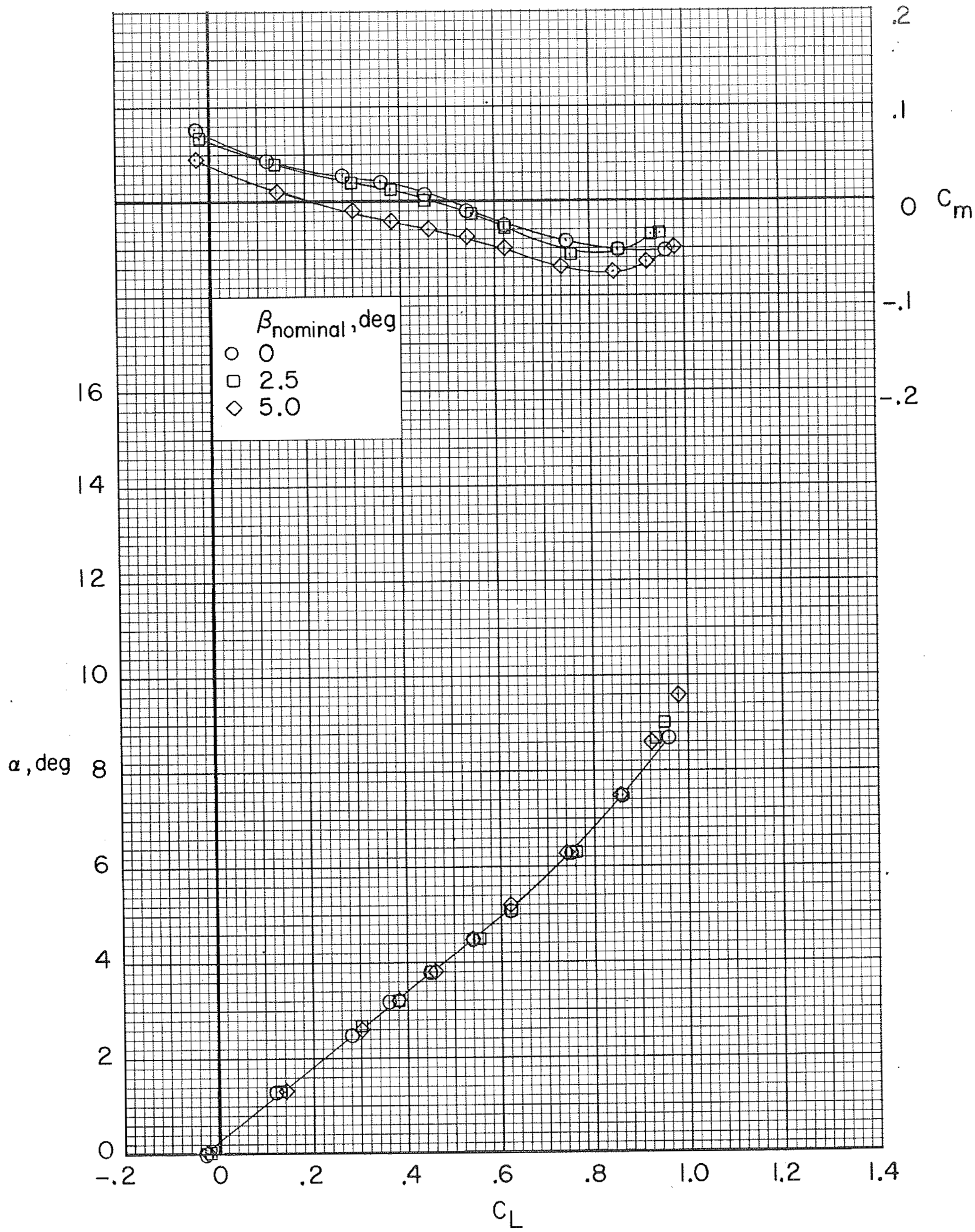

(c) M = 0.950. Concluded.

Figure 10.- Continued.

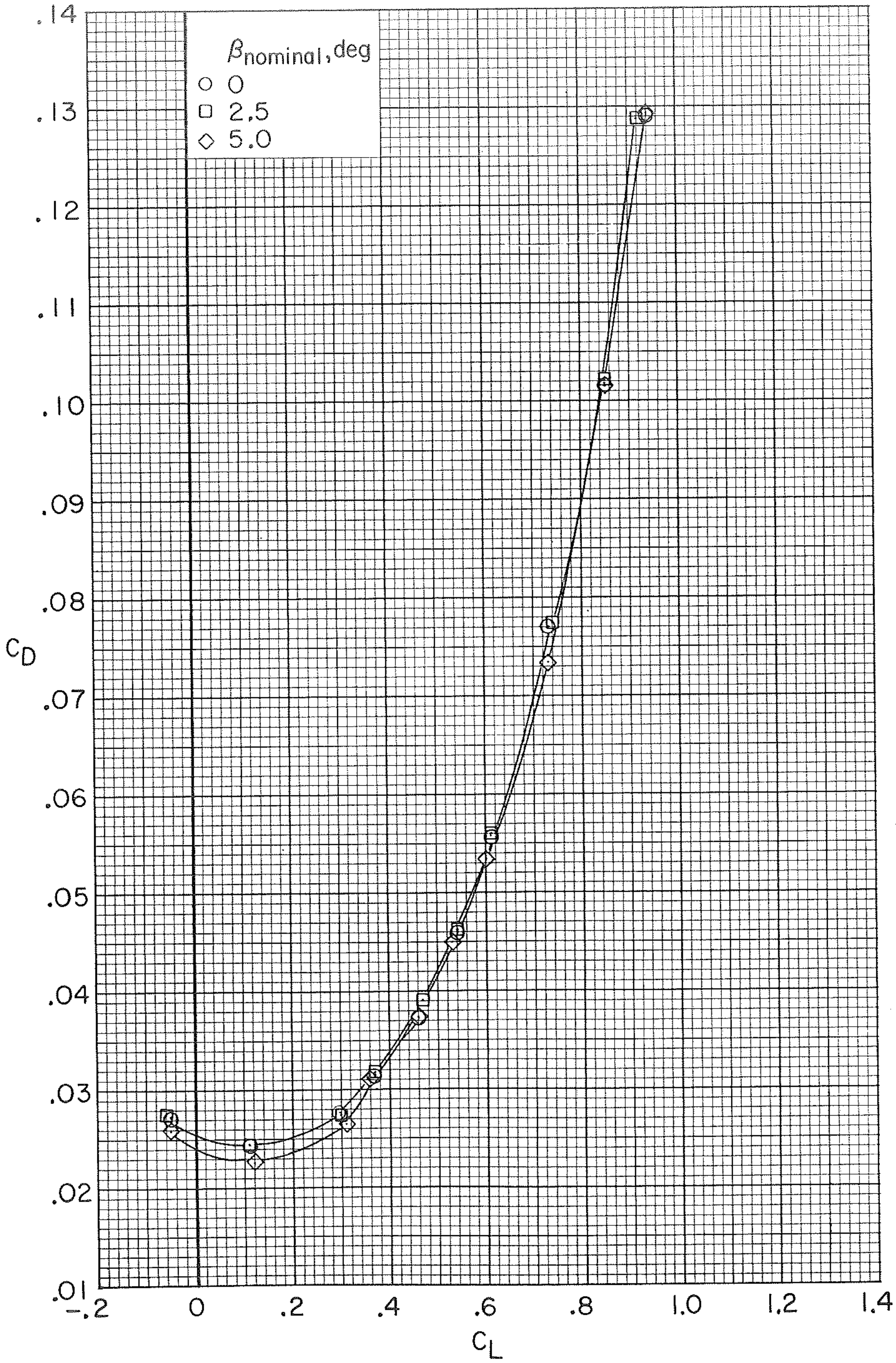

(d) M = 0.990.

Figure 10.- Continued.

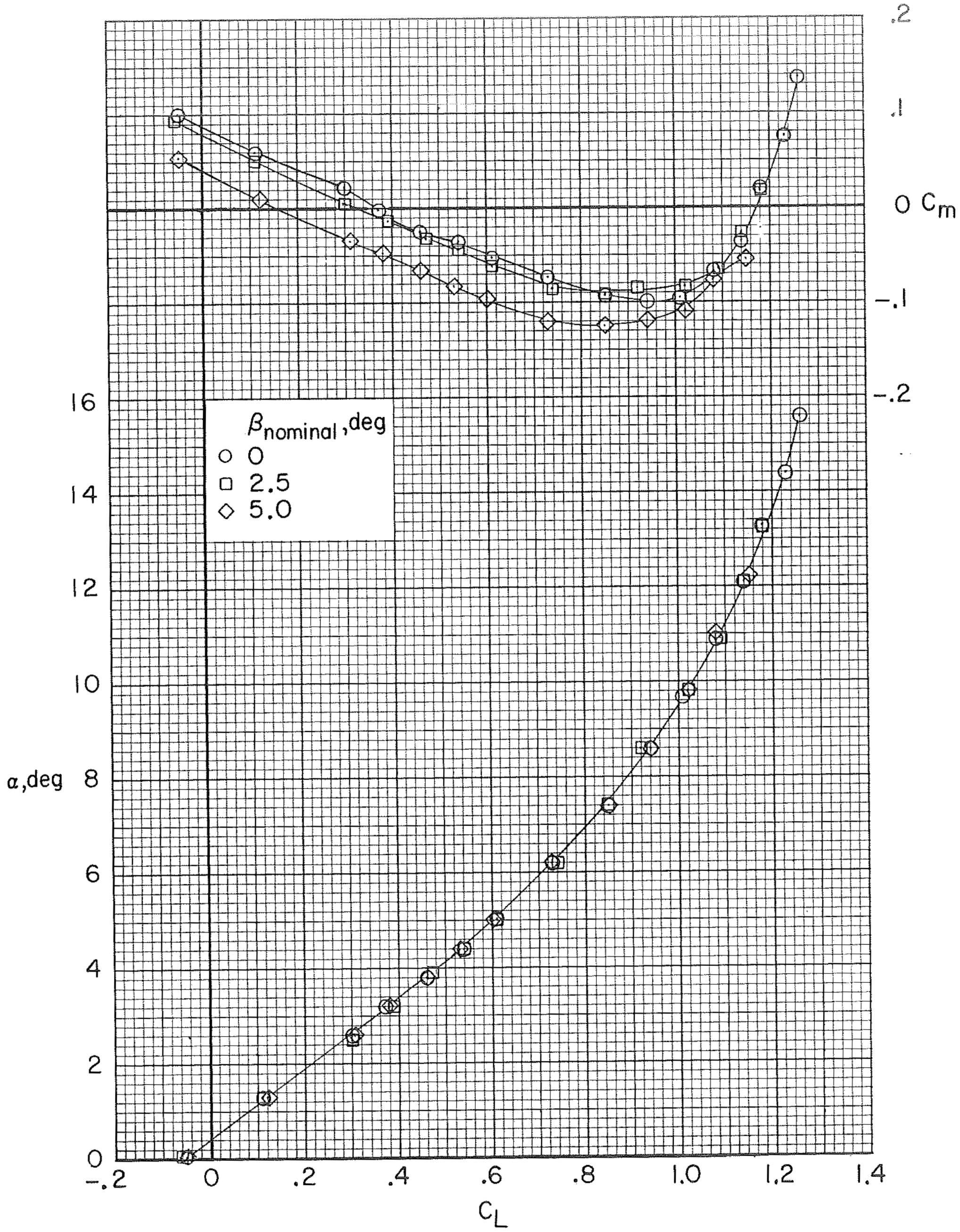

(d) M = 0.990. Concluded.

Figure 10.- Continued.

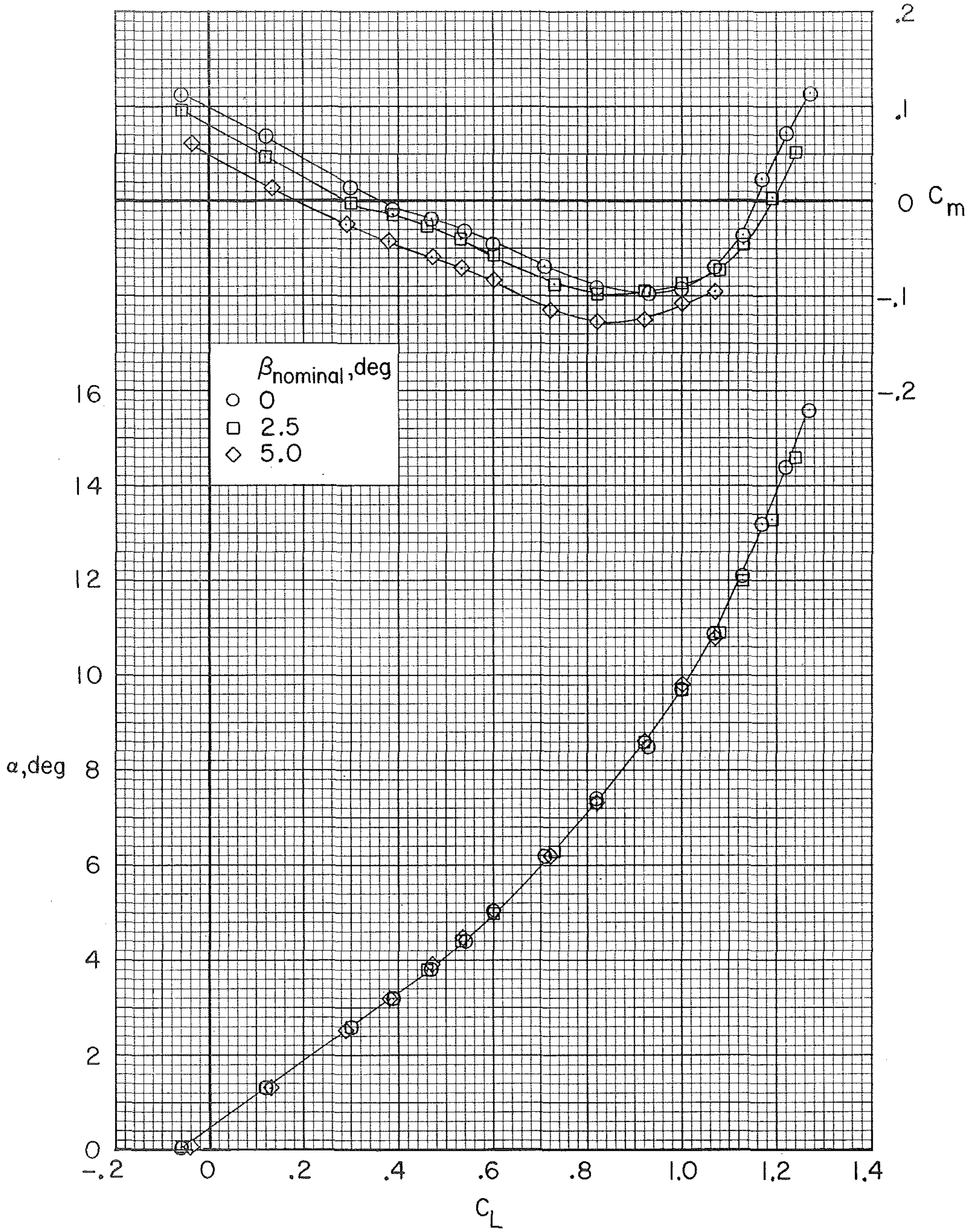

(e) M = 1.010.

Figure 10.- Concluded.

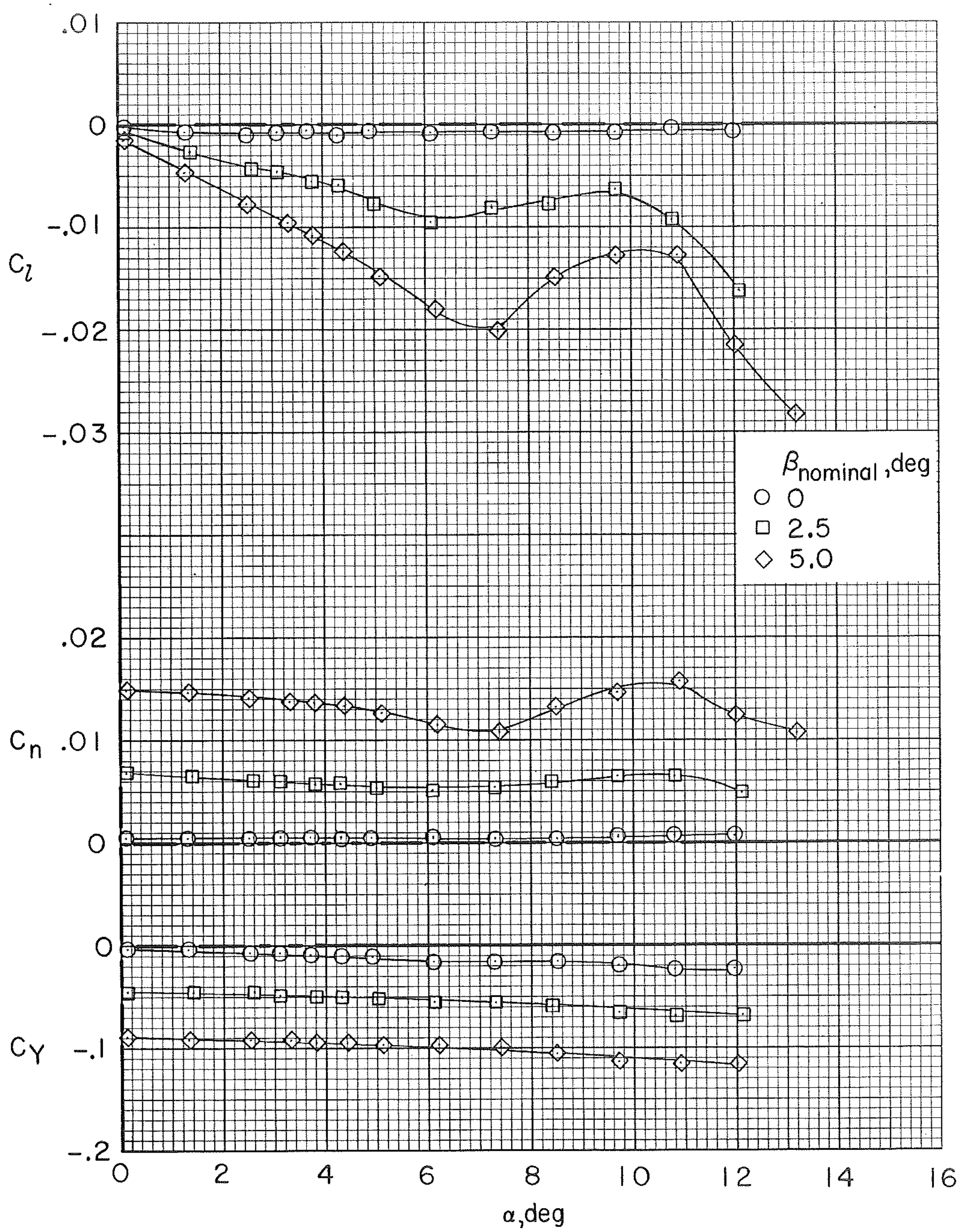

(a) M = 0.800.

Figure 11.- Effect of sideslip on lateral-directional aerodynamic characteristics. Transition type II; $\delta_h = -1.0^{\circ}$.

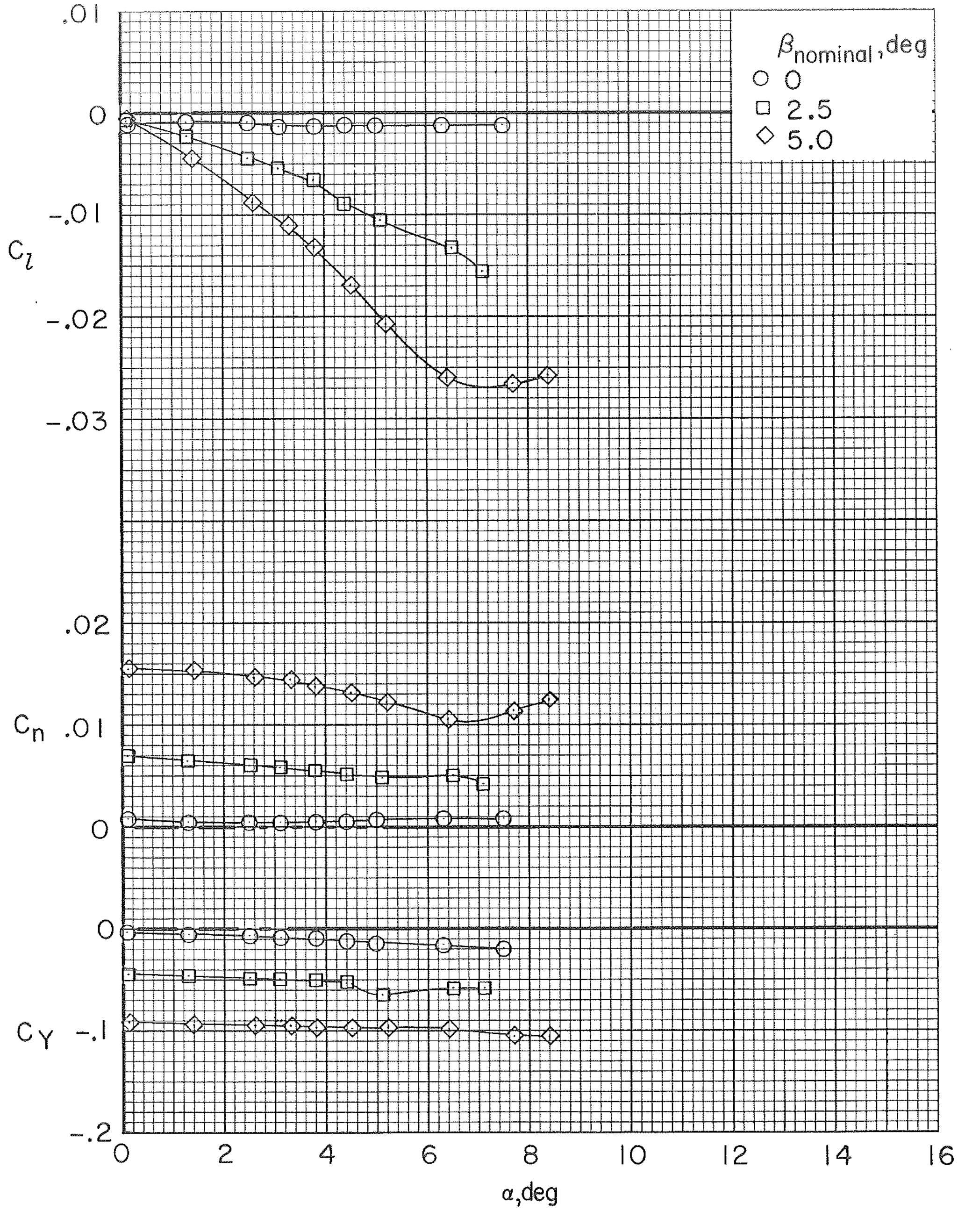

(b) M = 0.900.

Figure 11.- Continued.

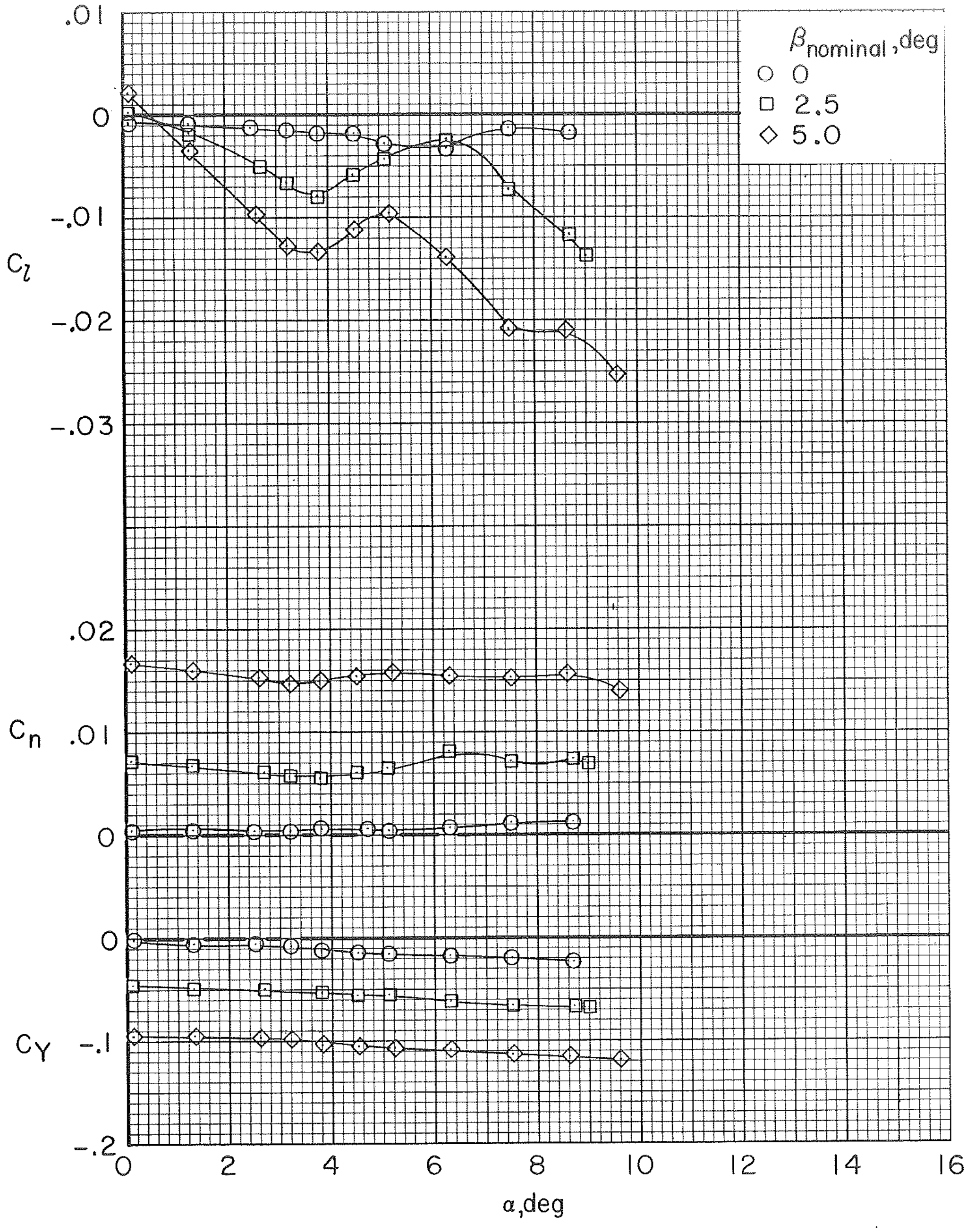

(c) M = 0.950.

Figure 11.- Continued.

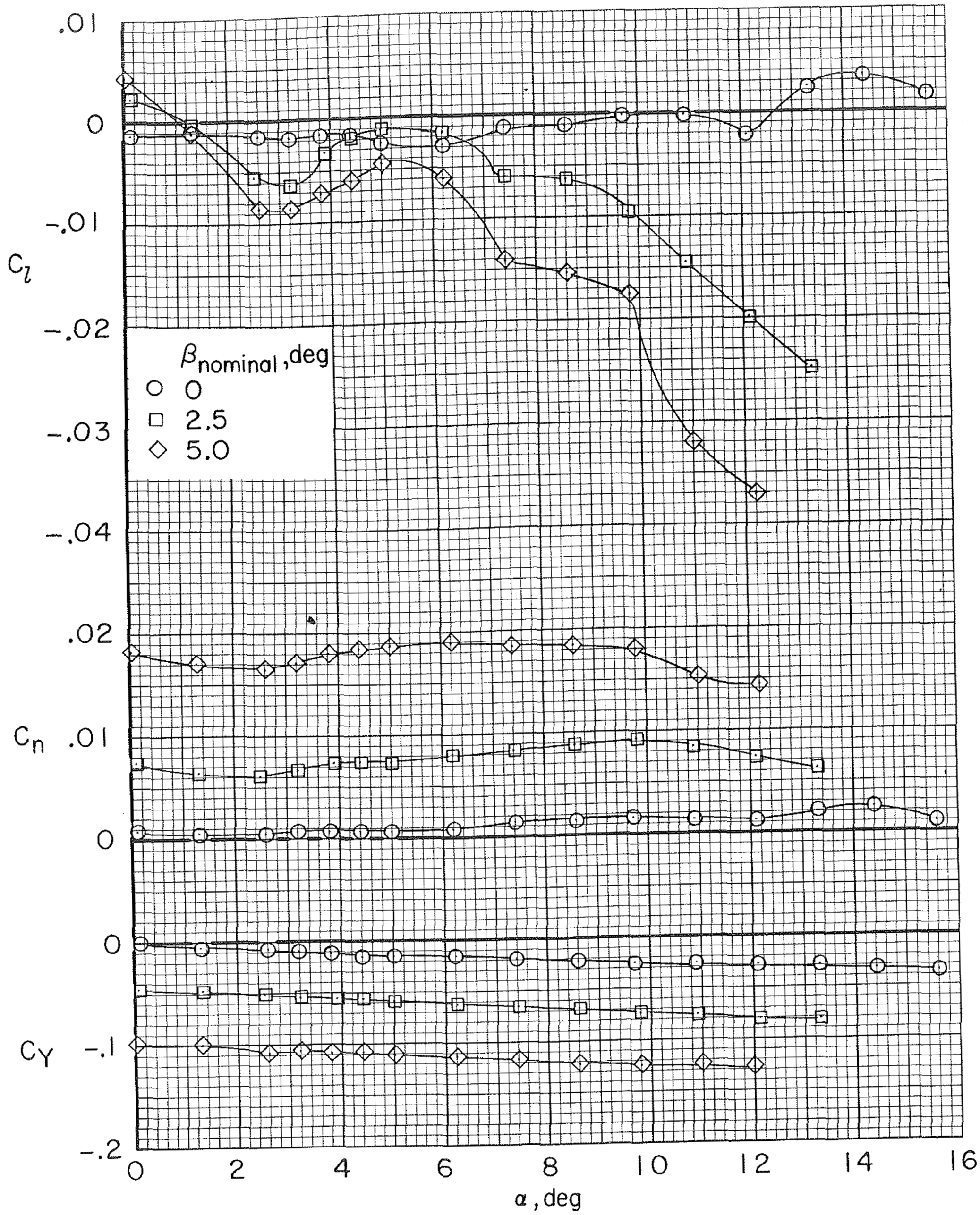

(d) M = 0.990.

Figure 11.- Continued.

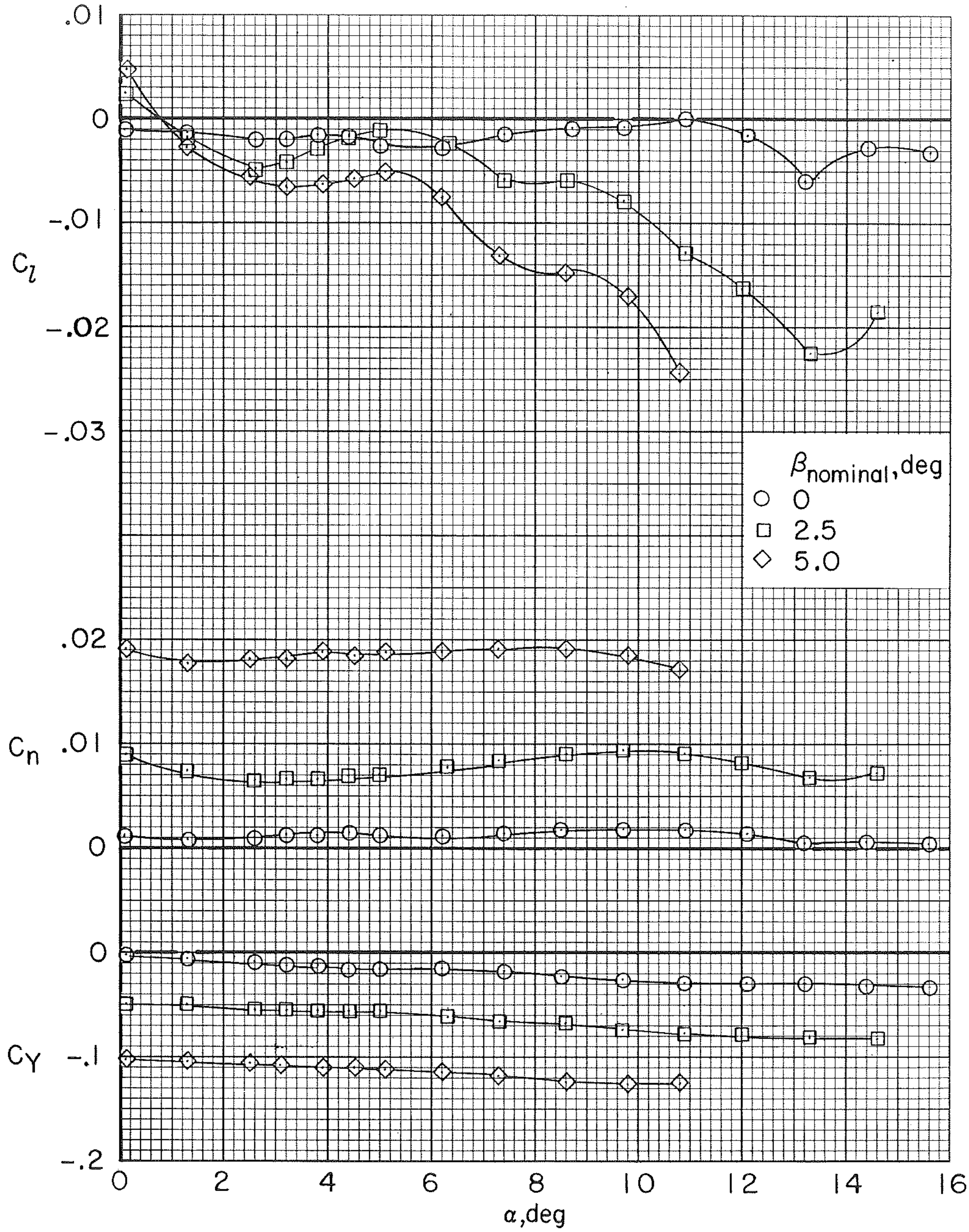

(e) M = 1.010.

Figure 11.- Concluded.

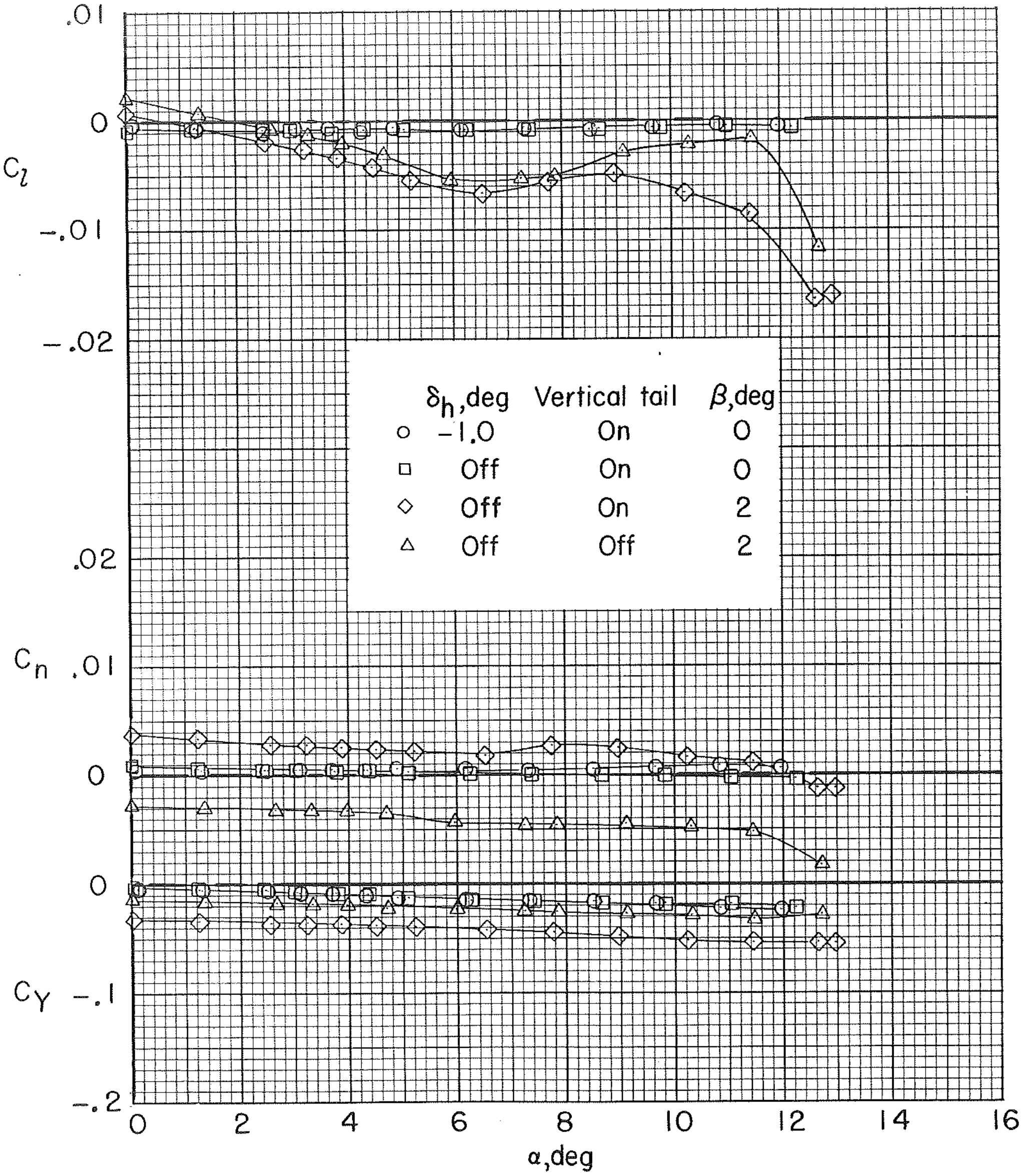

(a) M = 0.800.

Figure 12.- Effect of model components on lateral-directional aerodynamic characteristics. Transition type II.

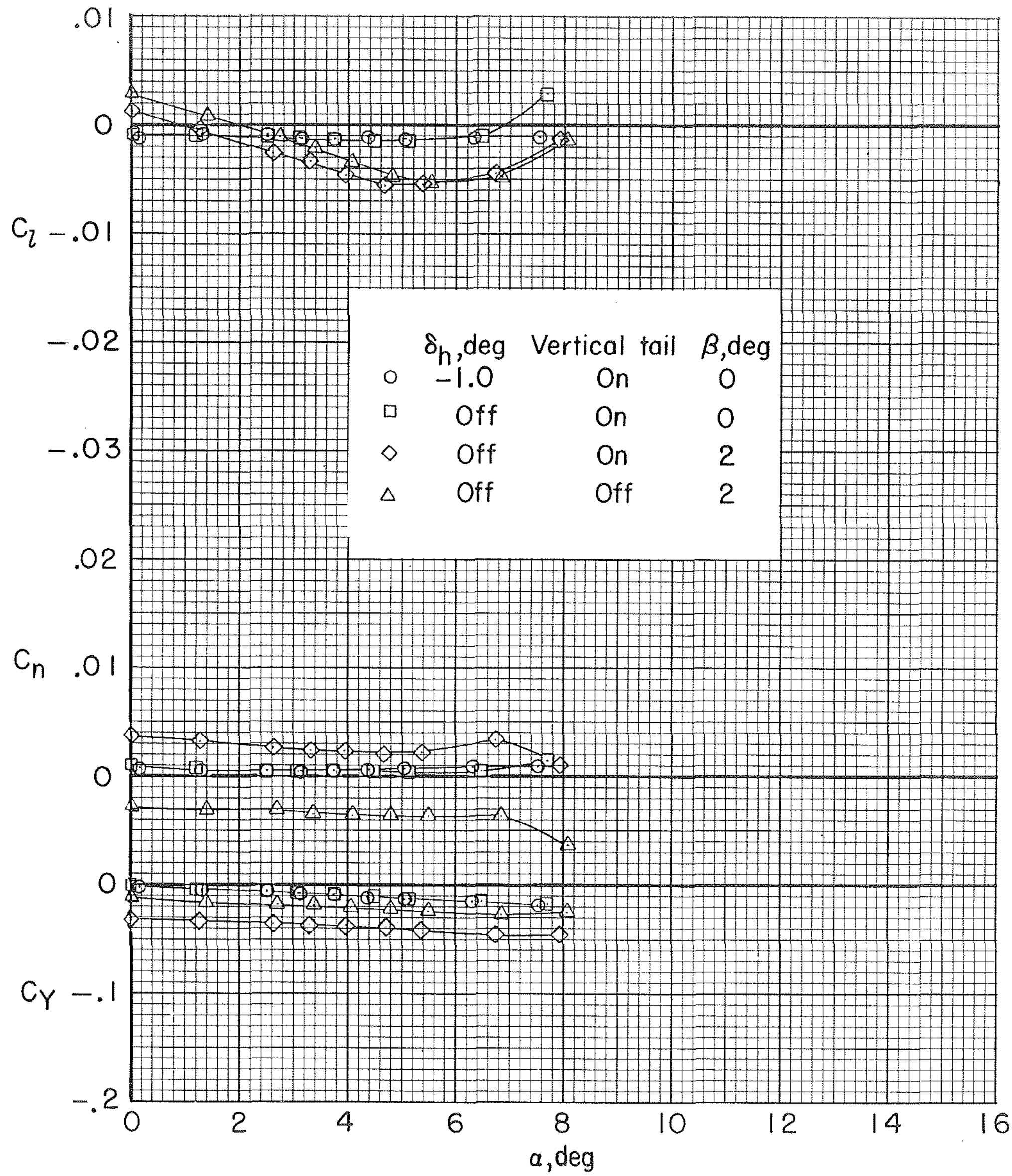

(b) M = 0.900.

Figure 12.- Continued.

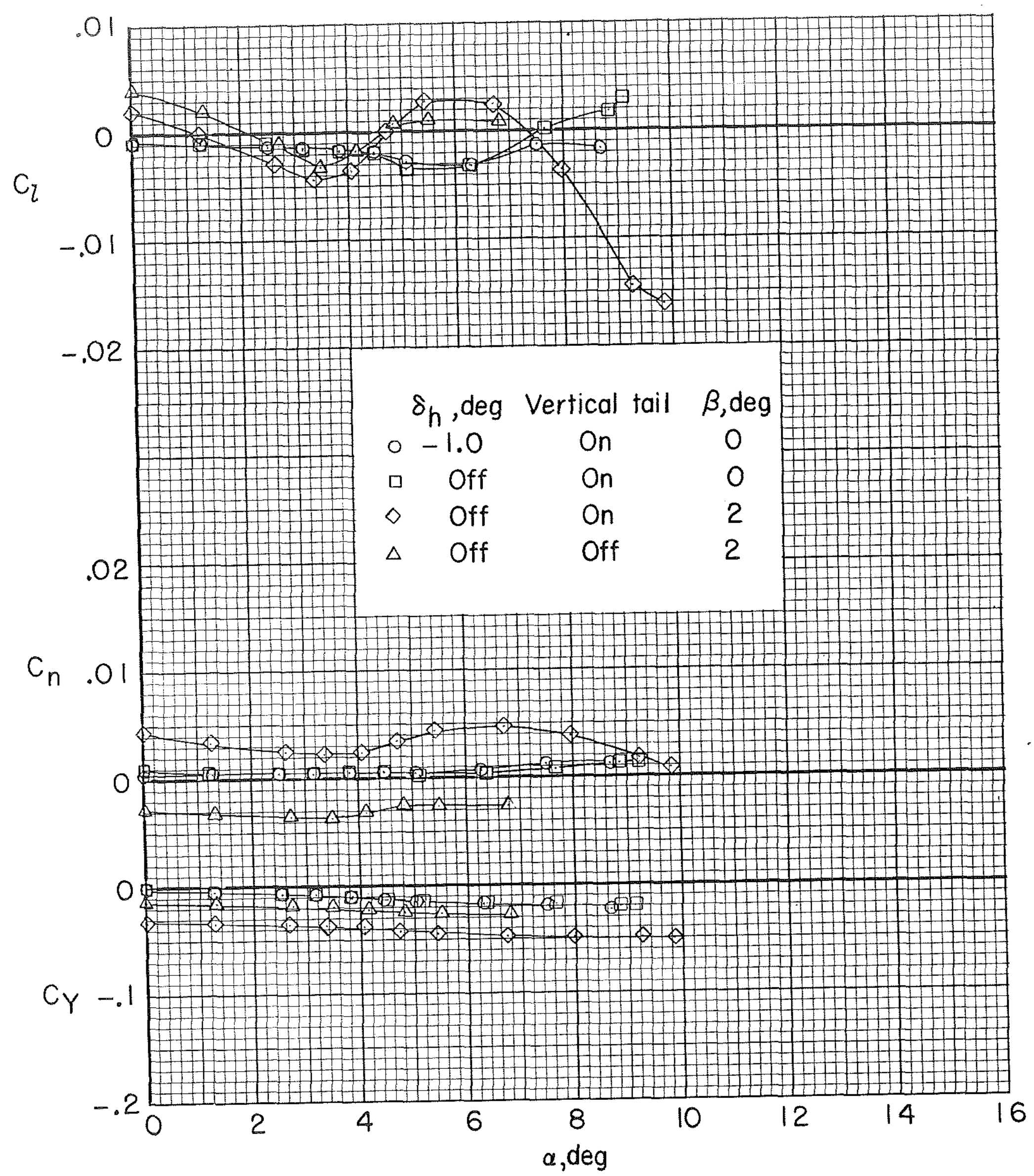

(c) M = 0.950.

Figure 12.- Continued.

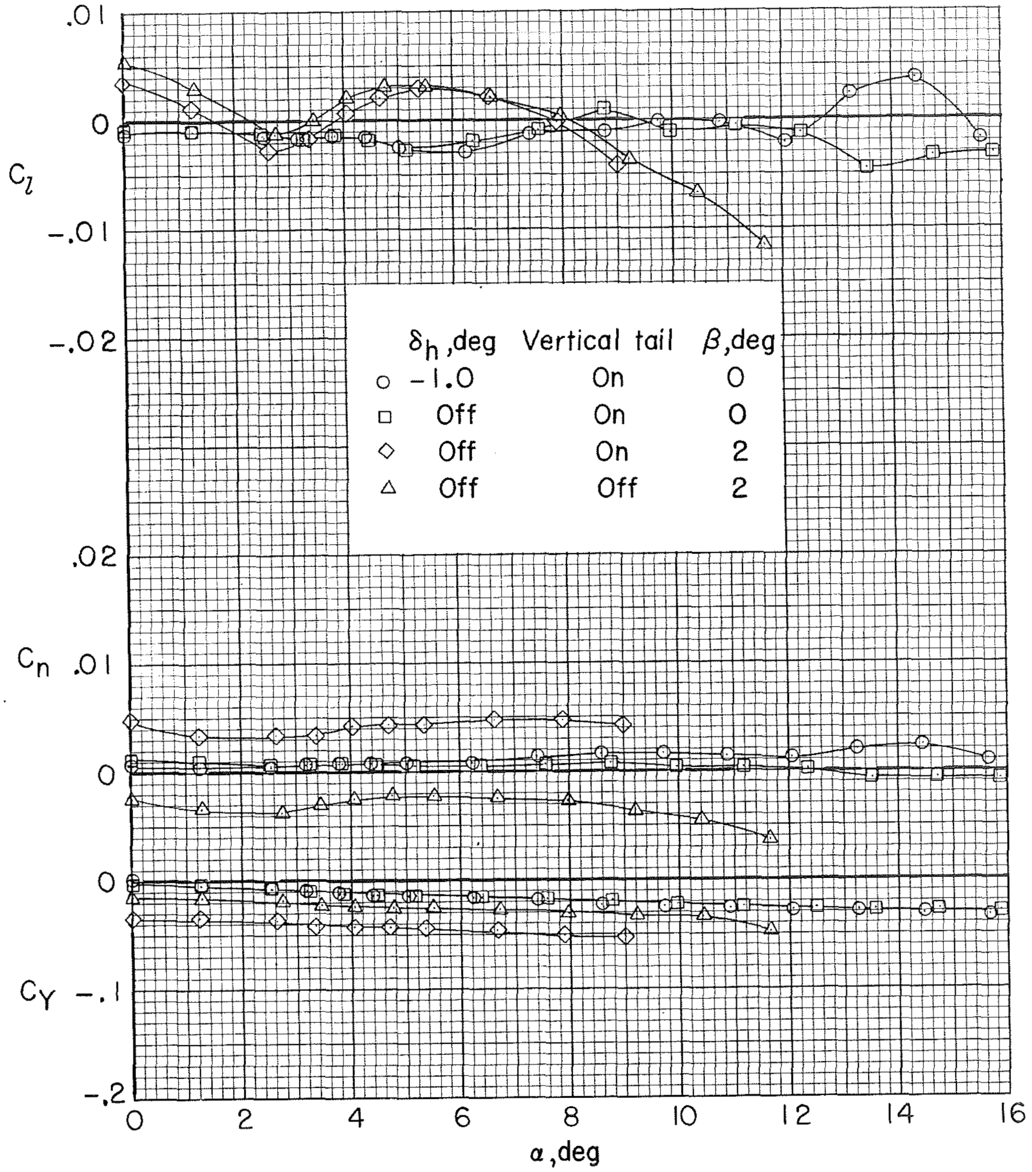

(d) M = 0.990.

Figure 12.- Concluded.

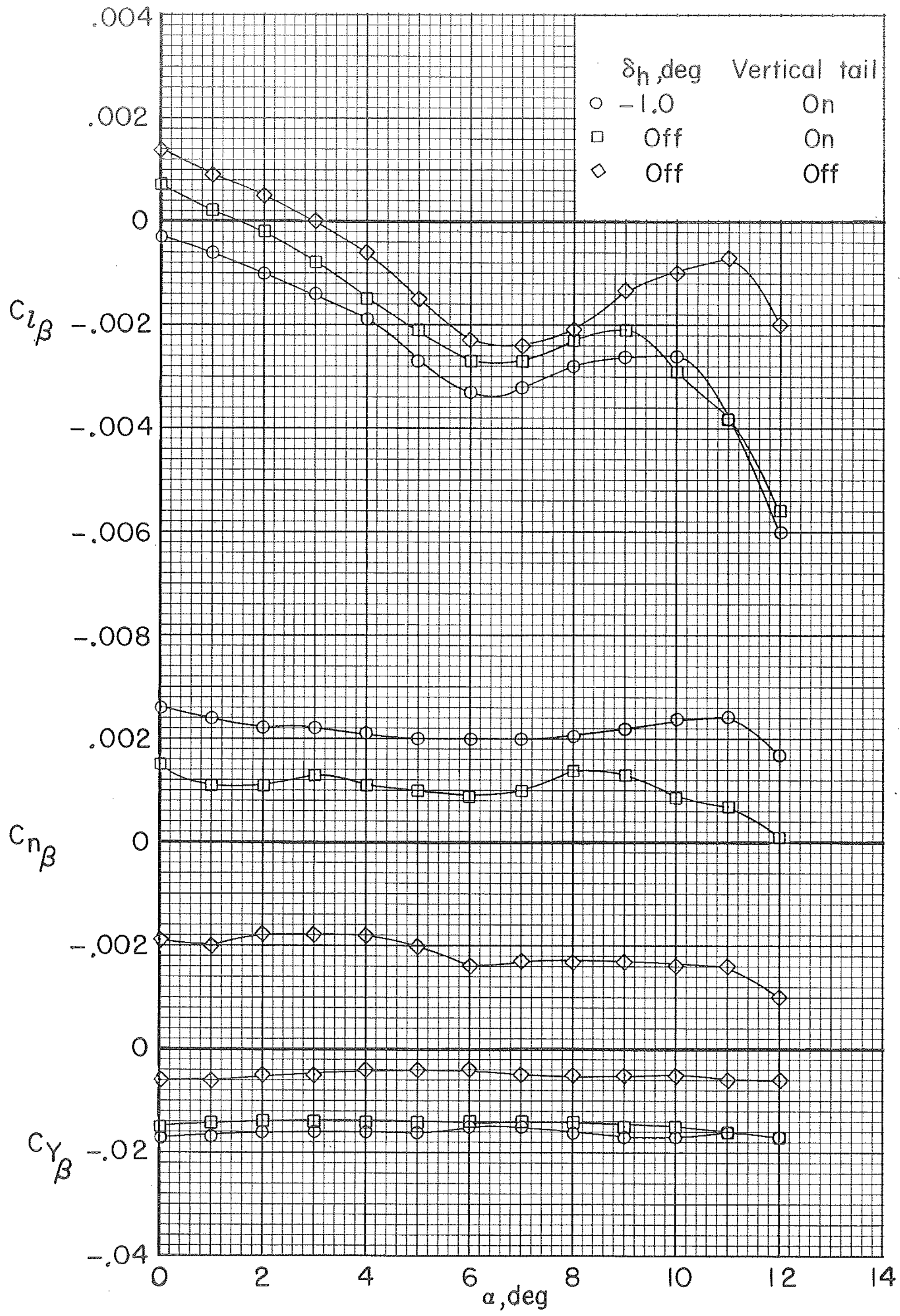

(a) M = 0.800.

Figure 13.- Effect of model components on lateral-directional stability parameters. Transition type II.

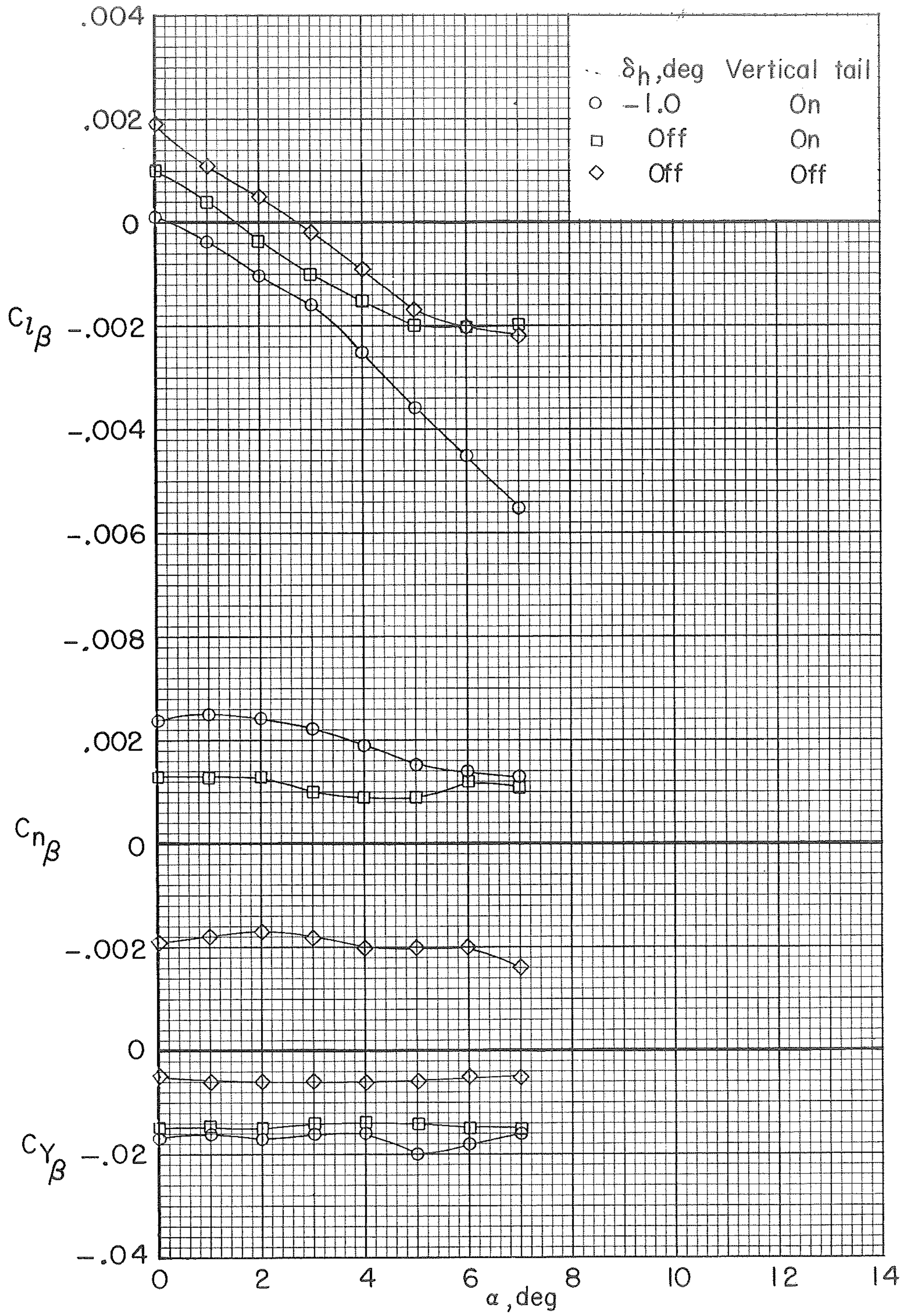

(b) M = 0.900.

Figure 13.- Continued.

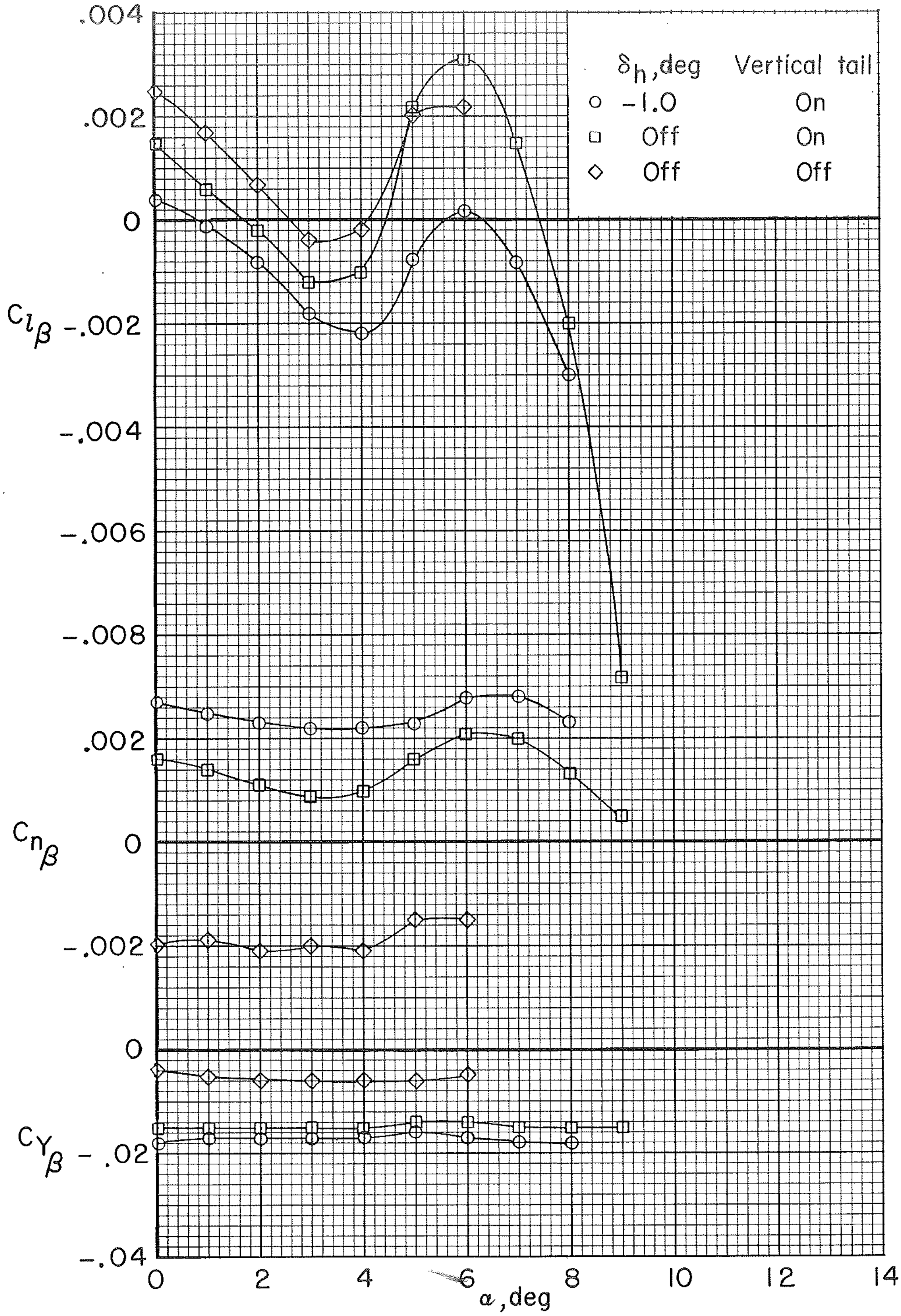

(c) M = 0.950.

Figure 13.- Continued.

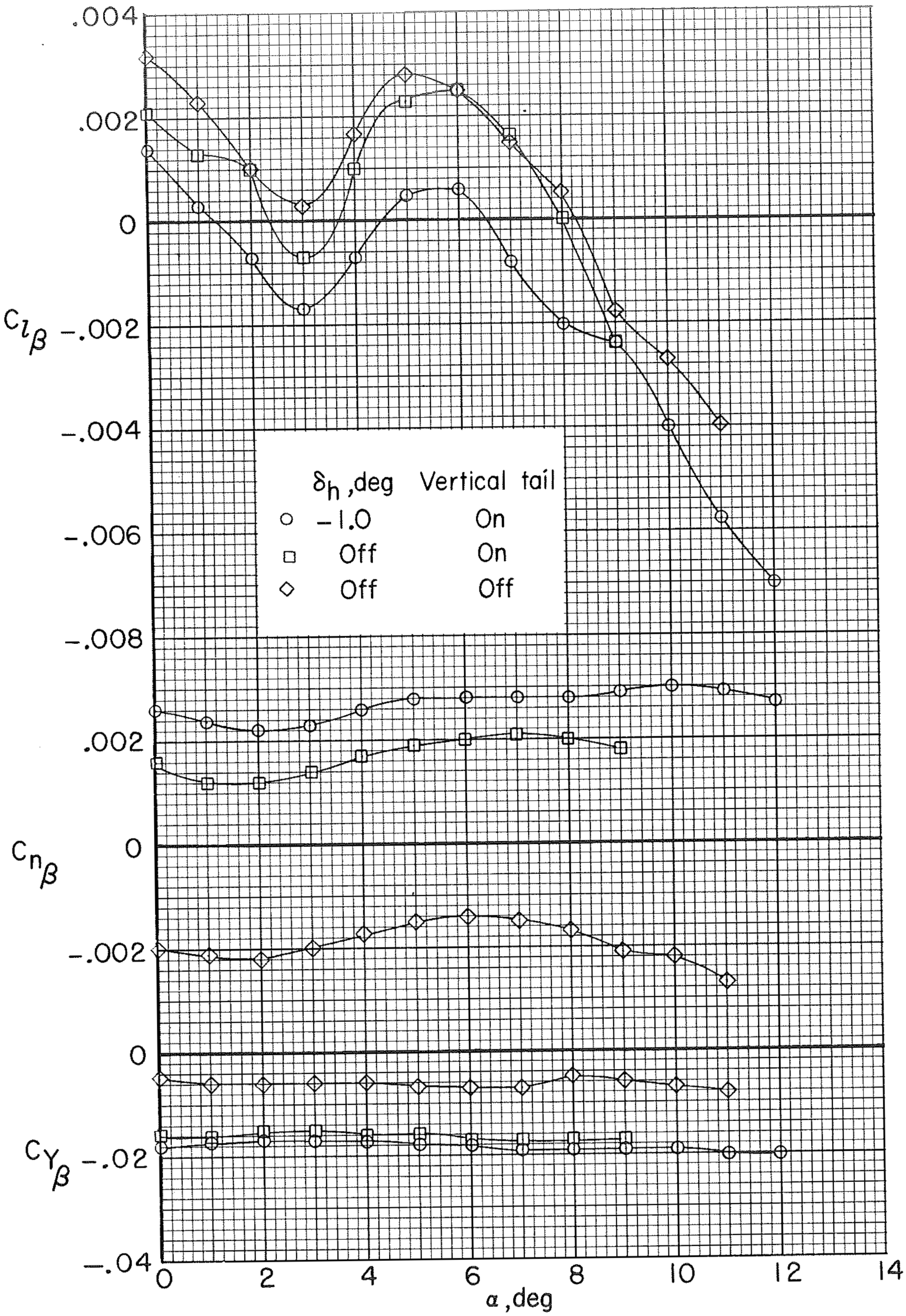

(d) M = 0.990.

Figure 13.- Continued.

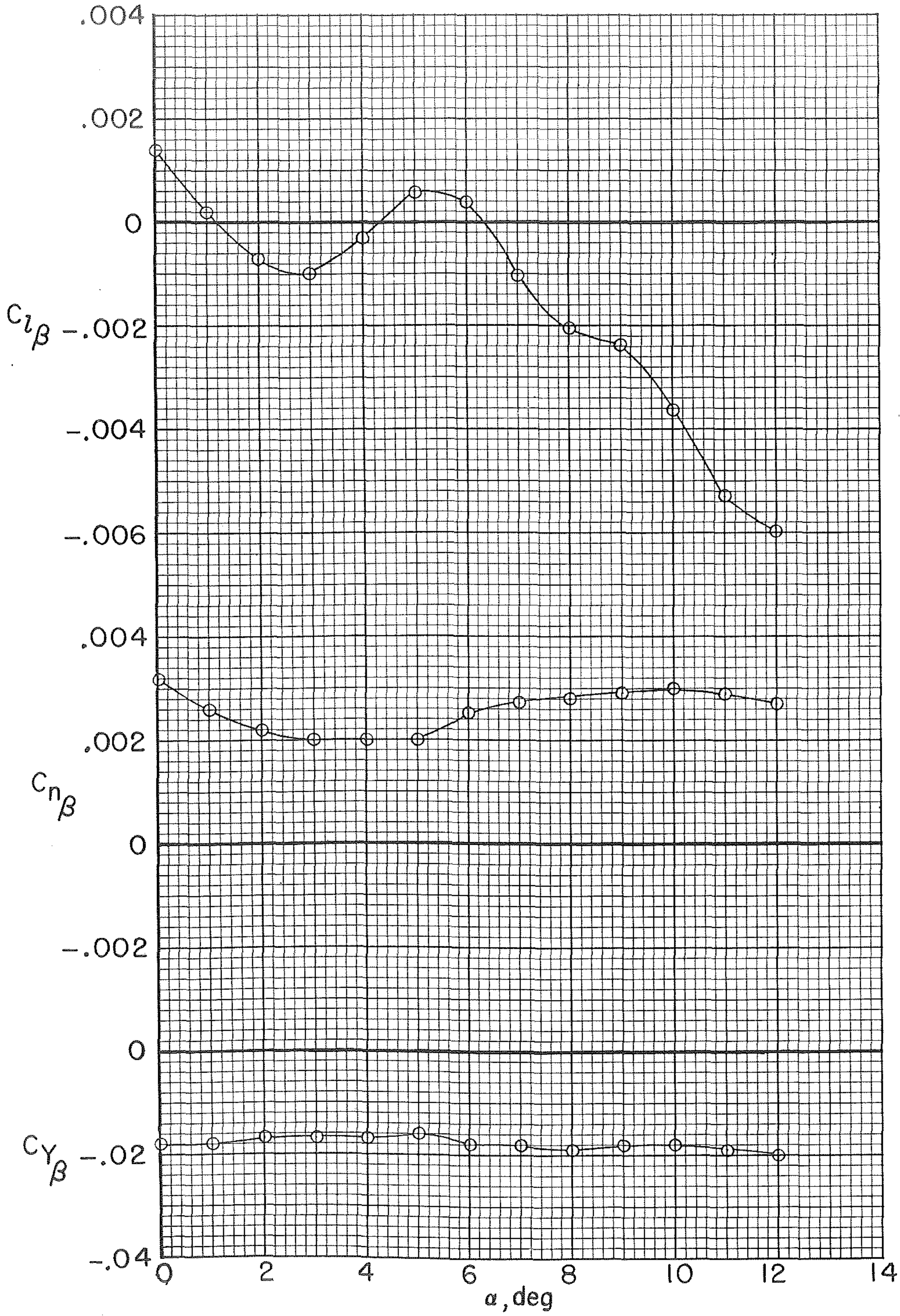

(e) M = 1.010.

Figure 13.- Concluded.

NASA-Langley, 1972 —— 1 L-8226

~~CONFIDENTIAL~~

"The aeronautical and space activities of the United States shall be conducted so as to contribute . . . to the expansion of human knowledge of phenomena in the atmosphere and space. The Administration shall provide for the widest practicable and appropriate dissemination of information concerning its activities and the results thereof."

—NATIONAL AERONAUTICS AND SPACE ACT OF 1958

NASA SCIENTIFIC AND TECHNICAL PUBLICATIONS

TECHNICAL REPORTS: Scientific and technical information considered important, complete, and a lasting contribution to existing knowledge.

TECHNICAL NOTES: Information less broad in scope but nevertheless of importance as a contribution to existing knowledge.

TECHNICAL MEMORANDUMS: Information receiving limited distribution because of preliminary data, security classification, or other reasons.

CONTRACTOR REPORTS: Scientific and technical information generated under a NASA contract or grant and considered an important contribution to existing knowledge.

TECHNICAL TRANSLATIONS: Information published in a foreign language considered to merit NASA distribution in English.

SPECIAL PUBLICATIONS: Information derived from or of value to NASA activities. Publications include conference proceedings, monographs, data compilations, handbooks, sourcebooks, and special bibliographies.

TECHNOLOGY UTILIZATION PUBLICATIONS: Information on technology used by NASA that may be of particular interest in commercial and other non-aerospace applications. Publications include Tech Briefs, Technology Utilization Reports and Notes, and Technology Surveys.

Details on the availability of these publications may be obtained from:

SCIENTIFIC AND TECHNICAL INFORMATION OFFICE

NATIONAL AERONAUTICS AND SPACE ADMINISTRATION

Washington, D.C. 20546

~~CONFIDENTIAL~~